ANL/FE-49628-TM04

STATE-OF-THE-ART OF ACOUSTIC INSTRUMENTATION FOR COAL-CONVERSION PLANTS

by

A. C. Raptis and T. K. Lau

ARGONNE NATIONAL LABORATORY

FOSSIL ENERGY PROGRAM

ARGONNE NATIONAL LABORATORY, ARGONNE, ILLINOIS

Prepared for the U. S. DEPARTMENT OF ENERGY
under Contract W-31-109-Eng-38

Printed in the United States of America
Available from
National Technical Information Service
U. S. Department of Commerce
5285 Port Royal Road
Springfield, VA 22161

NTIS price codes
Printed copy: A07
Microfiche copy: A01

Distribution Category:
Coal Conversion and Utilization--
Materials and Components (UC-90h)

ANL/FE-49628-TM04

ARGONNE NATIONAL LABORATORY
9700 South Cass Avenue
Argonne, Illinois 60439

STATE-OF-THE-ART OF ACOUSTIC INSTRUMENTATION FOR COAL-CONVERSION PLANTS

by

A. C. Raptis

Components Technology Division

and

T. K. Lau

U. S. Department of Energy
Fossil Energy

October 1981

TABLE OF CONTENTS

TABLE OF CONTENTS (Contd.)

LIST OF FIGURES

LIST OF FIGURES (Contd.)

LIST OF FIGURES (Contd.)

LIST OF TABLES

ABSTRACT

In developing process control instruments for coal conversion plants acoustic techniques have received considerable attention. The reasons for this attention are that instruments based on acoustic techniques are usually non-intrusive, easy to install and maintain, they have very fast response times. This report presents the State-of-the-Art in development of acoustic instruments for coal conversion plants. It discusses the feasibility for flow and temperature measurements in terms of important parameters of the Sonar Equation and environmental conditions i.e., (a) attenuation of sound in coal conversion media; (b) the noise background levels in coal conversion plants, and (c) acoustic transducer and other material charcteristics needed to meet the requirements of the hostile environment. Major emphasis is on the current state of development of the high temperature acoustic doppler flowmeter, active acoustic cross-correlation flowmeter, and the acoustic flow/no-flow indicator. Operating experience with these instruments and recommendations for further work are presented.

STATE-OF-THE-ART OF ACOUSTIC INSTRUMENTATION FOR COAL-CONVERSION PLANTS

I. INTRODUCTION

The instrumentation needs for the economic, safe, and optimum operation of coal-conversion pilot and demonstration plants were first presented by Argonne National Laboratory (ANL) in a State-of-the-Art report to ERDA-Fossil Energy.[1] These needs were subsequently confirmed by pilot plant engineers and reports from other organizations. The State-of-the-Art report pointed out that 90% of the instrumentation needs for large-scale coal gasification, liquefaction, and fluidized-bed conversion plants will be met with conventional petrochemical plant instrumentation. The remaining 10% cannot be met with commercially available instrumentation and, therefore, will have to be developed. This remaining 10% involves on-line composition analysis of process streams and measurements of mass flow rates of solids in liquids or gases, fluidized-bed and oil/water interface levels, and temperatures in reactors and combustors.

In the ANL instrument development program which followed publication of the original State-of-the-Art report, the main emphasis has been on development of instruments to measure mass flow rates and to perform on-line analysis of process flow streams unique to coal-conversion systems with less emphasis on temperature and level measurements.[2,3] The flow instruments under development are based on acoustic/ultrasonic, electromagnetic, optical, or nuclear techniques, and the program has focused on development of nonintrusive instruments. The primary focus on nonintrusive instruments has been necessitated by the presence of crush solids, usually coal, char or ash, and sometimes limestone, dolomite, powder iron, or alumina pellets moving with the liquid or gaseous process flow streams. Because of the solids content, these streams are very abrasive and corrosive in nature, and at pressures as high as 4500 psi and temperatures up to 2000°F or higher, nonintrusive instruments would be considered superior to intrusive instruments.

This report presents the state of the art of acoustic instrumentation. This study includes some of the findings of theoretical feasibility studies, laboratory experiments, and operating and experimental information from experiments on prototype instruments installed in pilot plants.[4,5,6]

The findings of some initial theoretical feasibility studies discussed in this report were based on limited theoretical and experimental work found in the literature. These studies estimated important parameters such as the attenuation of sound through the media and the noise background levels in coal-conversion plants. These studies also indicated that acoustic/ultrasonic flowmeters were feasible for instrument operating frequencies below 500 kHz, and the frequency selected should be dependent on the size of the pipe.

The laboratory and pilot-plant experiments reviewed in this report were performed to supplement and verify the initial theoretical findings. The sound-attenuation and noise-background measurements reviewed were obtained with experiments at the HYGAS pilot plant. These measurements confirmed that the frequency of operation for an acoustic flowmeter should be below 500 kHz and depended on pipe diameter. The measurements also indicated that transducer availability was an important consideration not only from the stand point of high temperature serviceability but also with regard to sensitivity of signal level transmission and reception.

Based on the theoretical studies and experimental results, the high-temperature acoustic doppler flowmeter was developed. This report reviews the results of the testing of this doppler flowmeter in the SRC-Pilot Plant at Fort Lewis, WA.

This report also reviews other acoustic techniques and instruments including: (a) The active acoustic cross-correlation flowmeter developed during the HYGAS experiments and refined with tests in the laboratory. This flowmeter was not retested under actual temperature and pressure in a pilot plant. (b) The acoustic flow/no-flow monitor developed for the char return line of the BI-GAS pilot plant. This instrument was needed because the char flow to the gasifier is essential for safe operation of the pilot plant. (c) The findings of the theoretical feasibility studies for temperature and level measurements using acoustic/ultrasonic techniques.[7]

II. FLOW MEASUREMENT

A variety of acoustic/ultrasonic flowmeters are commercially available. These flowmeters are based on approaches or methods of measurement that may be categorized according to the principle utilized, that is, (a) contrapropagating transmission (upstream-downstream), (b) reflection (doppler), (c) beam drift, ray rotation, turbulence, and attenuation, (d) correlation (active or passive), (e) vortex shedding, (f) liquid level (weirs, flurries, ducts), (g) noise, and (h) hot wire waveguide.[8] Thus far, acoustic/ultrasonic flowmeters have been used with all types of matter and their multiphase mixtures except plasma. Examples of multiphase or multi-component mixtures are: (a) liquid plus sediment or gas bubbles, (b) solid particulate matter which is fluid-borne (e.g., coal dust in air, coal particles in oil or water, microemboli in blood), and (c) liquid plus liquid (oil plus water).

Commercially available acoustic/ultrasonic flowmeters, however, have not performed well in coal conversion plants because they were not designed for the temperature and operating-frequency requirements of the multiphase streams found in coal conversion processes. It is the purpose of this report to examine the feasibility, development, and application of acoustic/ultrasonic flowmeters with respect to coal conversion process streams.

1.0 Feasibility Analysis - Theoretical

The figure of merit for a sonic system of measurement which utilizes the generation, transmission, and reception of sound is defined as the maximum allowable transmission loss. This value is derived from the sonar equation, which simply states that, "the received signal level equals the noise background level plus a measurement requirement," where the measurement requirement is set by the particular measurement under consideration.[9] This method is not unique to sonics and may be applied to radar, astronomy, and communication theory. The advantage of the sonar equation, which underlies the figure of merit computation, is that it permits quantitative comparison of various measurement schemes and selection of operating parameters on a common basis.[10,11]

A simple form of the sonar equation is,

Received Signal Level = Noise Background + Measurement Requirement (1)

The output signal-to-noise ratio for a signal transmitted through a system is given by

$$(S/N)_{out} = \frac{S_o \cdot T \cdot G_s}{N_o \cdot G_n} \quad . \tag{2}$$

where

S_o = the received signal

N_o = the received noise

G_s = the signal gain

G_n = the noise gain

T = the transmission coefficient

For a sonic flowmeter to operate, some signal-to-noise requirement $(S/N)_{req}$ must be satisfied. Using this signal-to-noise requirement and Eq. (1), the following relationship is established

$$\frac{(S/N)_{out}}{(S/N)_{req}} = \frac{S_o \cdot T \cdot G_s / G_n \cdot N_o^{-1}}{(S/N)_{req}} \quad . \tag{3}$$

By calling the left-hand side of Eq. (3) the excess signal R required for flowmeter applications, and taking the logarithm of both sides of Eq. (3) the result is

$$10 \log (R) = 10 \log(S_o) + 10 \log(T) + 10 \log(G_s/G_n) - 10 \log(N_o) - 10 \log[(S/N)_{req}] \tag{4}$$

Equation (4), for simplicity, can be rewritten as

$$SE = SL - TL + PG + DG - NL + MR \tag{5}$$

where

SE = the signal excess
SL = the source level
TL = the transmission loss
PG = the processing gain
DG = the directivity gain
NL = the noise level
MR = the measurement requirement

The normal procedure is to write Eq. (5), the sonar equation, on a spectral basis where the sound intensities are referenced to a 1-H_z bandwidth. For a broad-band system, however, such as a flowmeter, as long as all variables are referenced to the same bandwidth, the equation is satisfied.

The processed signal level (PSL) of a one-way transmission system, as shown in Fig. 1, may be defined as

$$PSL = SL - TL + PG + DG \tag{6}$$

The processed signal level is the received signal level increased by a factor that accounts for the gain in the signal-to-noise ratio due to signal processing. Equation (6) is used in establishing the method of showing feasibility.[12]

The first attempt to determine the feasibility of using acoustic/ultrasonic techniques to measure mass flow in coal conversion process streams was based on limited theoretical and experimental results found in the literature.[9] This theoretical feasibility study was limited in nature, because important terms in the sonar equation such as the transmission loss and noise background level [see Eq. (5)] were estimated.[13] The other terms, such as, source level, processing gain, and directivity gain of the transducers, depend on the choice of transducers and instrumentation and, therefore, are known quantities. Although incomplete

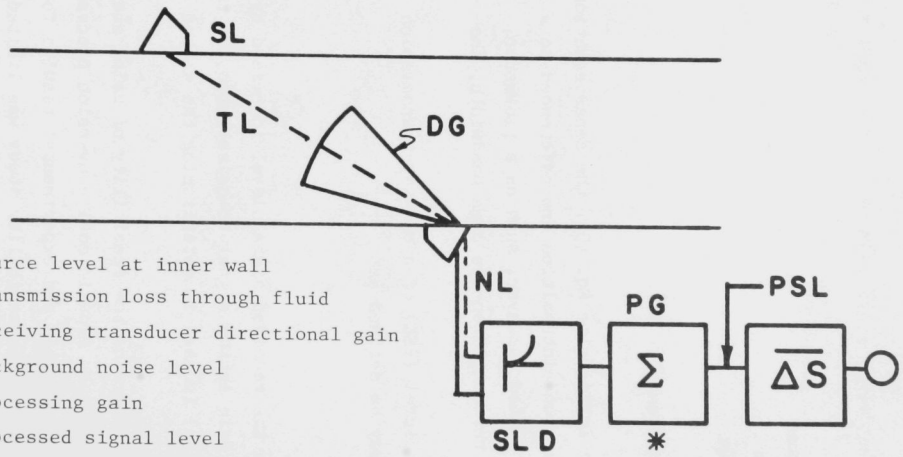

SL, Source level at inner wall
TL, Transmission loss through fluid
DG, Receiving transducer directional gain
NL, Background noise level
PG, Processing gain
PSL, Processed signal level
ΔS, Averaged measurement parameter (Δf, $\Delta \phi$, Δt, etc)
SLD, Square law detector
*, Summation

Fig. 1 An Elementary Sonic Transmission Flow Velocity Measurement Scheme

because of the unavailability of experimental data, the theoretical feasibility study became the basis for further developments of acoustic/ultrasonic flowmeters for coal conversion plants. The theoretical feasibility study established the need for experiments to determine (1) noise background levels in coal conversion plants and (2) the signal losses in the media found in the streams of such plants.

2.0 Attenuation and Noise Background Experiment

To determine the noise background levels in coal conversion plants and the attenuation of sound waves in coal-slurries an experiment was performed using the low-pressure coal slurry line of the HYGAS pilot plant.[14] The HYGAS pilot plant uses a gasification process that utilizes a fluidized-bed reactor operating at pressures of 1000 to 1500 psig and temperatures of 1300-1800°F to convert the major part of the carbon in coal to gases. Between 5 to 10 wt % of the coal feed is converted to a light aromatic oil, principally toluene. The process maximizes methanol production in the reactor by using direct hydrogenation of coal.[15]

For the experiment, a test section was designed, built, and installed in the low-pressure line of the HYGAS plant. The design specifications and criteria as obtained from HYGAS engineers are summarized in Table I. The test section, shown in Fig. 2, is 182.82 cm (72 in.) long with six transducer housings along its length. An important feature of the test section is the isolation of the transducer housings from the abrasive properties of the toluene-benzene-coal slurry and from the pipe vibration. This was accomplished by using (1) a concave acoustic window structure made of Teflon to fit the pipe contour, thus isolating the transducers from the slurry; and (2) Viton gaskets to isolate the transducers from the pipe vibration. The transducers, were chosen to operate in the frequency range of 100 kHz to 1 MHz based on the theoretical feasibility study. The transducers tested were (1) the Acoustic Emission (AE) Model FAC-500 which has a rather flat frequency response from 100 kHz to 1 MHz, and (2) the Dunegan Endevco (D/E) Model D9203, which has a very non-uniform response but much higher sensitivity than the AE at certain frequencies (100 kHz and 500 kHz).

Table I

SUMMARY OF HYGAS TEST SECTION DESIGN CONDITIONS

Pipe material:	Carbon steel, 150 psi class, ASTM-A-106GRB
Flanges:	SA-1891-II, ASTM-A-181GRII
Pipe dimensions:	Nominal 2" pipe
Pipe schedule:	40
Pipe life:	2 years
Welding:	Code to be used ANSI B31.3-1973, Petroleum refinery piping
Flow rates:	70-100 gpm
Transporting Vehicle:	85% Toluene, 15% Benzene
Temperature of Vehicle:	150°F maximum
Char:	15-200 Mesh
Weight fraction:	Char 25-50%
Pressure of slurry:	30-40 psig
Bulk density:	40-50 lbs/ft^3, Particle density ~ 90 lbs/ft^3
Standard under which the total assembly has to be tested:	ANSI B31.3-1973; Design pressure: 90 psig and hydrostatic pressure = 135 psig
Special tests:	24 hr. 135 psi test with toluene
Stress analysis:	Stress analysis is required on non-standard components.

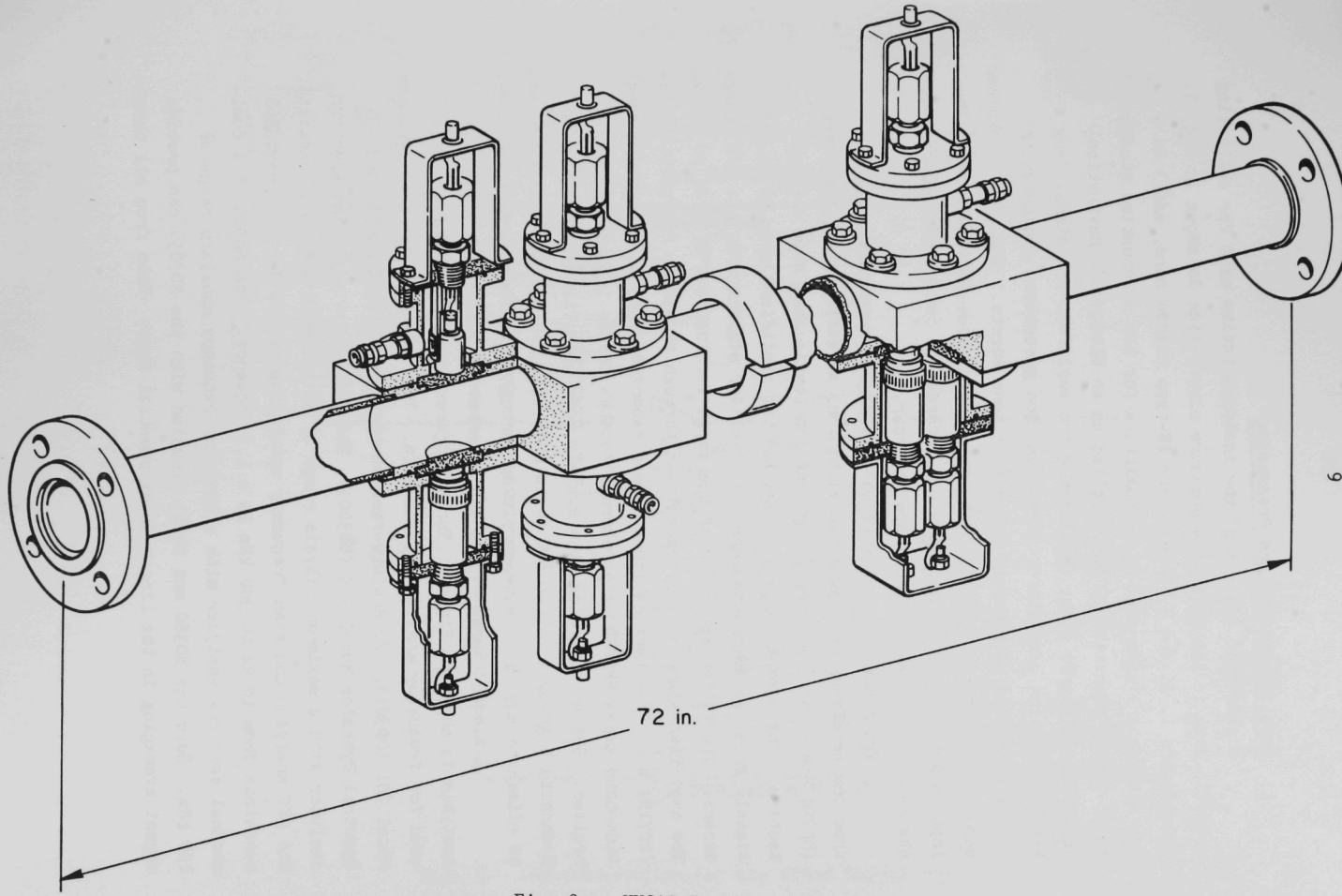

Fig. 2 HYGAS Test Section.

(a) Data Acquisition and Processing

A schematic diagram of the instrumentation used for collecting acoustic data in the HYGAS low-pressure slurry line is shown in Fig. 3. Transducers 1, 2, and 3 (1 and 2 are AE-type transducers, and 3 is a D/E transducer) were used as transmitters for the attenuation studies. Power to the transmitters was supplied by an Electronic Navigation Industries (ENI-rf) power amplifier which amplifies the signal from a Wavetek function generator. Three function generators connected in series were used to generate three sine tone bursts. The tone bursts had separate controls for pulse width, repetition rate, and amplitude. The input signal to the transmitters was recorded on two direct record channels of the Ampex PR2230 tape recorder.

Transducers 4 to 7 were used as signal receivers. Signals from the receivers were conditioned by four ac differential amplifiers (ORTEC Model 9454) enclosed in a junction box located near the test section. The nominal gain settings for the amplifiers were 60 dB for signals from the AE transducers and 40 dB for signals from the D/E transducers. The filter bandwidth of the amplifiers was set at 0.01 to 1 MHz. The amplified signals were transmitted through 90 meters of coaxial cable (RG71B) with 91-Ω termination and were recorded with the fourteen-channel wide-band Ampex PR2230 tape recorder located in the instrumentation trailer. Before recording, the signals were also filtered by using a Krohnhite high-pass filter set at 10 kHz. The purpose of this filter was to eliminate any low-frequency pickup through the 90-m transmission line.

A block diagram of the instrumentation employed for the data analysis is shown in Fig. 4. Three different spectrum analyzers were used for frequency analysis of the data. They were (1) Spectral Dynamics Model 301 (SD301), (2) Hewlett-Packard (H/P) Model 8553B/8552, and (3) Spectral Dynamics Model 360 (SD360). The SD301 is a real-time spectrum analyzer with a maximum analysis range of 50 kHz with a 150-Hz bandwidth. The H/P analyzer can scan frequency spectra up to 110 MHz and provide a bandwidth from 10 Hz to 300 kHz in a 1,3 sequence. The SD360 is a dual-channel spectrum analyzer with a maximum frequency analysis range of 150 kHz. Both the SD360 and SD361 (coupled with the SD309) can provide signal averaging in the linear or exponential form. Data from all three

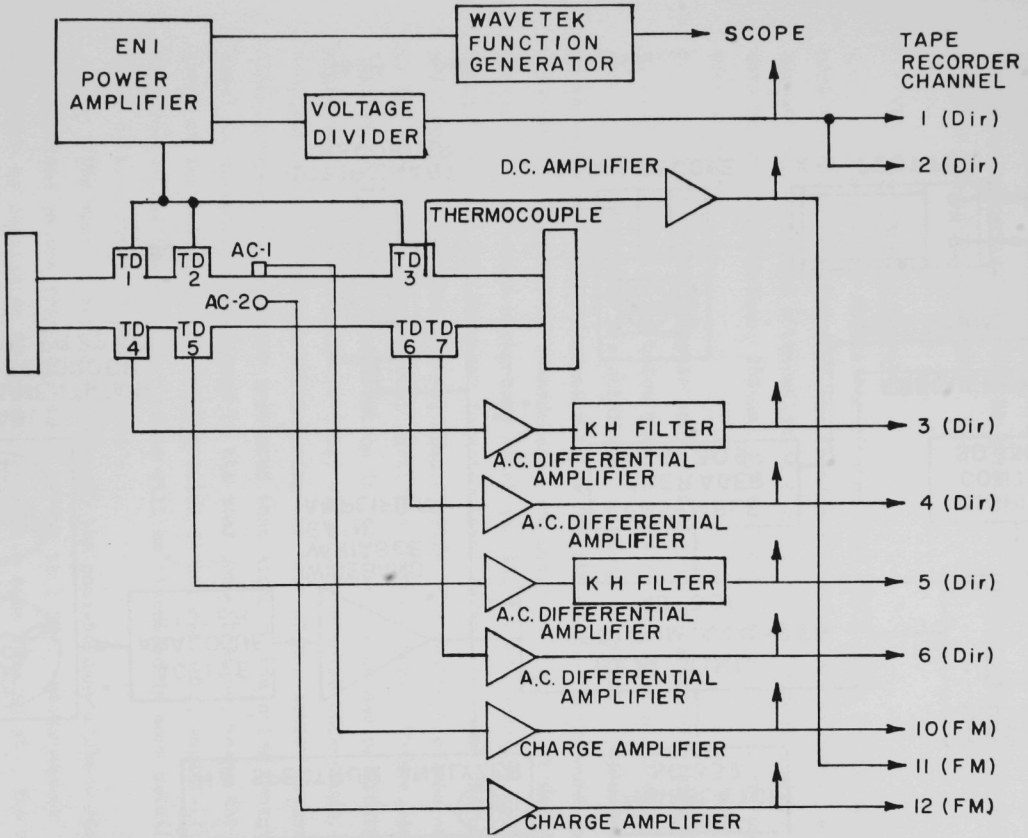

Fig. 3 Instrumentation for the HYGAS Experiment.

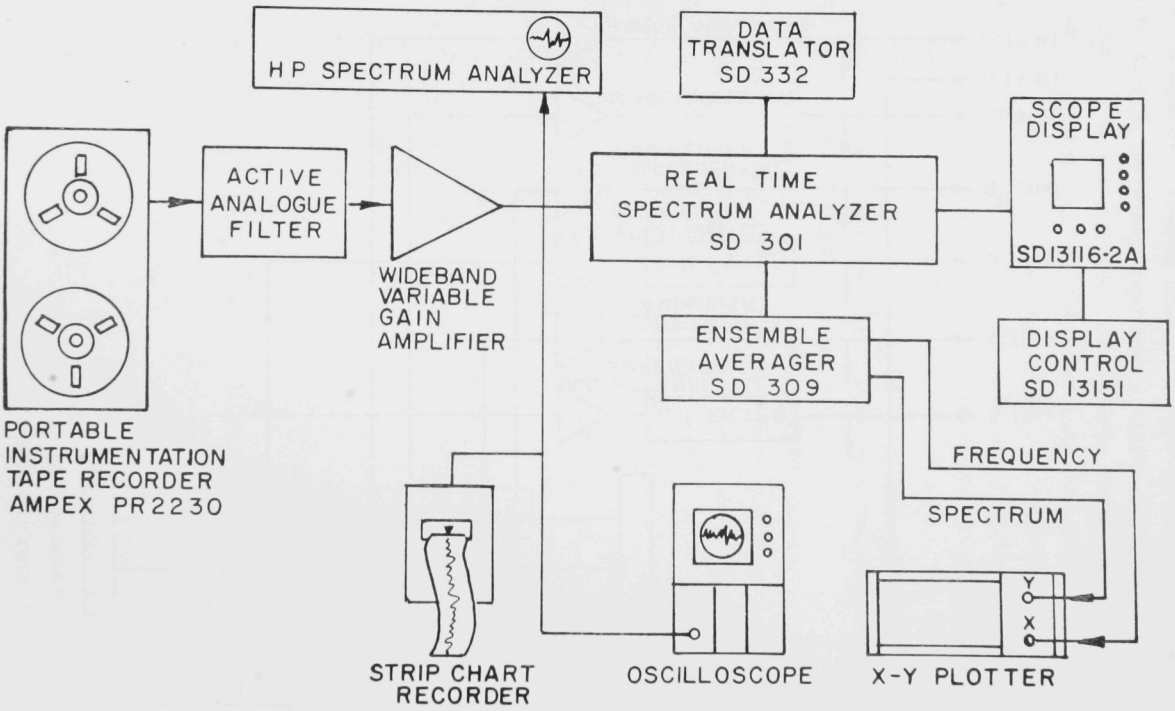

Fig. 4 Data Processing System.

analyzers are displayed on CRT units and can also be plotted on an X-Y recorder. The sound transmission was examined in the real time domain. A camera was used to capture the driving and the received signals displayed on a Tektronix oscilloscope. The logarithmic root-mean-square values of the noise background can also be plotted on a six-channel strip-chart recorder (Gould Model 2600).

(b) Experimental Results

The primary objectives of the HYGAS tests were: (1) to determine the noise background in the frequency range of 0.1 to 1 MHz, and (2) investigate the sound attenuation in a coal-toluene-benzene slurry. The data for toluene-benzene, 18%-and 33% coal-toluene-benzene slurry have been analyzed.

Most of the acoustic energy of the noise-background measurements at HYGAS was found to be below 500 kHz. There were some peaks observed near 1.5 MHz, but they are attributed to stray rf pickup. Representative linear-averaged expanded spectra below 400 kHz for the background noise, obtained by using the AE transducers, are shown in Fig. 5. It was observed that the noise-background level decreased with increased coal concentration. This decrease in noise level is due mainly to the noise attenuation in the coal slurry, specifically, the scattering loss caused by the increased number of coal particles in the slurry. This observation implies that the coal concentration in the slurry line may be obtained by measuring the root-mean-square (rms) value of the noise background. Additional experiments at HYGAS during the test of the active acoustic cross-correlation flowmeter indicated that although the noise background level is somewhat proportional to the coal concentration, using the noise level to indicate the coal concentration is not reliable, especially for high concentrations of coal. This will be discussed in more detail later (Active Acoustic Flowmeter).

The sound transmission through the coal-toluene-benzene slurry was examined in the frequency range of 0.1 to 1 MHz. Measurements were made by pulsing an AE transducer with a sine tone burst. The tone burst travels through the medium and is received by another AE transducer directly across the pipe. The AE transducers, because of their flat

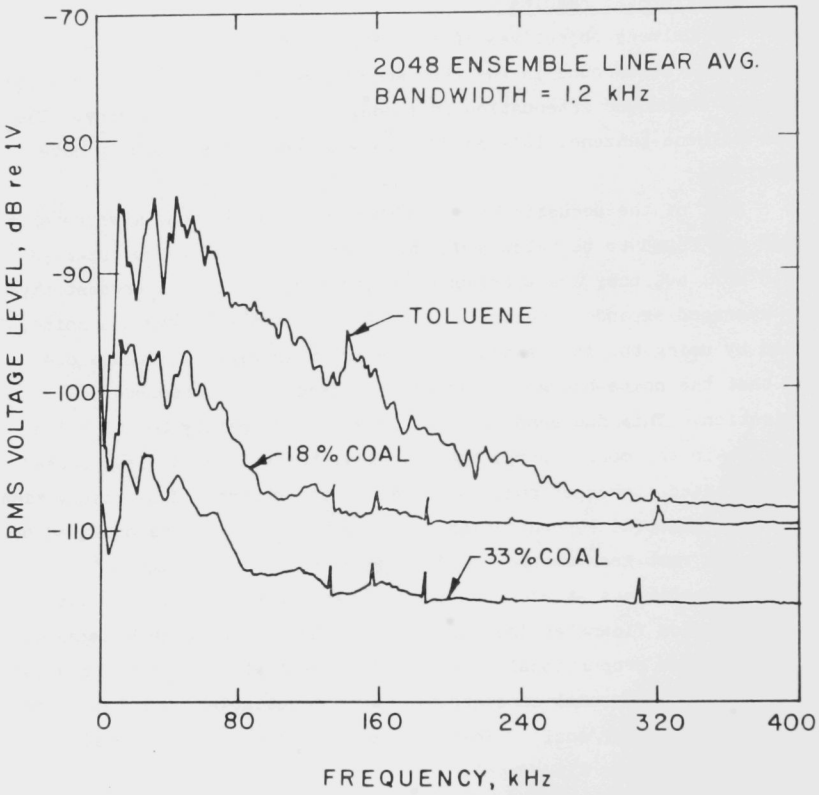

Fig. 5 Noise-Background Level Obtained with the Acoustic-Emission Transducers.

frequency response, were chosen for this study. A sine tone burst with a pulse width of 75 μs and a repetition rate of 0.2 ms was used to drive the transmitters. Since the AE transducer is not designed for pulsing, the output pressure was not constant over the frequency range. Therefore, a calibration curve of the driving voltage *versus* the received voltage with only toluene-benzene in the line was used to normalize the results.

To obtain the absolute sound attenuation in the coal slurry, the diffraction loss, the acoustic mismatch loss, the attenuation loss due to the teflon window, and the oil coupling must be calculated. Because of the complexity of the problem, only the relative attenuation loss is considered in the present analysis. The relative attenuation loss for a given coal concentration means that the output voltage at a coal concentration is conpared with that of pure toluene-benzene. This can be expressed by

$$\alpha(\text{dB/cm}) = [20 \log V_1 | V_o]/d \quad , \tag{7}$$

where

α = relative attenuation loss in dB/cm,
d = separation between two teflon windows (5.08 cm),
V_o = ratio of the received voltage and the driving voltage in toluene-benzene,
V_1 = ratio of the received voltage and driving voltage in coal-toluene-benzene slurry.

Results for sound attenuation in the 18%-and 33%-coal slurry concentration are shown in Fig. 6. It is noted that sound attenuation increases linearly at a rate of 0.7 dB/cm/100 kHz for the 18%-coal slurry, while for the 33%-coal slurry, the attenuation increases much faster and the transmitted signal is below the noise level beyond 250 kHz. The maximum input power used in the present measurement was around 10 W across 50 Ω.

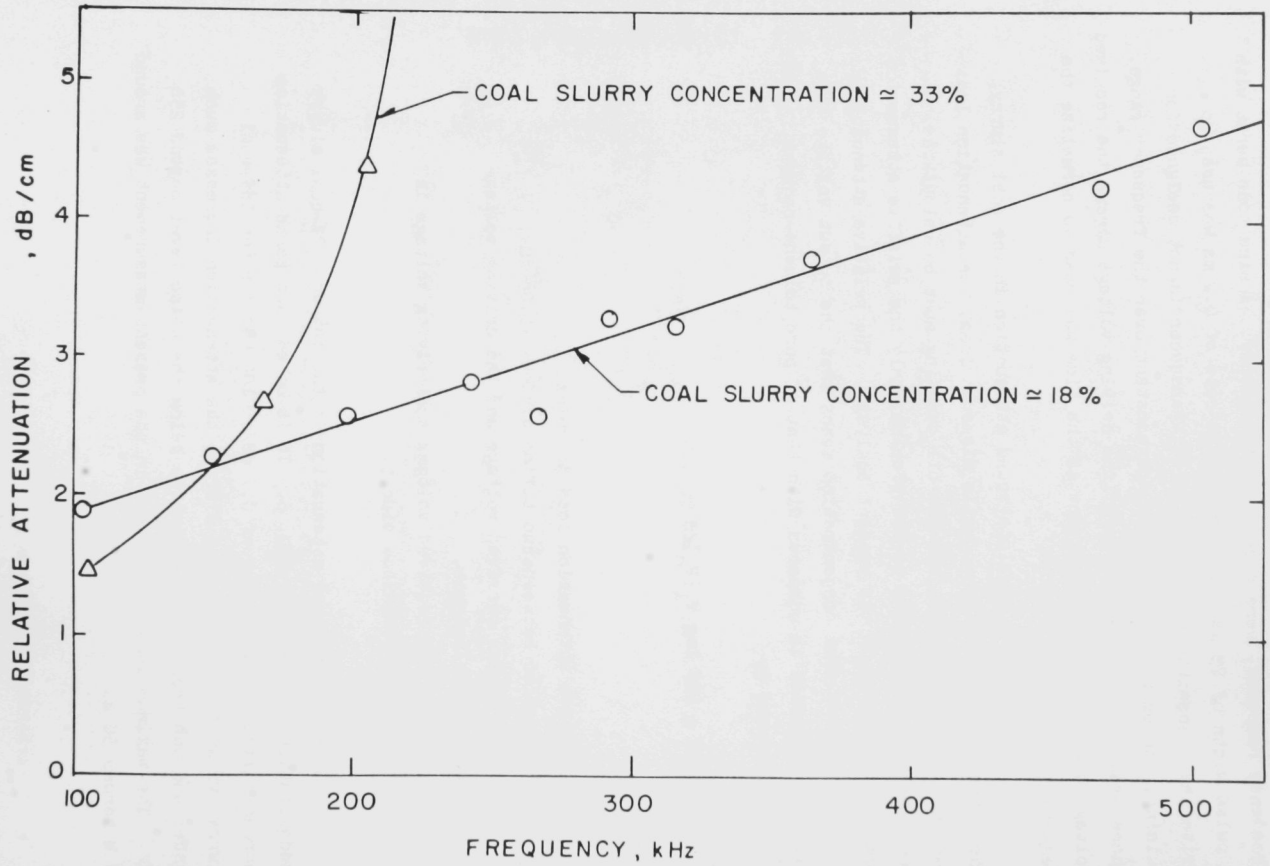

Fig. 6 Relative Attenuation Loss *vs.* Frequency for 18% and 33% Coal in Toluene-Benzene.

(c) Experimental Feasibility

In accordance with the sonar equation, Eq. (5), the condition for detection for a transmitted wave is

$$PSL = NL + MR \tag{8}$$

where PSL is given by Eq. (6), NL is the noise-background level and MR is the measurement requirement, which is set by the instrument developer and dictates the amount of signal above the noise background that a flowmeter must have for a satisfactory performance. In the theoretical feasibility study, two important parameters such as the noise background, NL, and the transmission losses, SL, were estimated based on very limited data found in the literature. In the HYGAS experiment, the values of these quantities were determined. Therefore, a better understanding of the feasibility and operation of acoustic flowmeters in coal conversion plants can now be established.

A least-squares linear fit was applied to the attenuation data of Fig. 6. The result was an empirical linear equation that represents the attenuation data. The equation for absolute attenuation in a slurry, α_A, is given in the form,

$$\alpha_A \text{ (dB/cm)} = B_1 + B_2 (f-100) + B_3 F^2 \tag{9}$$

where

F = the sound frequency in kHz
$B_1 = 1.86$, $B_2 = 0.0067$ for 18% concentration
$B_1 = 1.14$, $B_2 = 0.0287$ for 33% concentration
$B_3 = 1.04 \times 10^{-8}$, dB•s^2/cm.

The last term in Eq. (9) is the attenuation in a toluene-benzene mixture[9] with approximately 0.2 mole fraction of benzene. The overall transmission loss at r centimeters from the transmitter is given as

$$TL = \alpha_A r + DL + 20 \log r \quad , \tag{10}$$

where 20 log r is the beam spreading loss, and DL is the transducer diffraction loss which is neglected in the present work.

The noise level was analyzed with 50 kHz bandwidth and was found to have a frequency dependence of $F^{-2.8}$. Based on this dependence, the noise level (NL) can be represented by

$$NL \text{ (dB re } \mu Pa) = A - 56 \log F, \tag{11}$$

where

F = is the frequency in kHz

A = 170.9 and 163.9 for 18% and 33% concentrations respectively.

For comparison purposes, the values used in this study for SL and PG will be those used in the theoretical feasibility study.[4] That is, SL = 180 dB re μPa at 1 cm at 100 kHz, and PG = 5 dB. Substituting Eqs. (9 and 10), and the values for SL and PG in Eq. (6), the PSL is given by

$$PSL = 185 - 20 \log r - [B_1 + B_2 \times (F - 100) + B_3 F^2]r \tag{12}$$

The PSL and NL for the HYGAS test are plotted in Fig. 7 for the frequency range of 100 to 500 kHz. It is noted that the PSL is higher than the NL for the entire frequency range of interest. The results also indicate that the transmission loss is the primary factor that will limit the utility of any acoustic/ultrasonic device. The noise background is relatively small, especially in the higher frequency range.

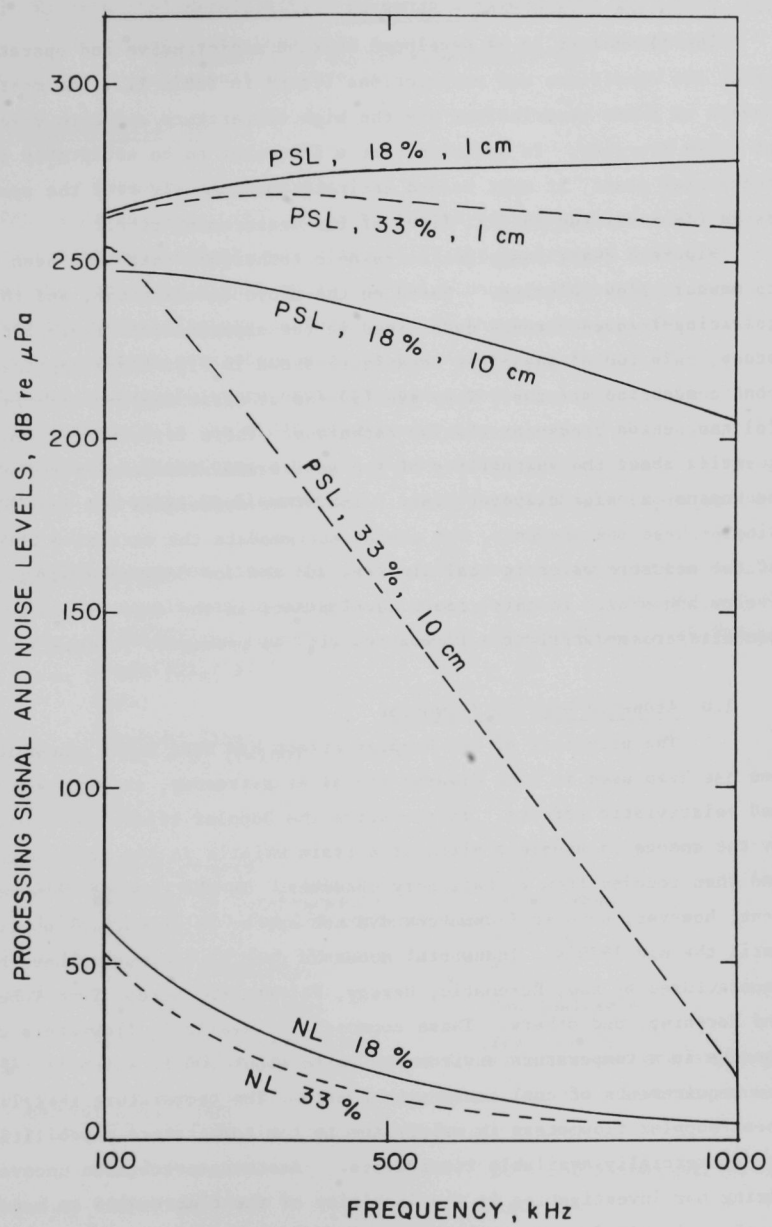

Fig. 7 Processed Signal Level (PSL) *vs.* Frequency.

III. FLOWMETER DEVELOPMENT - SLURRIES

The flowmeters to be developed must be nonintrusive and operate under the conditions and restrictions listed in Table II. The most severe of these restrictions are the high temperature and high viscosity of these slurries. In addition, for a flowmeter to be acceptable in an industrial plant, it must record entirely autonomously over the specified range (from startup to full flow) of the measurement site.

Figure 8 describes eight ultrasonic techniques that have been used to measure flow velocity. Based on the above restrictions, and the operating-frequency range determined in the experimental feasibility study, only two of the eight techniques shown in Fig. 8 are applicable to coal conversion streams. They are (a) the acoustic doppler technique and (b) the active cross-correlation technique. There is, however, some question about the suitability of the active acoustic cross-correlation technique on large diameter pipes. The other techniques are feasible for single-phase measurements, but cannot accommodate the excessive attenuation of the acoustic waves in coal slurries and the low frequency of operation (below 500 kHz). In this report developments in the doppler and active acoustic cross-correlation flowmeters will be presented in detail.

1.0 Acoustic Doppler Flowmeter

The principle of the Doppler effect has been known since 1842 and has been used in such diverse fields as astronomy, atomic spectra, and relativistic effects. In acoustics the Doppler effect is illustrated by the change in apparent pitch of a train whistle as the train approaches and then recedes from a stationary observer. In the case of flow measurement, however, doppler flowmeters did not appear in industrial applications until the mid 1970's. Industrial acoustic doppler flowmeters have been manufactured by EDO, Euromatic, Hersey, Polysonics, Sirco, Tech Tube, Leeds and Northrup, and others. These commercially available flowmeters can operate in a temperature environment up to about 300°F, which is far below the requirements of coal conversion plants. The temperature restriction of these doppler flowmeters is mainly due to the temperature capabilities of the commercially available transducers. Another restriction uncovered during our investigation is the inability of the electronics to handle doppler signals from the highly viscous media found in coal conversion streams.

Table II

REPRESENTATIVE SLURRY FLOW CONDITIONS

- CHARACTERIZATION

Transporting Vehicle:	Oil
% Solids:	5 - 45 wt %
Temperature:	350 - 750°F
Flow Rate:	0.5 - 4.5 ft/s
Viscosity:	400 CP
Pressure:	300 psi
Conductivity:	?
Sp. Gr.:	1.0 to 1.2
Compressability:	6% at 3000 psi
Particle Size:	95% through 100 Mesh

- RESTRICTIONS

Accuracy:	5% Acceptable - 2% Desired
Repeatability:	± 2%
Life:	1-Year Minimum
Response Time:	20 s

- MECHANICAL

Pipe Dimension:	2 inches
Material of Construction:	Carbon Steel
Configuration:	Vertical
Codes or Standards:	?
Obstruction of Flow:	Not Desirable
Pressure Drop Permitted:	Yes -500 lb

- AMBIENT CONDITIONS

Temperature:	20 - 130°F (Depends on location)
Vibration:	Some
Explosive:	Yes
Provisions for Servicing:	Should be Available

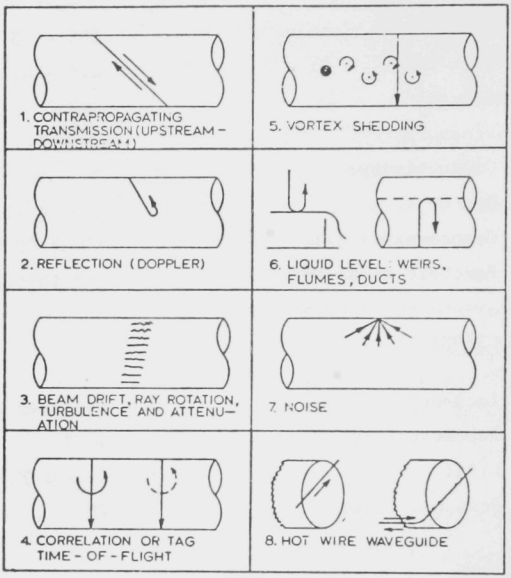

Fig. 8 Summary of Eight Categories of Ultrasonic Flow Measurement Principles and Methods.

Doppler flowmeters usually are based on the principle that the frequency of ultrasonic waves reflected from scatterers within the moving medium is shifted in proportion to the velocity of the scatterers. It is usually presumed and sometimes verified, that the scatterers travel at the local fluid velocity, but this condition is not always satisfied. In a physical situation, as shown in Fig. 9, if a sound signal is transmitted at a frequency, f_o, an angle, θ_t, with the direction of motion, and a scatterer is traveling with velocity, u, in a fluid with sound velocity, c, and scattering the soundwave in direction, θ_r, then the change in frequency, f_d, is given by

$$f_d = f_o(u/c)(\cos \theta_t + \cos \theta_r) \quad . \tag{13}$$

Typically the incident and scattered directions are fixed by the configuration of the source transducers, hence

$$\theta_t = \theta_r = \theta \quad . \tag{14}$$

In addition, if the sound energy is injected into the pipe via a wedge, as shown in Fig. 10, then Snell's law requires that

$$\frac{\cos \theta}{c} = \frac{\cos \beta}{c_w} \quad , \tag{15}$$

where the wedge angle, β, and the velocity of sound in the wedge, c_w, are constants characteristic of the apparatus. Substituting Eqs. (14 and 15) in Eq. (13) and solving for the flow velocity the result is

$$u = (c_w/2\, f_o \cos \beta)\, f_d \quad . \tag{16}$$

The volume flow rate, V, is the product of the pipe cross-sectional area $(\pi/4)d^2$ and the average flow velocity. If a profile correction factor, K, is used to account for the non-uniform weighting of various pipe regions and non-uniform scattering, then

$$V = K\, (\pi/4)d^2(cw/2\, f_o \cos \beta)\, f_d \quad . \tag{17}$$

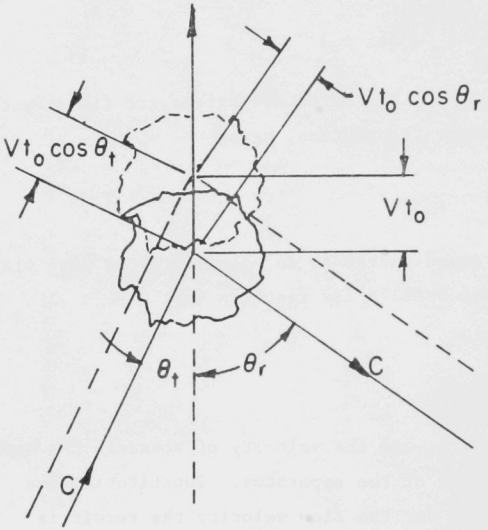

Fig. 9 Scattering of Sound from a Moving Particle.

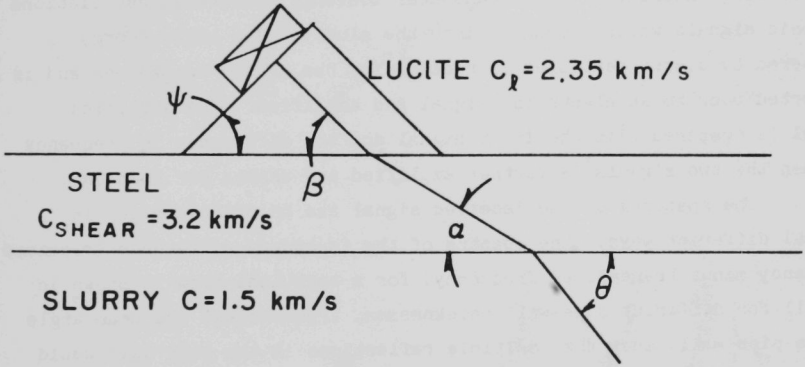

Fig. 10 Refraction at the Outer and Liner Surface of a Pipe Obeys Shell's Law.

$$\cos \beta / c_\ell = \cos \alpha / c_s = \cos \theta / c$$

The profile correction factor, K, should be close to unity and will be determined empirically for a wide range of conditions. In this study the effects of multiple scattering, flow fluctuations, and finite beam width of the transducers were not considered.

In the development of the acoustic doppler flowmeter at ANL, we first developed a low-temperature unit that could be tested in a small circulation loop at the laboratory and then, based on the experience of this device, a high-temperature version was developed and is currently being tested at the SRC-II pilot plant.[16]

(a) Low-Temperature Acoustic Doppler Flowmeter

The acoustic doppler flowmeter consists of two electro-acoustic transducers, an electronic signal conditioning package, and a readout or recording instrument. One transducer converts electrical oscillations to sonic signals which propagate into the slurry. The sonic energy scattered by slurry particles is received by the second transducer and is converted back to an electrical signal and amplified. The amplified signal is compared with the input signal and the difference in frequency between the two signals is further amplified and shaped for counting.

The spectrum of the received signal can be characterized in several different ways. The spectra of the frequency difference (received frequency minus transmitted frequency) for a turbulent flow is shown in Fig. 11 for different pipe-wall thicknesses, frequencies, and beam angle in the pipe wall, such that multiple reflections in the pipe wall would emerge in phase in the fluid. The condition is

$$ZW \sin \alpha = n\lambda \qquad (18)$$

where W is the wall thickness, α is the angle between the propagation direction and the pipe axis, n is an integer, and λ is the acoustic wavelength in the pipe wall. Reinforcement occurs in the 4-mm pipe wall for a coupling wedge angle of 24° and f = 500 kHz, while in the 9.5-mm pipe wall and a wedge angle of 34°, f = 240 kHz (n = 1) or

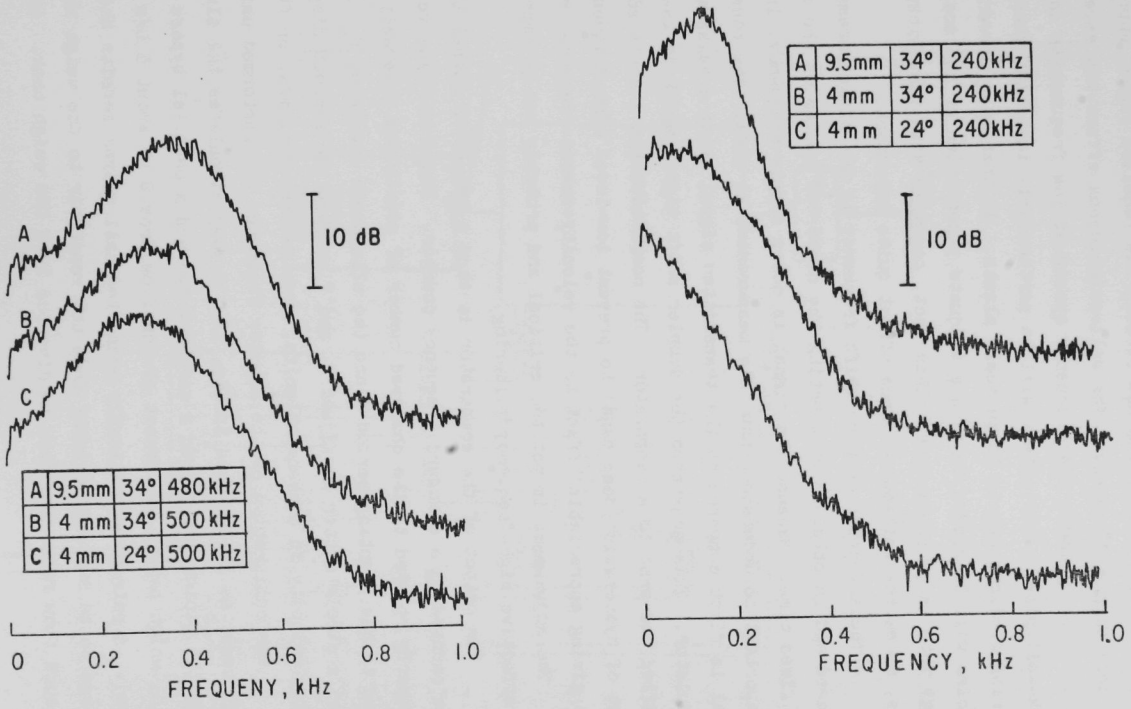

Fig. 11 Spectra of Doppler Signals for Varying Pipe-Wall Thickness, Frequency and Beam Angle in Pipe.

480 kHz (n = 2). A detailed study of this effect measured the ratio of the center frequency to the frequency spread of the received signal. Such a measurement indicates how closely the received signal approaches the ideal single frequency. The wall-coincidence effect was especially effective in narrowing the frequency spread at low frequencies in the thick-wall pipe. This effect will be particularly important when considering applications to large-scale plants. In that case, lower frequencies will be needed to assure adequate penetration of the acoustic energy into large pipes used. This fact, combined with the thicker pipe walls, makes the wall-coincidence effect quite important.

The effective doppler shift frequency is the basic parameter measured and is obtained by counting the number of cycles of the signal in a fixed time. Because the signal is not a single frequency, it is important to understand how this measurement is made. The received signal is first compared to the transmitted signal using a balanced demodulator. This generates the doppler shift signal which is then amplified and sent to a comparator. The comparator has a small adjustable amount of hysteresis (dead band) to prevent low-level high-frequency noise giving appreciable offset to the velocity-*versus*-frequency relationship. The adjustment is not too critical and probably can be improved by more effective high-frequency filtering.

The output of the comparator is then a two-level signal that can be counted in a standard frequency counter. Since the flow velocity is linearly related to the observed number of counts and inversely related to the counting period T and the ultrasonic frequency f_o, it becomes a simple matter to adjust f_o and T so that the readout displays the flow velocity in convenient units, such as L/s, gpm, m/s, or ft/s.

The calibration of the doppler flowmeter was performed using a weigh tank, as illustrated in Fig. 12. A pump circulates the slurry through the piping system *via* a series valve and a parallel bypass circuit, which permit adjustment of the flow from 0 to about 5 L/s (80 gpm). A pair of mechanically connected ball valves permits the flow discharge to be switched quickly from the reservoir to the weigh tank. To measure flow rate, the flow is diverted into the weigh tank. As the

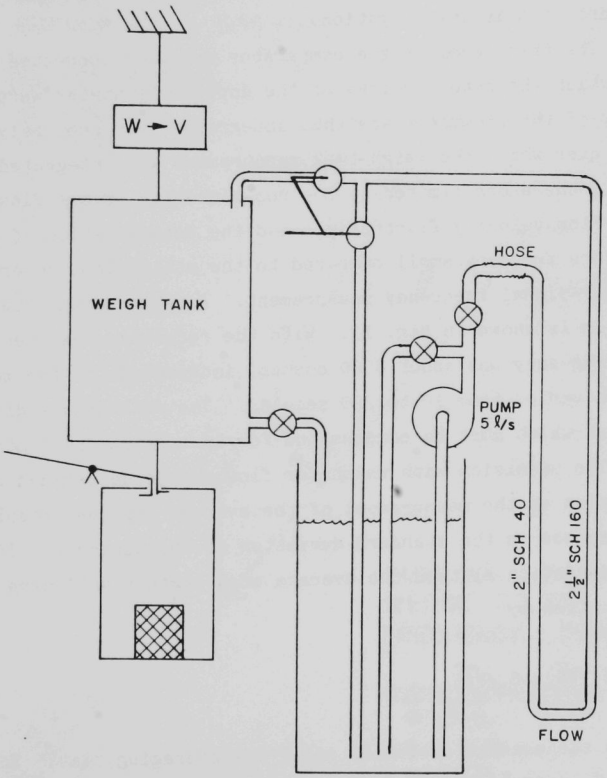

Fig. 12 Weigh-Tank Calibration Apparatus.

voltage output of the force gauge increases, a clock is started at a preset trip level. While the fluid accumulates in the tank, the reference mass is removed from the tank. When the weight of the fluid which has accumulated in the tank is exactly equal to the reference mass removed, the same trip level is reached again and the clock is stopped. Mass flow rate is then the quotient of the reference mass divided by the time interval between trip levels. This technique serves to cancel trip errors, non-linearities, etc., and has potential precision beyond the requirement of this investigation.

The trip level of the comparator was also connected to a gate through which the output pulses of the doppler flowmeter were passed. The frequency of the flowmeter was thus integrated over precisely the same time interval over which the weigh-tank measurement was integrated. Systematic errors are therefore limited to the non-linearity of the flowmeter over the range of flow velocity fluctuations and the determination of mass and time. These errors are very small compared to the statistical uncertainties of the doppler signal frequency measurement. A calibration obtained by using this system is shown in Fig. 13. With the reference mass set at 70 kg, the doppler frequency was about 3000 counts, independent of the measurement time which varied from 10 to 200 seconds. The data show a discernible zero offset which must be compensated for in a measuring instrument.

The precision with which the flow can be determined depends on the precision of the measurement of the average doppler frequency. This in turn depends on the standard deviation of the period τ. If τ has a standard deviation S, then the average of N periods will have a standard deviation given by

$$S = S_1/\sqrt{N} = S_1/\sqrt{fT} \qquad (19)$$

where f is the average frequency and T the averaging time. The standard deviation S, depends on the spectral distribution of the received signal, with $S_1 = 0$ for a pure tone. Preliminary measurements of the doppler signal for coal slurries indicate $S_1 \sim 0.31$. For a mean frequency of 1 kHz and standard deviation of 10%, this means the required integration time is 0.01S. To decrease the standard deviation to 1%, integration must be extended to one second.

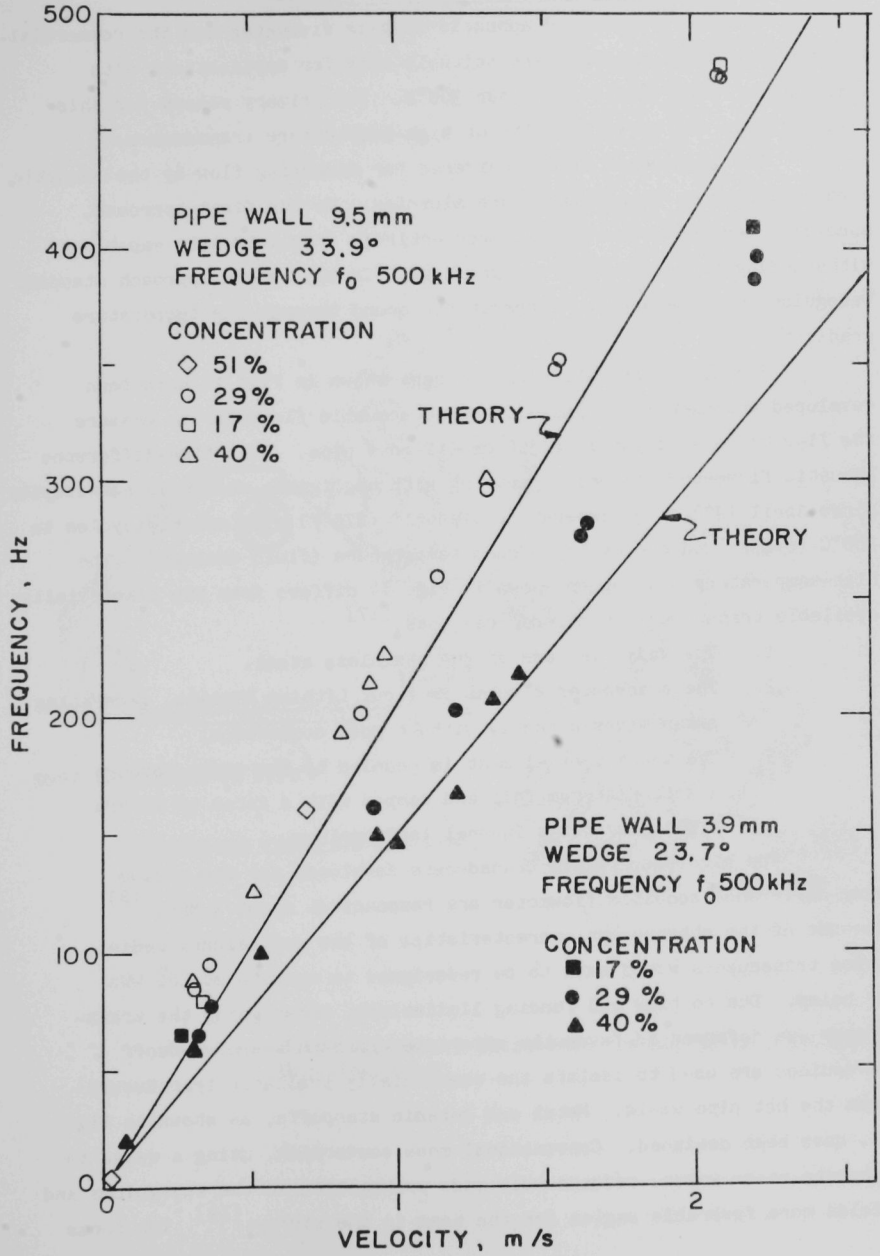

Fig. 13 Calibration of Doppler Flowmeter.

(b) High Temperature Acoustic Doppler Flowmeter

The above described acoustic doppler flowmeter and the commercially available doppler meters are suitable only for applications with temperature requirements less than 300°F. The primary reason for this limitation is the unavailability of high-temperature transducers.

Two approaches were considered for measuring flow by the acoustic doppler method in high-temperature slurries. In the first approach, specially designed transducers, made entirely from materials capable of withstanding high temperatures, are used. In the second approach standoff waveguides will be used to transmit the sound through the temperature gradient.

The high temperature transducers shown in Fig. 14 have been developed and used in a time-difference acoustic flowmeter to measure the flow of pure sodium in a 300-mm (12-in.) pipe. This time-difference acoustic flowmeter has been operating with negligible change in sensitivity since April 1978 at a temperature of 465°C (870°F) with monthly cycles to 300°C (570°F) and one cycle to room temperature (fluid drained). The high-temperature transducer shown in Fig. 14 differs from the commercially available transducers in several respects.[17]

1. The wedge is made of 304 stainless steel.
2. The transducer element is X-cut Lithium Niobate, generating shear waves directly without mode conversion.
3. The transducer element is coupled to the wedge through a soft platinum foil and damped with a force of 10 MPa (1500 psi) using Inconel leaf springs.

The high-temperature transducers devoloped for the sodium time-difference acoustic flowmeter are resonant at about 3 MHz.[18] Because of the attenuation characteristics of the coal-slurry media, these transducers would have to be redesigned to operate at 500 kHz or below. Due to time and funding limitations, redesigning the transducers was deferred in favor the alternate approach where standoff waveguides are used to isolate the commercially available transducers from the hot pipe walls. Metal and ceramic standoffs, as shown in Fig. 15, have been designed. Conventional mode conversion, using a wedge to generate shear waves, reduces multimode propagation in the waveguides and yields more favorable angles for the beam in the slurry.[19] Two forms

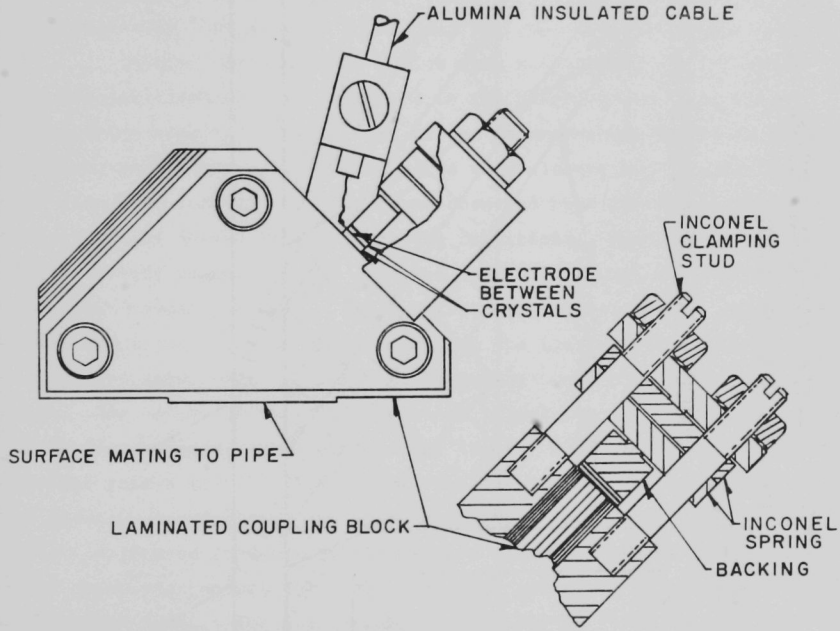

Fig. 14 High-Temperature Ultrasonic Transducer on a Laminated Coupling Block.

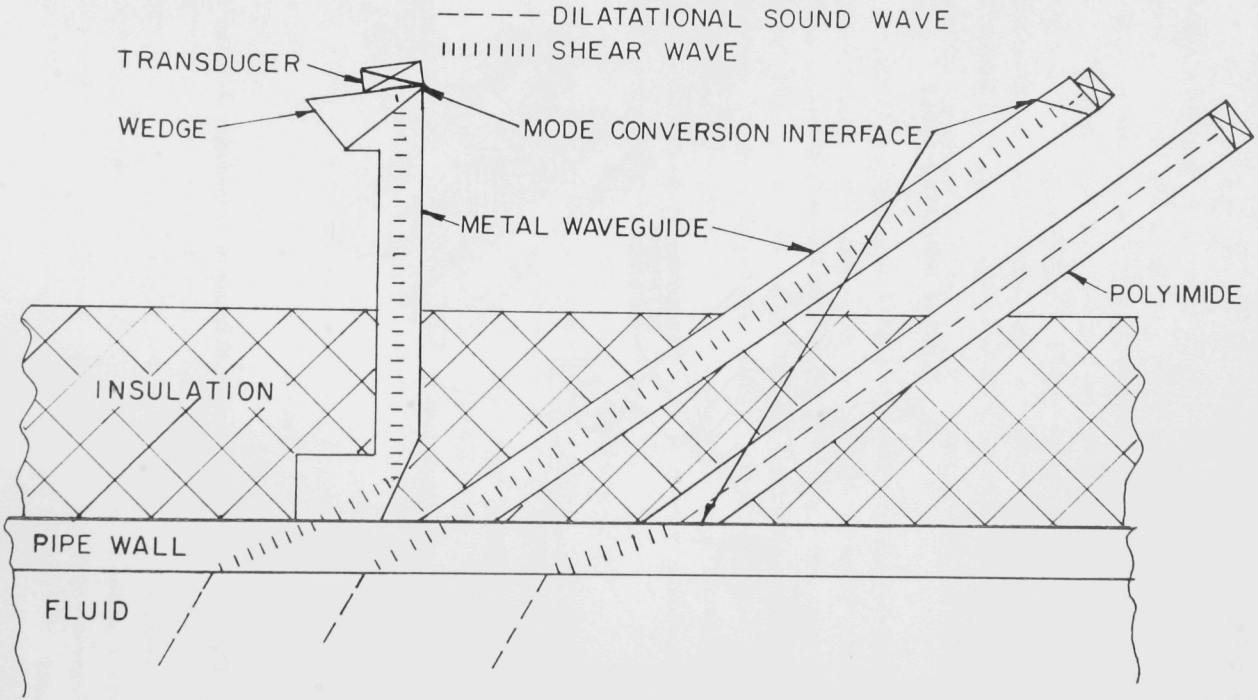

Fig. 15 Three Forms of Thermally Isolating Waveguides.

of waveguides are shown. The one to the right is made from polyamide (Vespel) and can be used at moderate temperatures (250°C, 500°F). The other two are made from metal (usually the same material as the pipe) and can be used for high temperatures. The one in the middle conducts the sound wave in the desired direction into the pipe. The waveguide to the left uses the reflection property from a free surface to permit a shorter path. A pair of these guides has been installed at the inlet to the preheater slurry line of the SRC-II pilot plant in Fort Lewis, WA, and is shown in Fig. 16. Figure 17 shows the transducers attached at the end of the waveguides. The electronics used to process the doppler signal were initially identical to those used for the low-temperature version.

Initial tests of this device were successful, and the output of the doppler flowmeter was connected to the SRC-II pilot-plant data-acquisition computer. The output of the flowmeter was monitored over a six-hour period and was found to agree very closely to the material balance for that time period. Later, it was observed that the flowmeter readings were drifting during stable operating conditions. Upon checking the doppler-shift signal, it was observed that this signal was contaminated by a low-frequency signal. The low-frequency signal caused the doppler frequency signal to rise above and below the reference line of the zero crossing counter used to count the frequency content of the doppler waveform. The nature of this low-frequency signal was not easy to determine. It is now, however, attributed to the laminar flow conditions in the line. Another reason for the drifting of the flowmeter is the small quantities of hydrogen leaking from the snubber installed behind the charge pump, which is located in front of the doppler flowmeter. Hydrogen in the line will greatly attenuate the received signal and place it below the noise background level. The conditions found at SRC-II (Table II) of flow velocity, and high viscosity clearly indicate that the flow is laminar. The flowmter initially tested at SRC-II was developed based on experiments in a laboratory loop, where the flow is turbulent. In Fig. 18, where the velocity of particles normalized to mean velocity is plotted *versus* the number of particles. It can be seen that for the case of turbulent flow, the particles are concentrated at the mean of the velocity range, while for laminar flow particles are uniformly distributed over a range that is twice that of the mean. This observation agrees with the results observed by taking the spectra of the doppler signal under turbulent conditions in the laboratory and under laminar conditions at the SRC-II pilot plant.

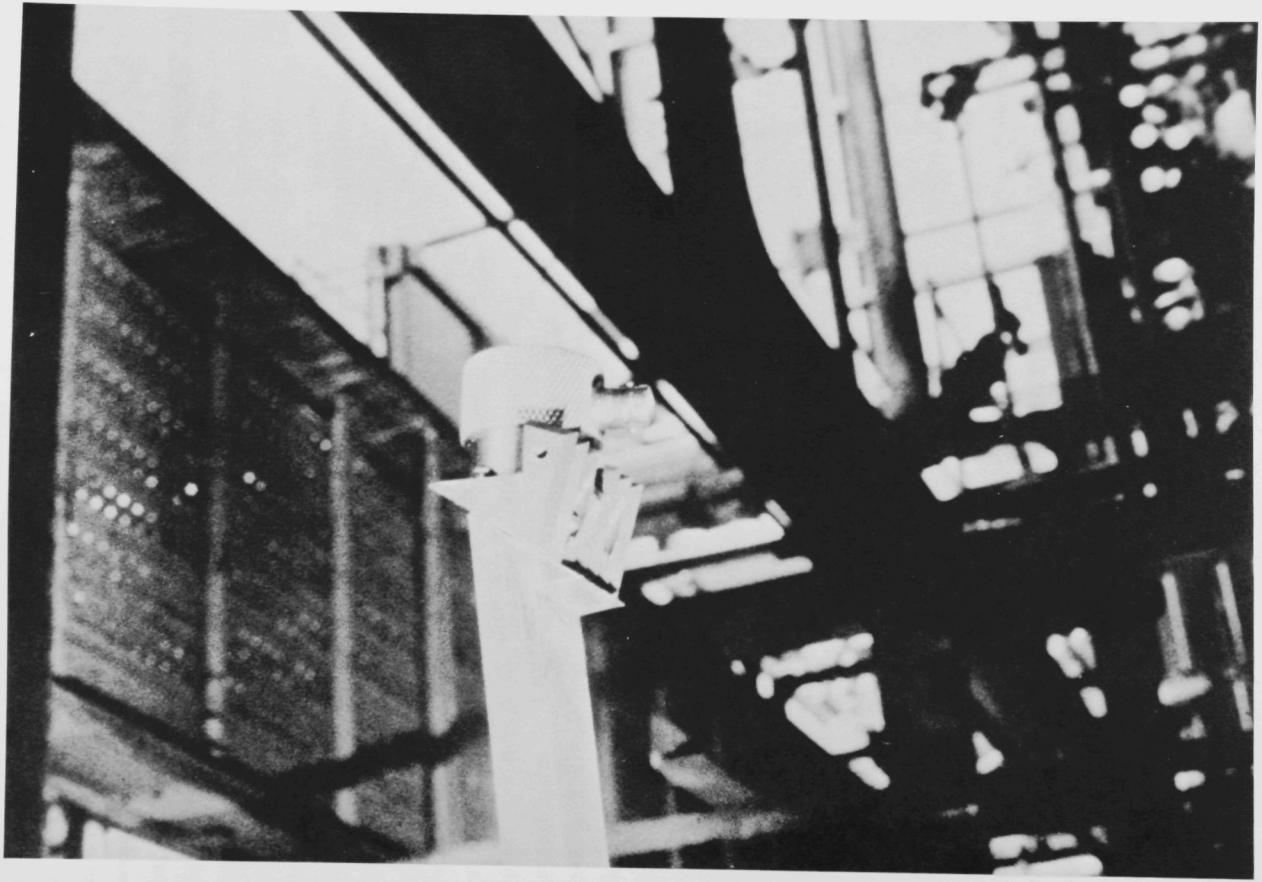

Fig. 16. Installation in Recycle-Slurry Line of SRC-II Pilot Plant, Fort Lewis, WA.

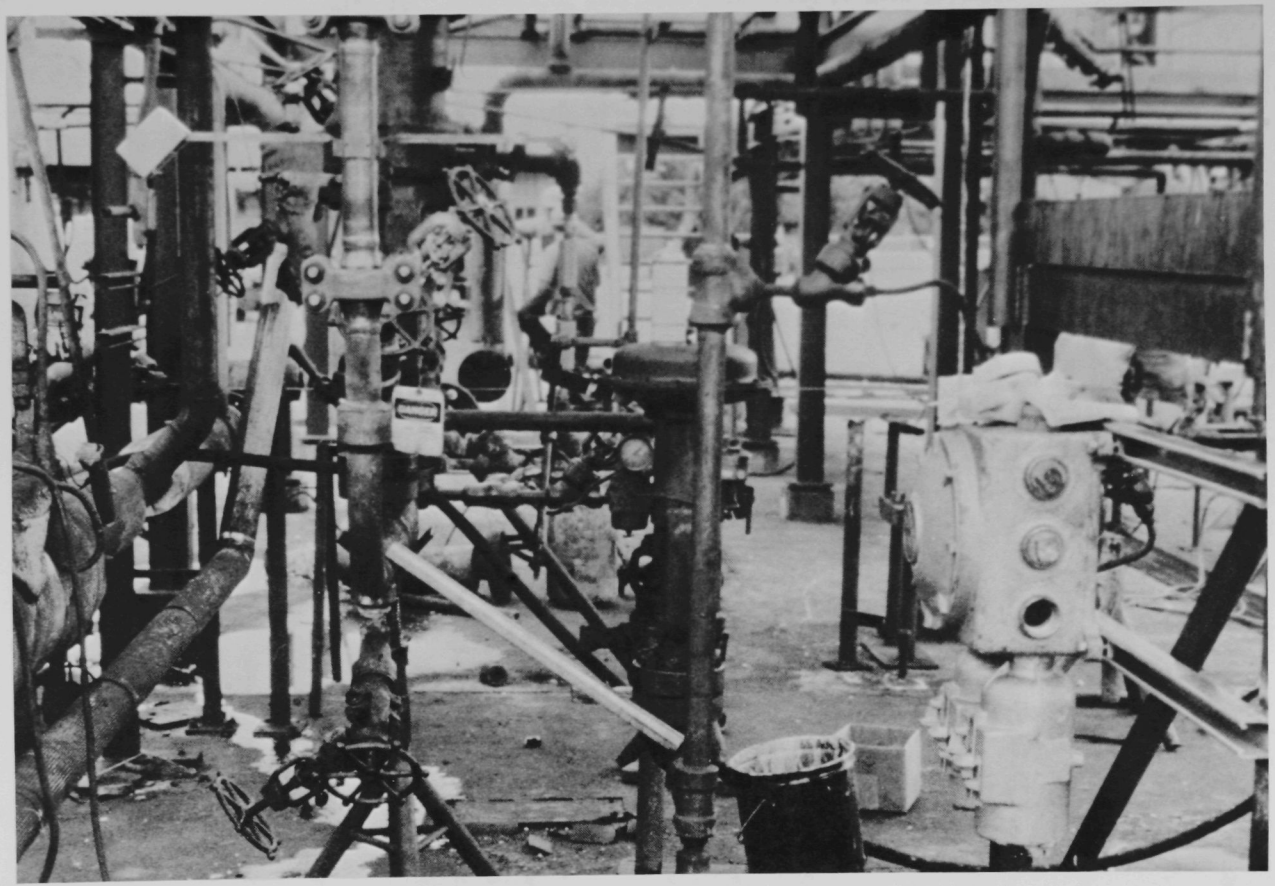

Fig. 17. Installation of Transducers at the End of the Waveguides.

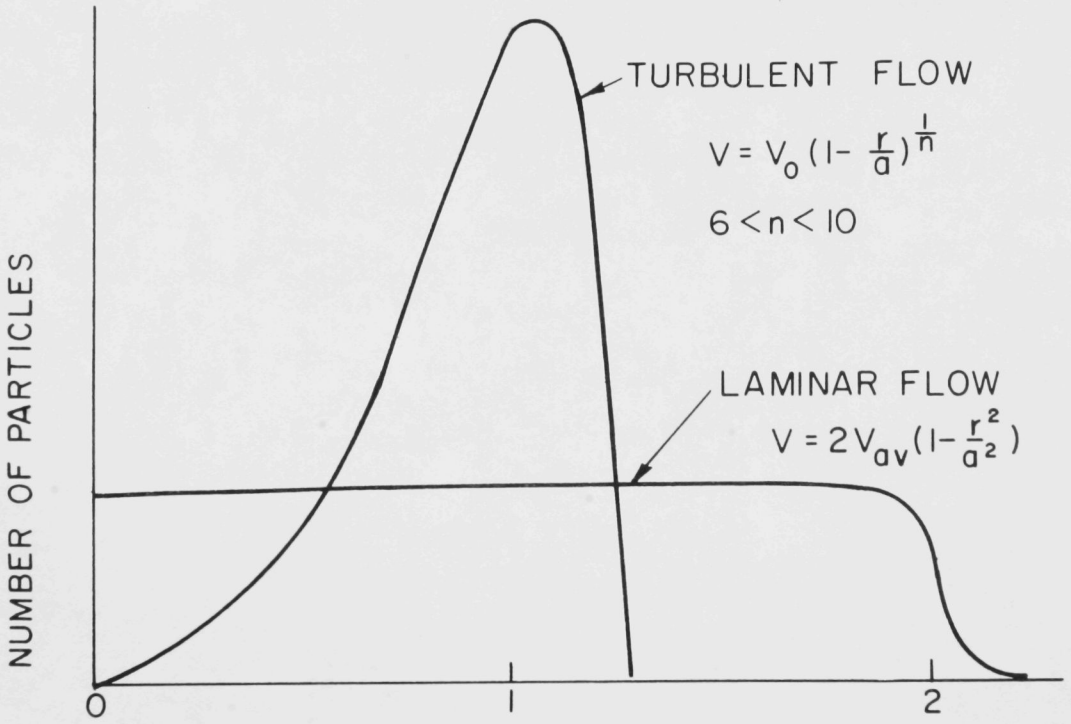

Fig. 18 Velocity of Particles Normalized to Mean Velocity, *vs.* Number of Particles.

These spectra are shown in Figs. 11 and 19. For the turbulent case (Fig. 11) the frequency content of the waveform is concentrated about the doppler frequency; for the laminar case (Fig. 19), the frequency is distributed over the frequency range.

In Fig. 19 it can be seen that the corner frequency of each spectrum corresponds to the doppler frequency and consequently to medium flow velocity. An electronic circuit to calculate this frequency was built and tested at SRC-II pilot plant. This test successfully demonstrated the use of the acoustic doppler flowmeter to measure flow velocity in hot slurries. Results of this performance test will be published in the near future.

2.0 Active Acoustic Cross-Correlation Flowmeter

A special test was provided by the HYGAS pilot plant, where the flow velocity and concentration of coal in the slurry line were varied. Three coal concentrations (5, 15 and 20 wt %) and two flow rates for the 5- and 15-wt % concentrations were achieved in the test. The coal-slurry flow cycle was established from the coal-mixing tank through a low-pressure pump, to the acoustic test section, through a throttle valve, and back into the mixing tank. To vary the coal concentration, we added a precalculated amount of coal into the mixing tank and allowed about one-half hour mixing time to establish the expected concentration. The flow rate was varied by adjusting the opening of the dowstream throttle valve. Problems in reducing the flow rate arose from coal particles settling in the slurry. The settling was clearly detected by a capacitive instrument in the line. When settling of coal was detected during the test, the throttle valve was immediately opened to establish full flow conditions in order to avoid any plugging in the slurry line. Only one reduced flow rate was established for each of the 5% and 15% coal concentrations.

The test section, the data-acquisition instrumentation, and data-analysis instrumentation are as shown in Figs. 1, 2 and 3, respectively. Acoustic data from each test run include measurements of acoustic background noise, sound transmission using sine-tone bursts between 100 and 500 kHz, and active cross-correlation using cw waves at 100, 200, and 300 kHz.

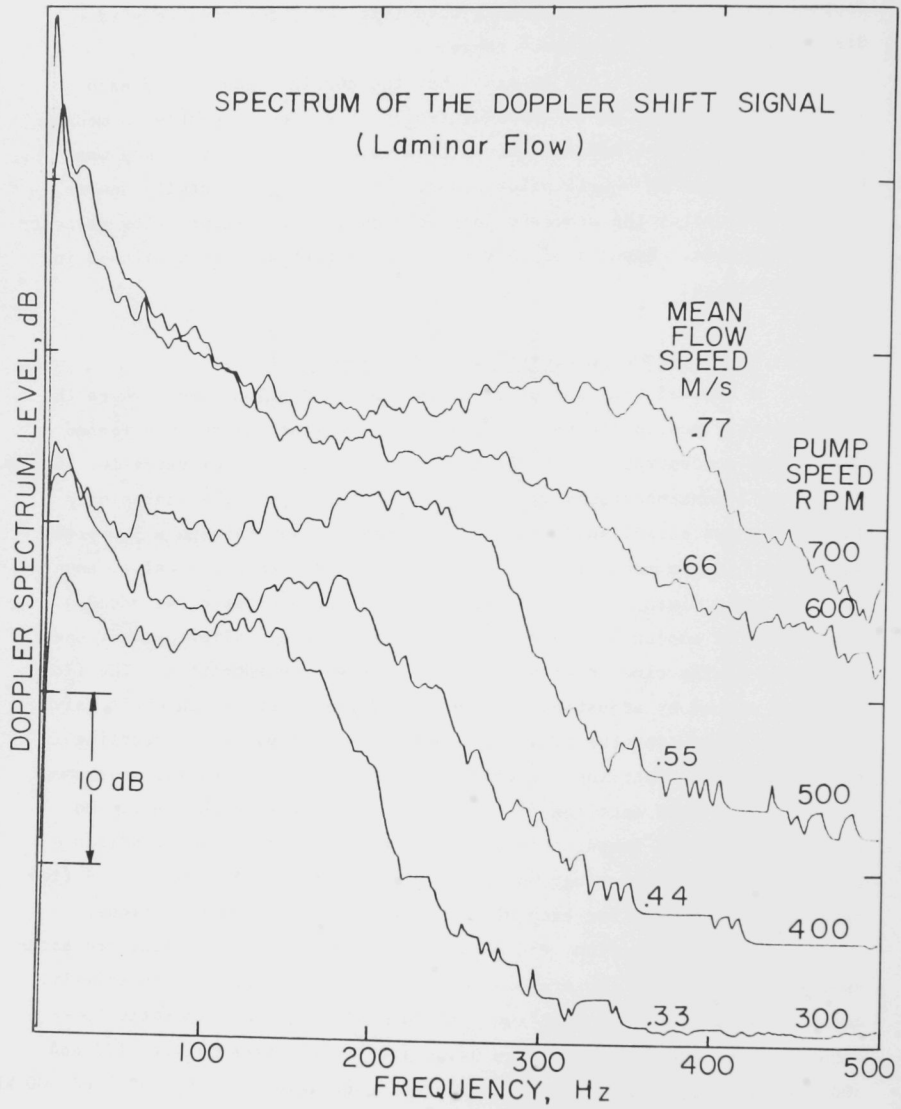

Fig. 19 Doppler Frequency Spectra for Laminar Flow at Various Flow Rates at SRC-II.

All data were recorded at a speed of 60 inches per second (ips). Each active cross-correlation measurement contains 40 seconds of data. In the active acoustic cross-correlation, transducers TD1 and TD4 in Fig. 3 constitute the first station, while transducers TD2 and TD5 constitute the second station. A flow disturbance at the first station modulates the waveform transmitted by TD1, and if the same flow disturbance persists until the second station it will also modulate the waveform transmitted by TD2. The modulated waveforms are then received by transducers TD4 and TD5. The flow-modulated signals are demodulated by amplitude demodulators and then cross-correlated to yield flow velocity.

(a) Results of the Experiment

Acoustic noise background was analyzed for its frequency contents up to 120 kHz. Figures 20 to 22 show the frequency spectra for the toluene-benzene mixture (containing about 1 wt % coal), and for 5 and 15 wt % coal in toluene-benzene, respectively. The two spectra shown in each figure correspond to different flow velocities. In general, the spectra show a rather constant noise-background level beyond 60 kHz. Peaks appearing between 10 and 40 kHz are attributed to the resonance effect of the transducer. It is observed that, especially in the range from pure fluid to 5 wt % coal, the magnitude of the noise background decreases as the coal concentration is increased. This observation implies that the coal concentration in the slurry line may be obtained by measuring the root-mean-square (rms) value of the noise background. However, only a slight change in magnitude of the noise signal from 5 to 15 wt % in concentration is observable. Furthermore, by comparing the noise levels for different flow rates, it is found that as the flow rate is reduced, the noise level is also reduced. Again this observation is more distinct at low concentrations of coal. Based on these results, the following conclusions are drawn: (1) although the noise level is somewhat proportional to the coal concentration, using the noise level to indicate the coal concentration is not reliable, especially for high concentrations of coal; and (2) the noise level in low concentrations of coal may be used to estimate the mass flow rate, provided that the coal concentration is already known.

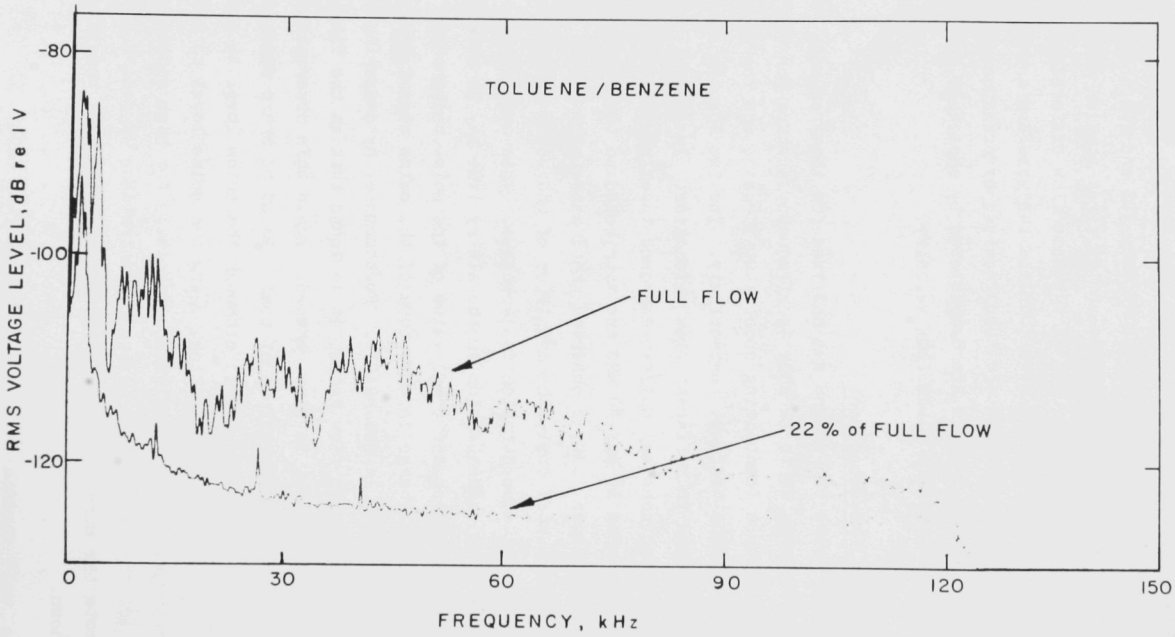

Fig. 20 Sound Frequency *vs.* RMS Voltage Level for the Background Noise in Toluene-Benzene Flow.

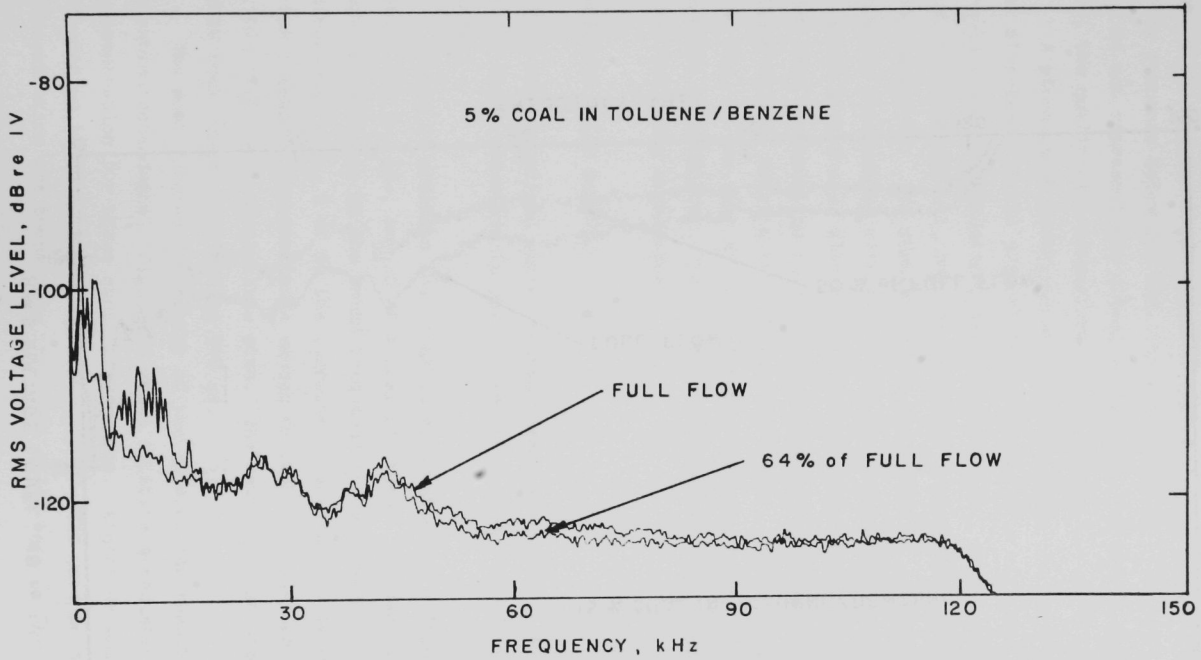

Fig. 21 Sound Frequency of the Background Noise *vs.* RMS Voltage Level in 5-wt % Coal Slurry.

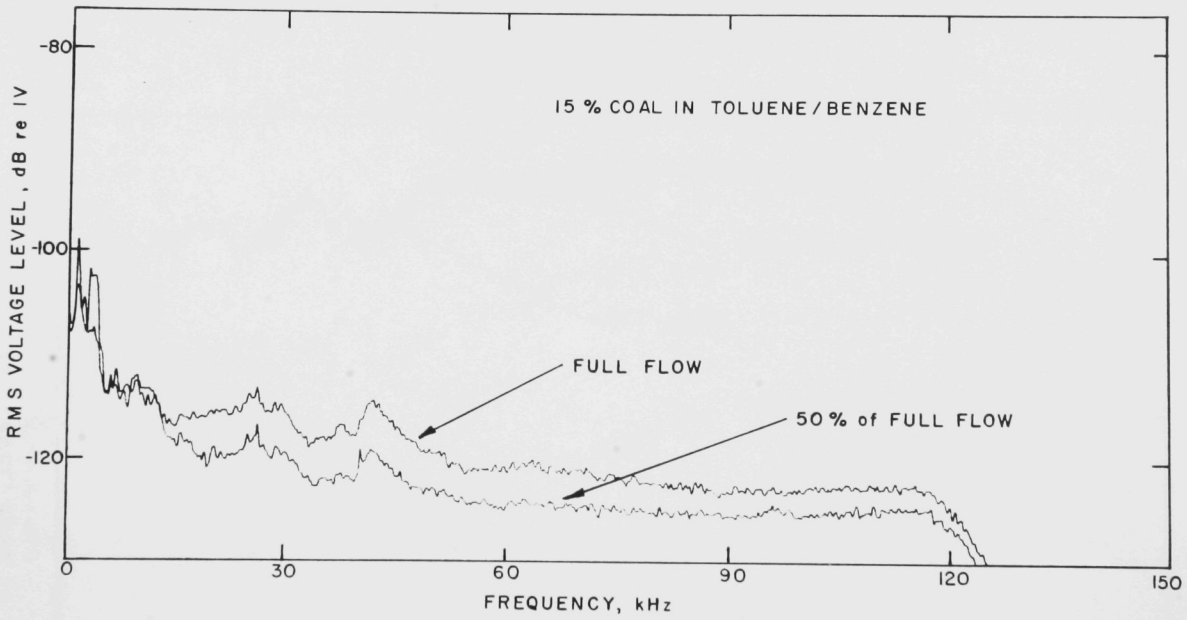

Fig. 22 Sound Frequency for the Background Noise *vs.* RMS Voltage Level in 15-wt % Coal Slurry.

Since the transducers (AE FAC 500) used in the noise measurement are not calibrated for their output levels as transmitters or for their frequency response below 100 kHz, the noise spectra discussed in this section do not represent the actual noise levels in the coal-slurry line. However, the qualitative comparison of the spectra is still valid.

A pitch-catch technique was used to obtain the sound attenuation in coal slurries. In the present experimental setup, in order to obtain the absolute sound attenuation, transmission losses due to the acoustic windows, the coupling oil, and the geometric arrangement of the transducers must be considered. The problem can be simplified by considering only the relative attenuation with respect to the attenuation in the transporting fluid (about 1 wt % coal slurry). Figure 23 shows the output voltages received when transmitting pulses through the transporting fluid are normalized to unit driving voltage for the pulses. The voltage from the curve in Fig. 23 was used as the reference voltage, V_o, to calculate the relative attenuation. The relative attenuation α is calculated by using the following expression,

$$\alpha(\text{dB/cm}) = [20 \log (V/V_o)]/d \quad , \tag{20}$$

where V is the normalized output voltage received in the coal slurry from which the attenuation is being calculated, and d is the transducer separation.

Figure 24 presents the relative attenuation as a function of frequency, for 5-, 15-, and 20 wt % coal slurries. In general, the attenuation increases as the sound frequency is increased. At low concentrations, e.g., 5 wt %, the increase in attenuation is not obvious until the frequency becomes large enough so that the sound-wavelength is compatible with the coal-particle size. The particle-size distribution for HYGAS coal ranges from 200 to 900 μm.

The most interesting aspect of the attenuation results is the concentration dependence. Figure 25 shows relative attenuation *verses* coal concentration for three sound frequencies. Linear dependence can be approximated up to 35 wt % coal concentration. [The data points at 33 wt % coal concentration are those from the first HYGAS test.] The dependence

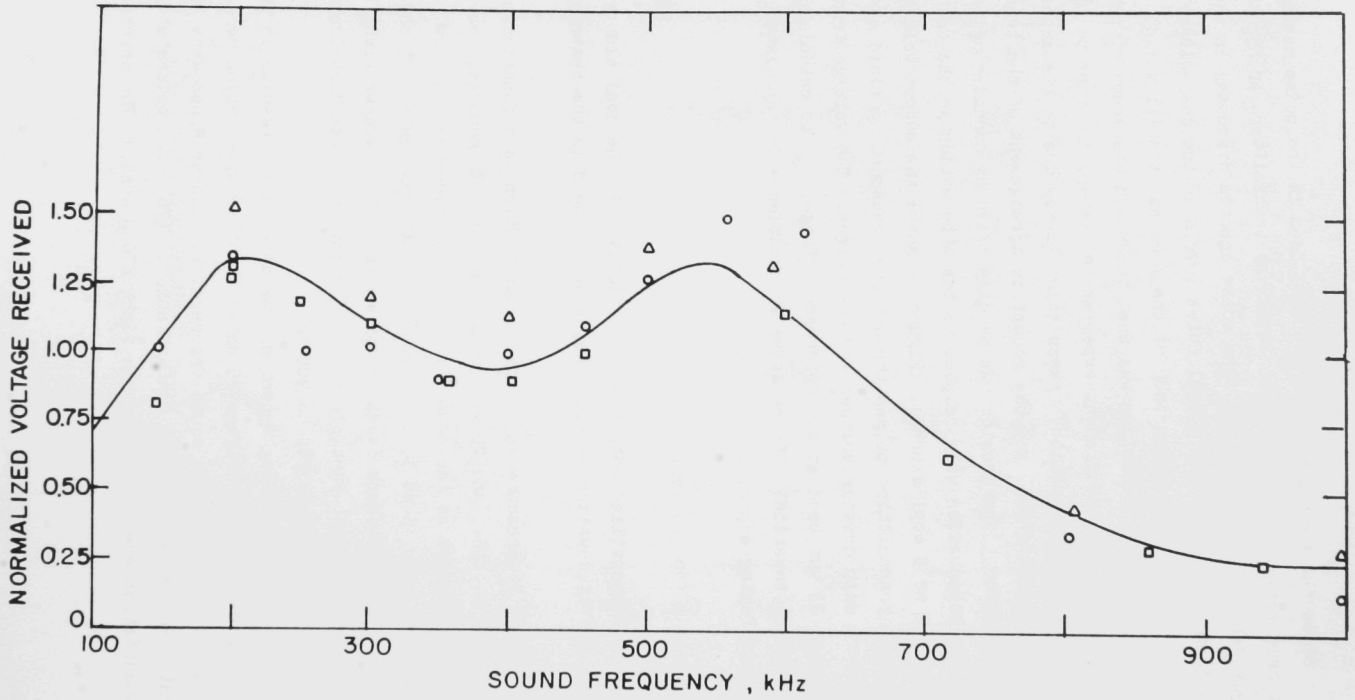

Fig. 23 Normalized Output Voltage *vs.* Sound Frequency in Toluene-Benzene Flow.

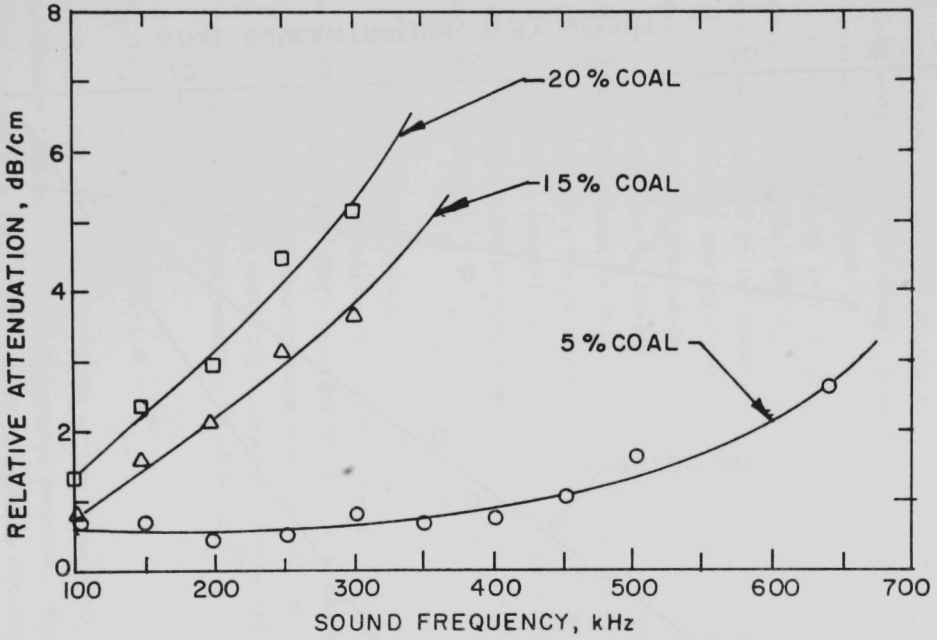

Fig. 24 Relative Sound Attenuation *vs.* Sound Frequency in Toluene-Benzene Flow.

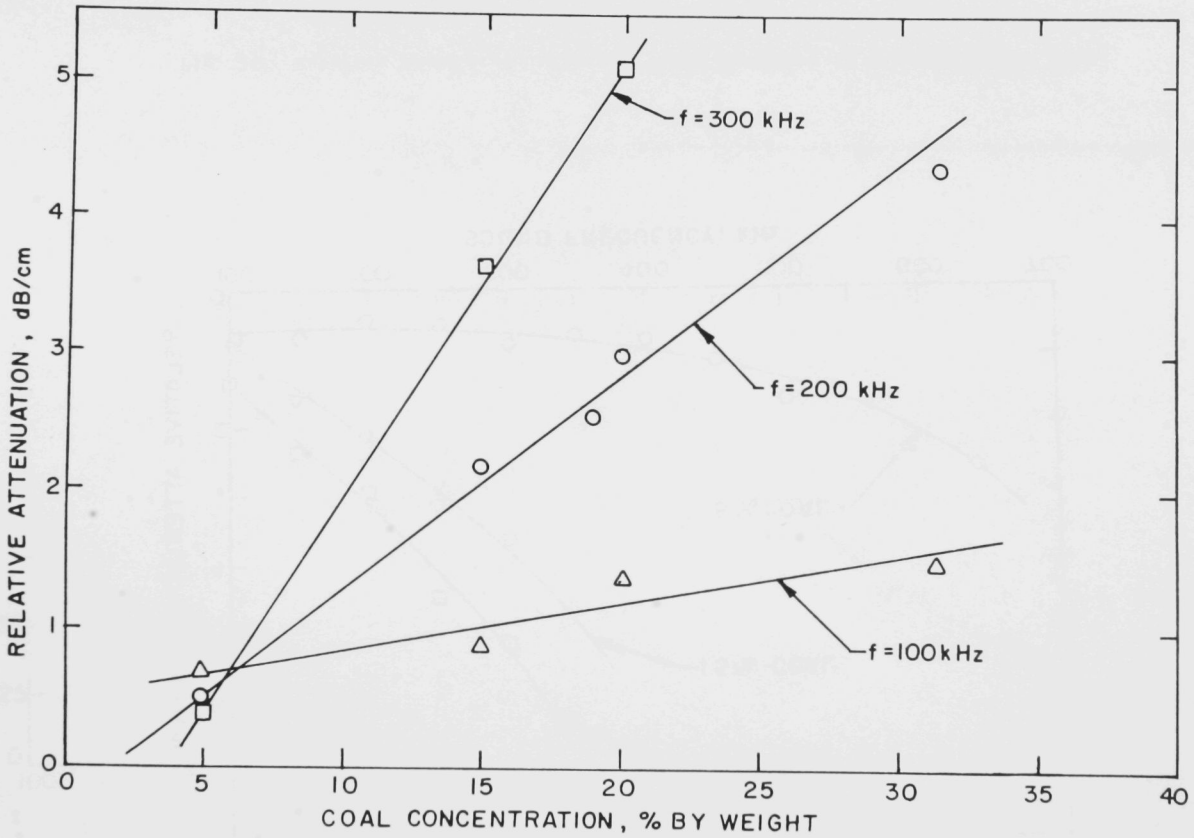

Fig. 25 Relative Sound Attenuation *vs.* Coal Concentration for Three Sound Frequencies.

of attenuation on coal concentration can be used to determine the coal concentration in slurries. This measurement, of course, will depend on particle-size distribution in the slurry. For example, at 200 kHz, the change in attenuation is about 0.16 dB/cm for each 1% variation in coal concentration. This sensitivity amounts to about a 10% change in the magnitude of the signal that is transmitted through the coal slurry in a 2-in-dia pipe. This 10% change is greater than the uncertainty of the measurement which is about 5%.

Another uncertainty in a concentration measurement based on sound attenuation may arise from the fluctuation of the flow velocity. This is also investigated in the present work. Figure 26 shows the relative attenuations for two given coal concentrations at two flowrates. In general, the change in attenuation due to the flow-rate change is rather small--for example, at 200 kHz the variation in attenuation is about 0.3% per 1% flow-velocity change. Under the normal steady-state operation of a coal plant, the attenuation change due to the fluctuation of the flow velocity is probably insignificant. Therefore, the sound-attenuation measurement can provide an estimate of the coal concentration with an accuracy of 5%.

(b) Cross-correlation Results

The operating principle of a cross-correlation flowmeter is to measure the time of flight (TOF) required for a flow disturbance to travel between two measuring points along the pipe. If the time-series signals detected at the two measuring points are represented by x(t) and y(t), their cross-correlation function, is given as[20]

$$R_{xy}(t) = \lim_{T\to\infty} \frac{1}{Y} \int_0^T x(t)\, y(t+\tau)\, dt \qquad (21)$$

where τ is the time shift applied to one of the signals for evaluating the convolution integral, and T is the signal duration. The maximum of a cross-correlation peak (t_{max}) is related to the measured volumetric flow, V_m, by

$$V_m = L/t_{max} \quad , \qquad (22)$$

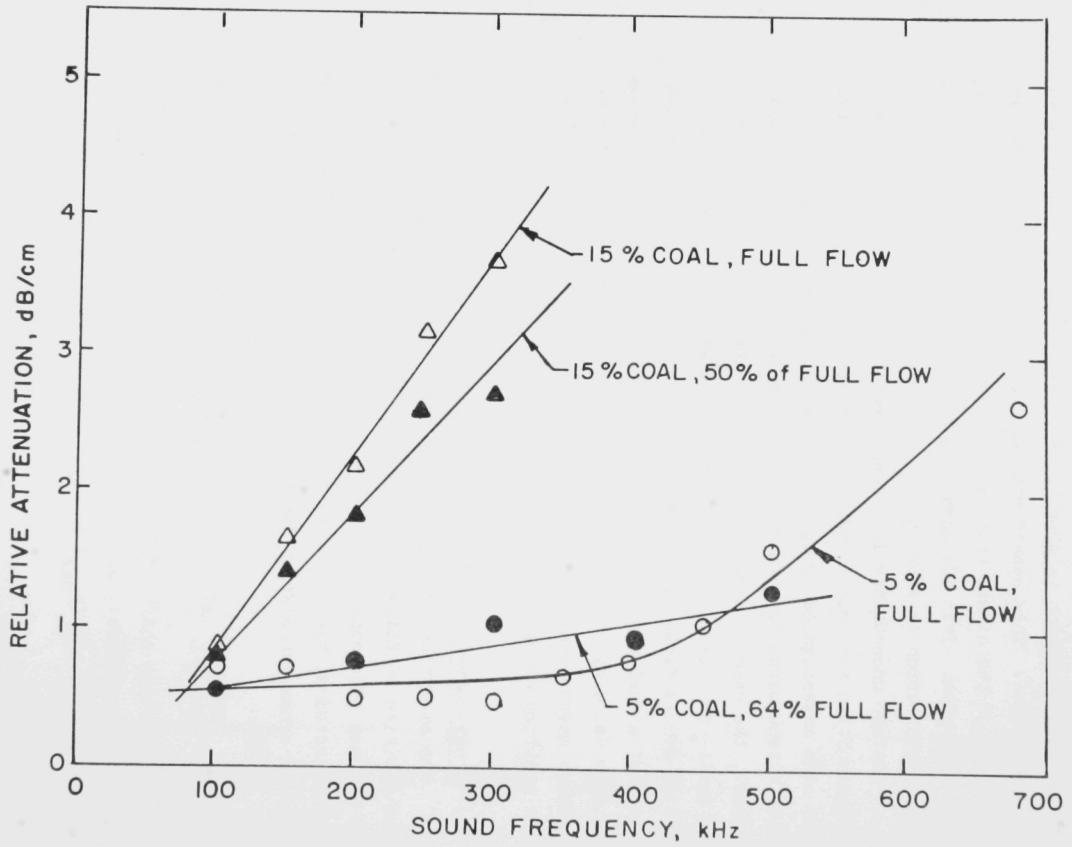

Fig. 26 Relative Sound Attenuation *vs.* Sound Frequency at Different Flow Velocities for Two Coal Concentrations.

where L is the distance between the two measuring points. However, a correction factor must be applied to the measured flow velocity to give the average volumetric flow velocity in the slurry line. The correction factor reflects the fact that the flow velocity averaged over the ultrasonic beam path differs from that averaged over the actual flow-velocity profile across the pipe. The corrected volumetric flow velocity is equal to 0.91 V_m.

Ultrasonic flowmeters using cross-correlation techniques may be operated in either the passive or the active mode. The passive technique requires cross-correlating the background noise received by two similar transducers without introducing any disturbance into the flowing medium being measured. On the other hand, the active cross-correlation technique requires sending a pressure wave (normally cw) into the medium. The medium in turn, modulates the pressure wave with the local flow disturbances. Such disturbances might be caused by the flow turbulence near the pipe wall and the boundaries of coal particles.

In this report only operation in the active cross-correlation mode will be presented. In that mode, the flow-modulated cw waves require demodulation and bandpass filtering before they are used for cross-correlation. The demodulation technique used in this paper is AM. If any constant tone, such as the electrical 60-Hz noise and the 5.7-Hz slurry pump in this case is present, the cross-correlation function will be dominated by those tones. It is, therefore, necessary to apply proper filtering to eliminate constant tones from the demodulated signals.

Figure 27 shows the auto- and cross-correlation functions for three filter bandwidths. It is noted that the 60-Hz tone is clearly observable in the auto- and cross-correlation functions at the top of the figure. By varying the filter bandwidth it was noticed that the variation of the peak position is less than 2%. This uncertainty can be neglected if the filter bandwidth is increased. Notice that the width of the cross-correlation function decreases as the filter bandwidth is increased.

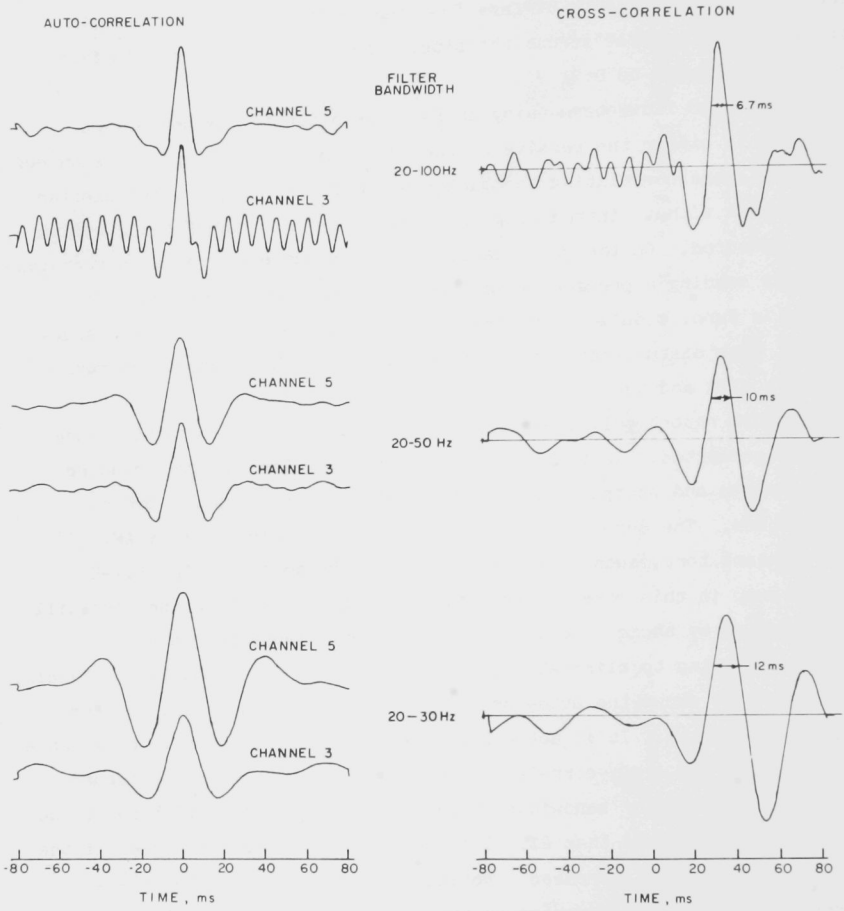

Fig. 27 Auto- and Cross-correlation Functions Obtained Using Different Filter Bandwidths.

Figure 28 is representative of the cross-correlation function for two flow velocities and 15 wt % coal concentration. From this and additional data at other concentrations, it was observed that the full-flow velocities for three coal concentrations were consistent within 1%; i.e., the increase in coal concentration introduces a very small change in flow velocity. Cross-correlations for two reduced flow rates, 64 and 50% of the full flow, have been obtained. Table III summarizes the results of the flow-velocity measurements. The results agree within 20%, with those obtained by the capacitive instrument in the line.

Table III HYGAS Coal-Slurry Flow Velocities Obtained by Ultrasonic Cross-Correlation Measurements.

	Time Delay of the Cross-correlation Peak (ms)	Measured Flow Velocity V_m (m/s)	Corrected Flow Velocity V (m/s)	Flow Velocity from Capacitive Measurement (m/s)
Full Flow	29.55	4.3	3.91	3.62
64% of Full Flow*	45.6	2.79	2.54	2.1
50% of Full Flow*	56.0	2.27	2.07	1.65

*Estimated from the opening of the throttle valves.

Flow velocities for coal concentrations below 1 wt % cannot be obtained using the active cross-correlation technique, because the flow disturbances present in a pure fluid are too small to be detected with the present setup. They can be determined, however, by using a set of transducers with higher sensitivity than the AE-FAC-500.

One necessary step in the active cross-correlation measurement is the elimination of the phase shift caused by the data-processing system. The primary source of the phase shift is the bandpass filters which may introduce an error as large as 8%. The use, therefore, of constant-phase filters is critical in the cross-correlation measurement.

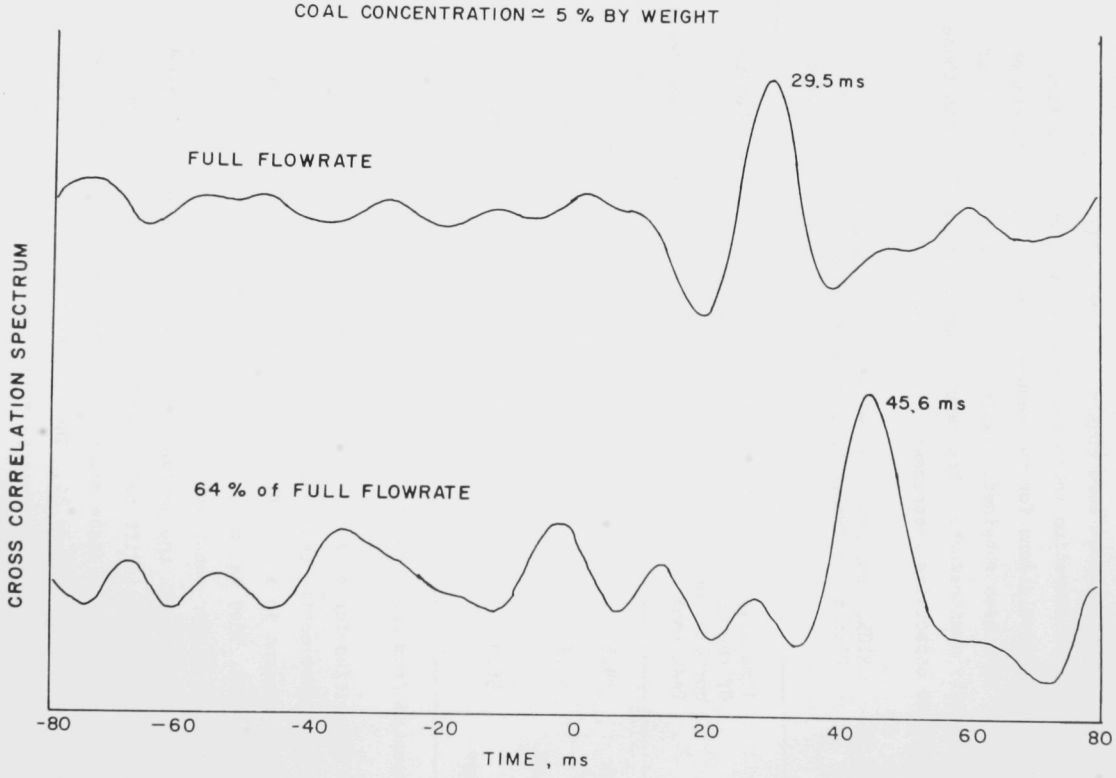

Fig. 28 Cross-Correlation Functions of Two Flow Velocities in 15-wt % Coal Concentration.

(c) On-Line Flowmeter

Based on the results obtained in this test as well as in the first HYGAS test, an on-line ultrasonic mass flowmeter can be designed. The flowmeter will measure the coal concentration by measuring the sound attenuation in the slurry; the flow velocity will be measured by using the active cross-correlation technique. Figure 29 is a schematic diagram of an on-line cross-correlation ultrasonic mass flowmeter. Two pairs of transducers are installed in transducer housings, which are separated from the coal slurry by Teflon windows. The main features of the data-processing system are AM demodulators with built-in filters and a low frequency cross-correlator. The coal concentration is indicated by the rms value of the transmitted signal, and the flow velocity is derived from the peak position of the cross-correlation function. Finally, the product of the flow velocity and coal concentration gives the mass flow rate of the coal slurry.

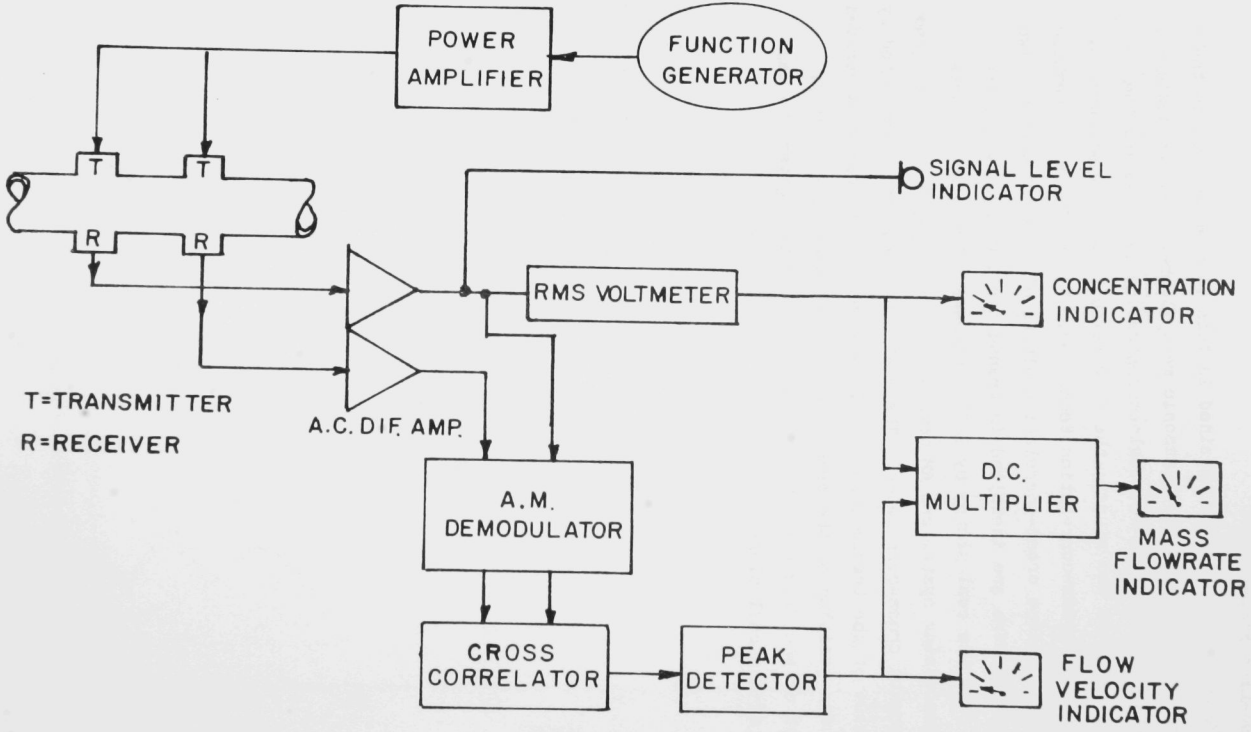

Fig. 29 Schematic Diagram of an On-Line Cross-correlation Ultrasonic Mass Flowmeter.

IV. SOLID/GAS MEDIA

The development of acoustic/ultrasonic techniques for solid/gas media has been limited because of priorities and funding to a theoretical feasibility study and the development of a flow/no-flow indicator for the char return line of the BI-GAS pilot plant. The results of the theoretical feasibility study and the development of the BI-GAS flow/no-flow indicator will be presented next.

1.0 Theoretical Feasibility Study - Solid/Gas Media

The criteria for feasibility of acoustic/ultrasonic techniques for flow measurement for solid/gas media in coal conversion streams will again be based on the sonar equation, Eq. (1). The important quantities again will be the transmission losses and noise background levels. This study will be restricted by the limits of present acoustic theory to ≤ 0.25 particle volume fraction. Furthermore the study includes only air, methane, and steam at selected pressures and temperatures. The characteristics of the media used in the feasibility study are shown in Table IV.

TABLE IV Characteristics of Media used in Feasibility Study on Solid/Gas Media

Item	Medium A	Medium B	Medium C	Medium D
Gas	Air, methane and/or steam at specified temperature and pressure			
Particle Size	100 μm	10 μm	1 μm	1000 μm
Particle Density	2.0 g/cm^3	1.0 gm/cm^3	0.5 gm/cm^3	2.0 gm/cm^3
Concentration	0.2 Vol. fract.	0.01 Vol. fract.	0.001 Vol. fract.	0.2 Vol. fract.
Path Length	15.24 cm	15.24 cm	152.4 cm	15.24 cm

The values of the attenuation constants for the media given in Table IV were based primarily on the studies by Epstein and Garhart[21] on the absorption of sound in suspensions and emulsions. From the results of this study, the attenuation of sound by particles suspended in a gas can be resolved into the following four terms:

1. A component representing the absorption of sound by the gas itself,
2. A scattering loss component due to a redistribution, rather than a dissipation of energy of the incident sound beam by the particles,
3. A viscous component due to the relative motion of the gas with respect to the particles, and
4. A thermal component due to irreversible heat transfer between the gas and the particles. Thus,

$$\alpha_t = \alpha_g + \alpha_s + \alpha_v + \alpha_k \tag{23}$$

where,

α_t = the total attenuation
α_g = the attenuation of the gas, itself
α_s = the attenuation due to the scattering loss from the particles
α_v = the attenuation due to particle-gas-viscous loss
α_k = the attenuation due to particle-gas-thermal loss

The classical expression for the absorption coefficient in a dilute fluid such as a gas is given by the Stokes-Kirchoff relationship.[22]

$$\alpha_g = \left[\frac{8}{3}\pi^2\right]\left[\frac{f^2}{c_o^3 \rho_o}\right]\left[\mu_o + \frac{3}{4}\left(\frac{\gamma - 1}{C_p}\right)\kappa\right] \tag{24}$$

where,

α_g = the attenuation in the gas (cm^{-1}),
c_o = the sound velocity in gas (cm/s),
ρ_o = the density of the gas (g/cm^3),
μ_o = the absolute viscosity of the gas (poise),
$\gamma = C_p/C_v$ = the ratio of specific heats for the gas,
C_p = the specific heat of the gas at constant pressure (cal/g·°C),
C_v = the specific heat of the gas at constant volume (cal/g·°C),
κ = the thermal conductivity of the gas (cal/s·cm·°C),
f = the frequency (Hz).

The first of these terms on the right was derived by Stokes in 1841 and represents a loss due to the viscosity of the gas. The second term represents a loss due to thermal conductivity as predicted by Kirchoff in 1868.

It should be noted that the classical value of absorption for an ideal gas increases as the square of the frequency. Measurements made on monatomic gases yield values that are in fair agreement with those predicted by the classical theory. Because of relaxation processes, this agreement is not found for most gases where both sound velocity and absorption depart from values predicted by classical equations. For the computations in this study, the classical equations for absorption are used. The errors are not serious for the selected gases (air, steam, and methane) since, in most instances, the particle-attenuation terms dominate. If other gases are used, the effect of relaxation should be studied before the classical equations for absorption are used.

The theory for the scattering loss of plane waves incident on a moveable spherical particle was developed by Lamp.[23] The attenuation due to the scattering loss is directly related to the total effective scattering cross section. For the case where the wavelength of sound is much greater than the particle size, an approximate expression for the attenuation coefficient is given by,

$$\alpha_s = \frac{8\pi^4}{3} C \left(\frac{f}{c_o}\right)^4 a^3 \qquad (25)$$

where:

α_s = the particle scattering loss (cm^{-1}),
C = the particle concentration (vol. fraction),
f = the frequency (Hz),
c_o = the sound velocity in the gas (cm/sec),
a = the particle radius (cm).

Equation 25 is only valid for low concentrations because at high concentrations the particle interactions become significant.

For the case where the incident wavelength is much greater than the particle size and the particle concentration is low, the possibility of particle interactions is eliminated. The sound attenuation due to the relative motion of the gas with respect to the suspended particles, that is, the particle viscous loss, is given by (see Refs. 21 and 24),

$$\alpha_v = 72\pi\,(C) \cdot \left(\frac{f}{c_o}\right) \frac{y^2\,(1+y)}{[16y^4 + 72\delta y^3 + 81\delta^2\,(1 + 2y + 2y^2)]} \qquad (26)$$

where:

α_v = the particle viscous loss (cm^{-1}),
C = the particle concentration (vol. fraction)),
f = the frequency (Hz),
c_o = the sound velocity in the gas (cm/s),
$\delta = \rho_o/\rho_1$,
ρ_o = the density of the gas (g/cm^3),
ρ_1 = the density of the particle (g/cm^3).

The dimensionless parameter y is given by,

$$y = (\pi f \rho_o/\mu_o)^{1/2} a \qquad (27)$$

where:

f = the frequency (Hz),
ρ_o = the density of the gas (g/cm^3),
μ_o = the absolute viscosity of the gas (poise),
a = the particle radius (cm).

Under the same conditions as given for the particle viscous loss, the attenuation due to the heat transfer between the gas and the particles, that is, the particle thermal loss, is given by (Refs. 21 and 24),

$$\alpha_\kappa = 72\pi\,(C) \times \left(\frac{f}{c_o}\right) \frac{P_r y^2(\gamma-1)\,(1 + P_r^{1/2} y)}{\left[4P_r^2 y^4 + 12\gamma(C_p/C'_p)P_r^{3/2} y^3 + 9\gamma^2(C_p/C_p')^2\right]} \qquad (28)$$

where:

α_κ = the particle thermal loss (cm^{-1}),
C = the particle concentration (vol. fraction),
f = the frequency (Hz),
c_o = the sound velocity in the gas (cm/sec),
δ = ρ_o/ρ_1,
ρ_o = the density of the gas (g/cm^3),
ρ_1 = the density of the particle (g/cm^3),
γ = C_p/C_v = ratio of specific heats for the gas,
C_p = the specific heat of the gas at constant pressure (cal/•g•°C),
C_v = the specific heat of the gas at constant volume (cal/g•°C),
C_p' = the specific heat of the particle (cal/gm.°C),
y = dimensionless parameter given by Eq. (27).

and P_r is the Prandtl number for the gas, given by,

$$P_r = \frac{\mu_o C_p}{\kappa} \qquad (29)$$

where:

μ_o = the absolute viscosity of the gas (poise),
C_p = the specific heat of the gas at constant pressure (cal/g•°C),
κ = the thermal conductivity of the gas (cal/s•cm•°C).

Using Eqs. 25, 26, and 28 and the media characteristics of Table IV, the total attenuation for solid/air systems at 300K and 1 atm was calculated for a 15.24-cm (6-in.) path length and a 152.4-cm (60 in.) path length. A frequency range of 0.1 to 1 MHz was covered. The results are shown in Fig. 30. The effects of temperature and pressure on attenuation are shown in Figs. 31 and 32. From Figs. 31 and 32, respectively, it is observed that the attenuation increases with temperature at constant pressure and decreases with increasing pressure at constant temperature.

The total attenuation for air, steam, and methane (the three gases used in the study) is shown in Fig. 33. The attenuation calculations shown in Fig. 33 are for a temperature of 1000 K and a pressure of 100 atm. It can be seen that the attenuation in the steam is somewhat higher, and the attenuation in the methane somewhat lower, than the attenuation in air for media A and B. For medium C however, methane shows an attenuation that is intermediate between air and steam, except for frequencies above approximately 1 MHz.

It was previously shown that the passive sonar equation can serve as a basis for evaluating the feasibility of an acoustic flowmeter with respect to whether or not a pulse from a transmitting transducer, after traversing the medium, will arrive at the receiving transducer with enough signal level to be detected above the local noise level. Reviewing Eq. (6), the processed signal level, PSL, at a receiver is defined as,

$$PSL = SL - TL + DG + PG \tag{30}$$

where,

PSL = the processed signal level of the receiver (dB re μPa),

SL = the source level at 1 cm (dB re μPa),

TL = the total transmission loss along the path between the source and receiver (dB),

DG = the directional gain of receiving transducer (dB),

PD = processing gain of the receiver detecting circuitry (dB).

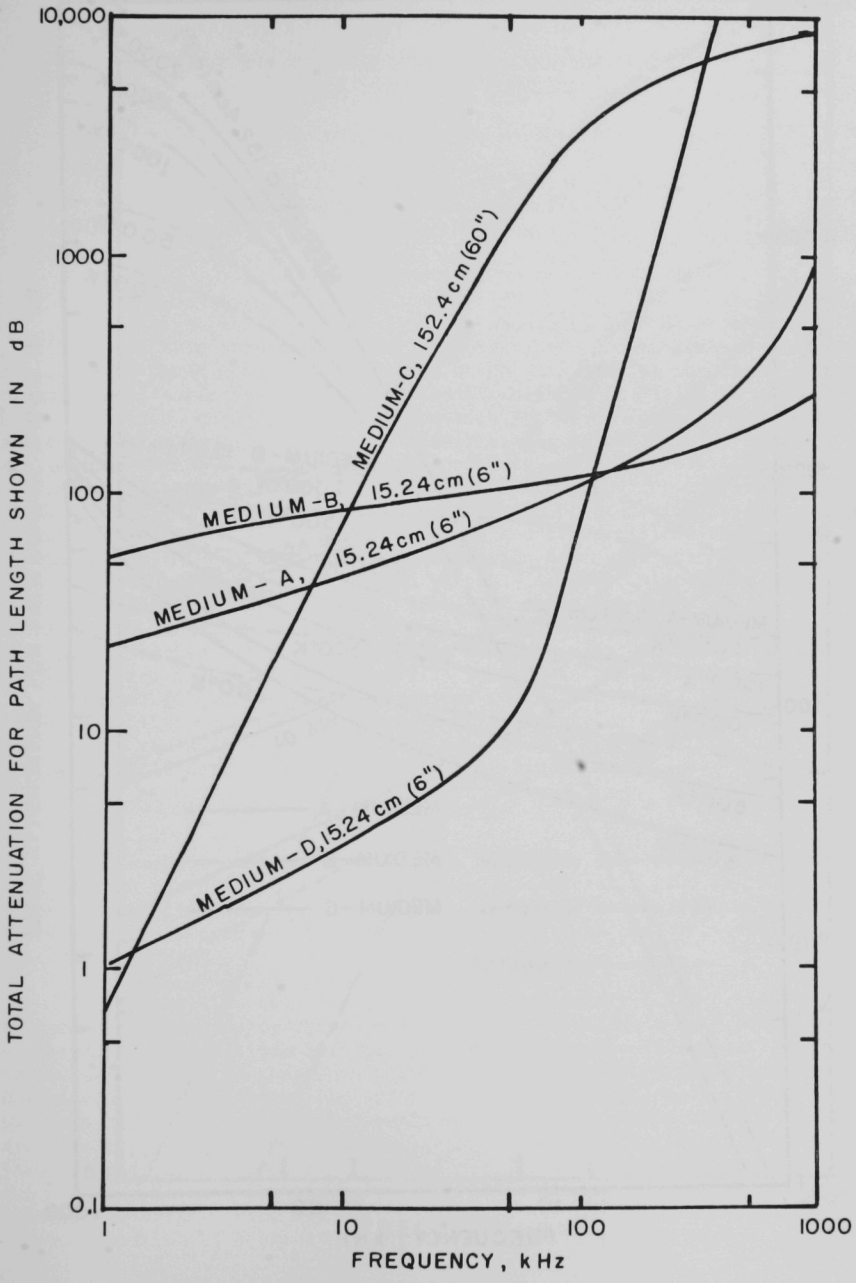

Fig. 30 Total Attenuation *vs.* Frequency for Solid/Air at 300 K and 1 atm.

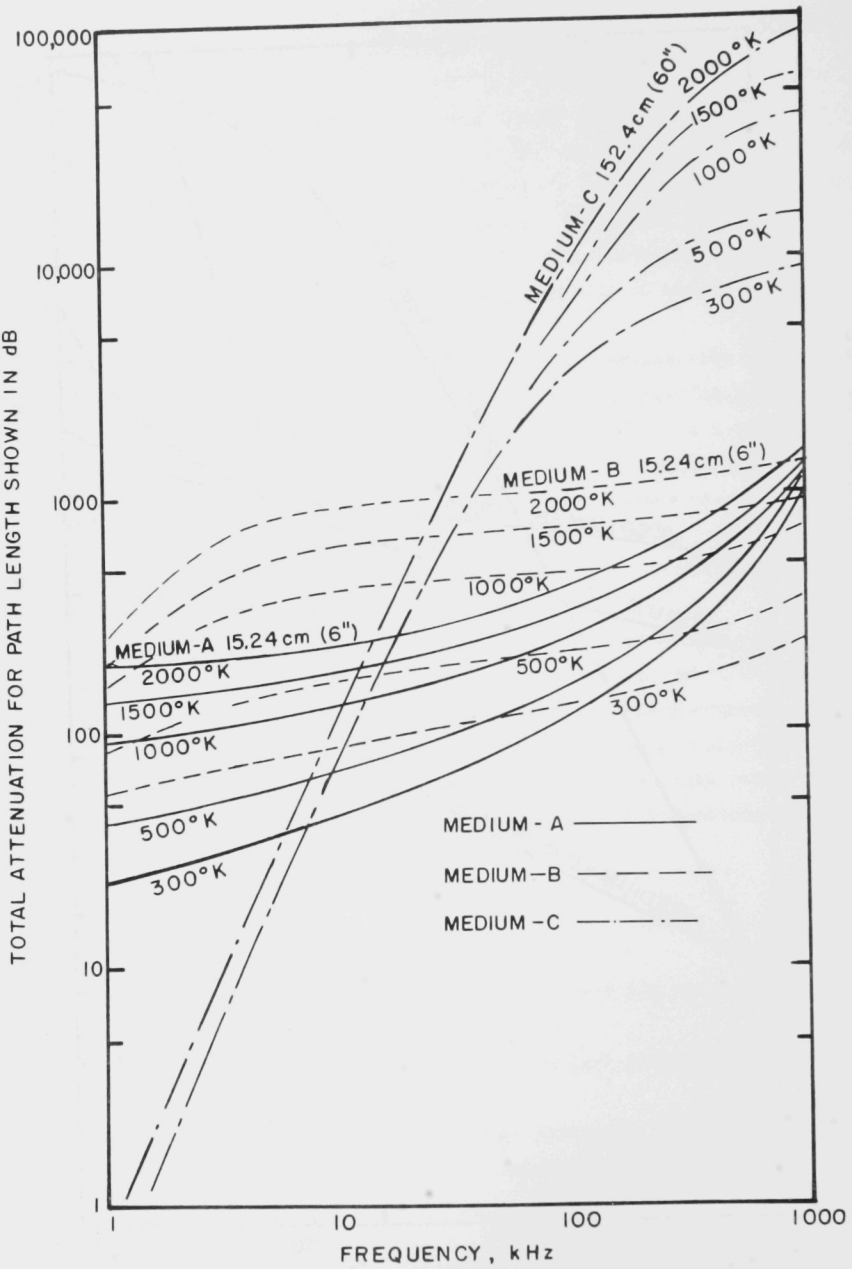

Fig. 31 Effect of Temperature on Total Attenuation for a Solid/Air System at Constant Pressure (1 atm).

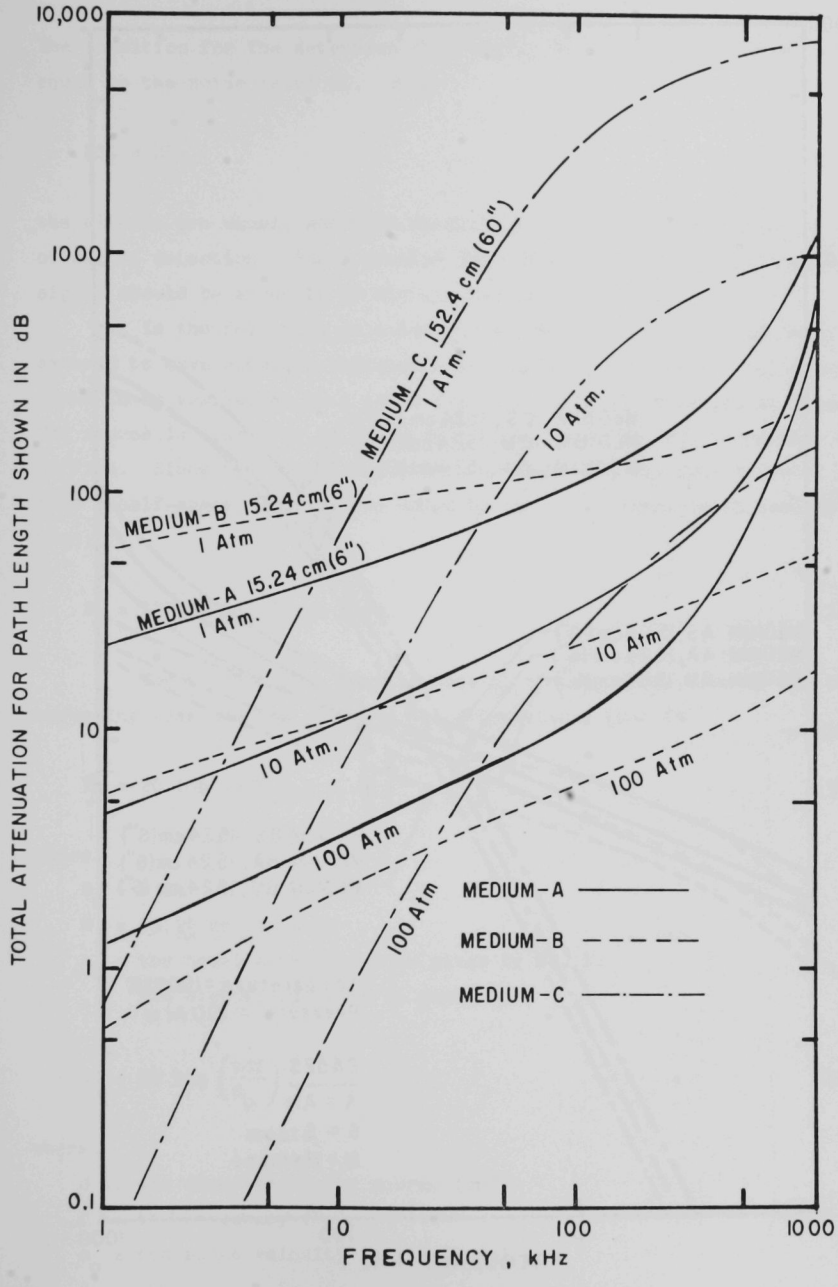

Fig. 32 Effect of Pressure on Total Attenuation for a Solid/Air System at Constant Temperature (300 K).

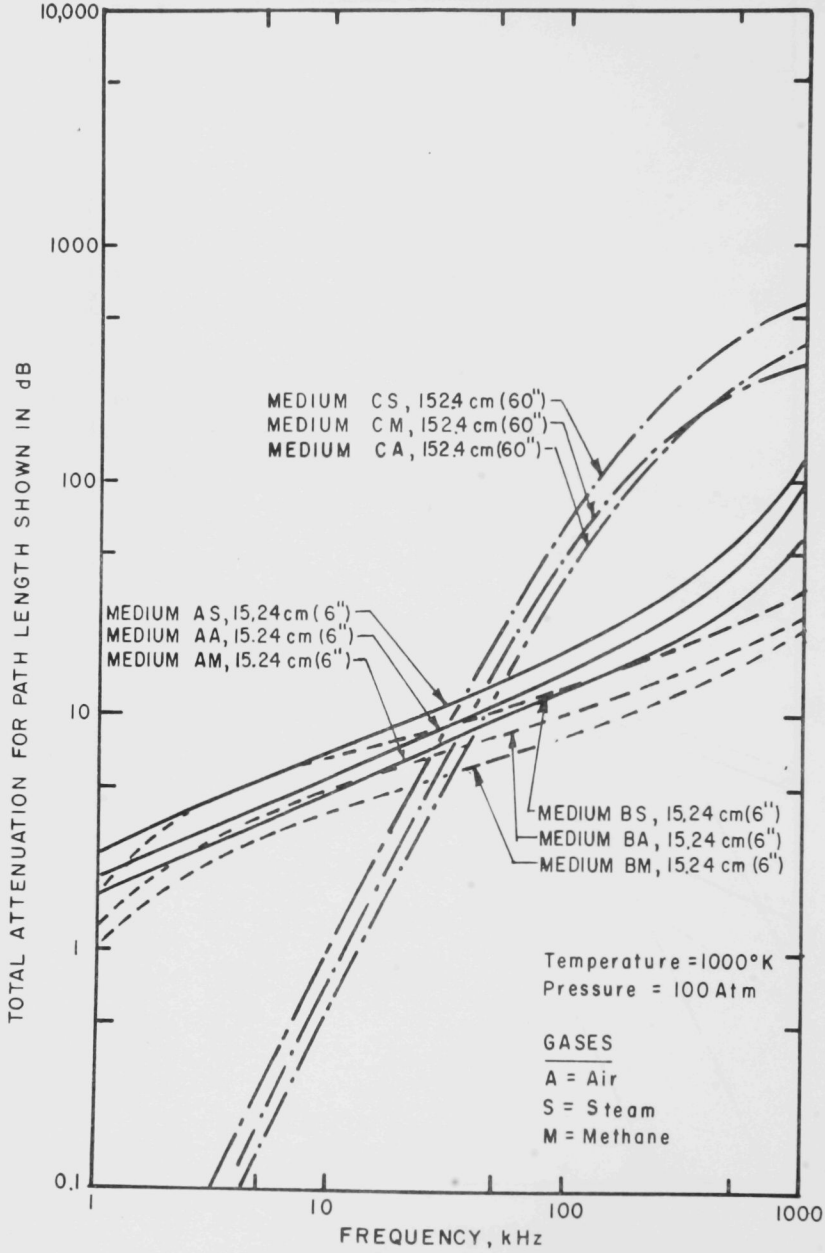

Fig. 33 Effect of Different Gases on Total Attenuation for Solid/Gas Systems at 1000 K and 100 atm.

The condition for the detection of a signal is that the PSL be at least equal to the noise level NL. When

$$PSL = NL, \tag{31}$$

the signals are equal, and this condition represents a 50% probability of signal detection. For a greater assurance of detection, the processed signal should be about 10 dB higher than the noise level.

In the following calculation, a spherical sound source level is assumed to have acoustic radiated power equal to 1 W. This source can be shown to be equivalent to a sound level, SL, of 175 dB re μPa at 1 cm. The source is likely to be inserted into a pipe wall and, therefore, be baffled. Since the source level will be radiating its full power of 1 W into a half-space, 3 dB may be added to SL. The source level assumed is, then,

$$SL = 178 \text{ dB re } \mu\text{Pa at 1 cm.} \tag{32}$$

The transmission loss is made up of two terms. One is due to the spreading loss and the other to the attenuation, that is

$$TL = 20 \log (R/R_o) + \alpha_t R \tag{33}$$

where,

R_o = 1 cm

R = 15.24 or 152.4 cm

α_t = the total attenuation as given by Eq. 1.

The directional gain is given by

$$DG = 20 \log \left(\frac{\pi d f}{c_o} \right) \tag{34}$$

where,

d = the diameter of the source (cm),

f = the frequency (Hz),

c_o = the sound velocity in air (cm/s).

A value of 5 dB is assumed for the processing gain, or PG = 5 dB. The actual value will depend on the signal level, the noise statistics, the integration time, and the receiving bandwidth. There is essentially no information available on the expected noise levels in pipe lines containing coal particles in gas flow, and the noise term is the most difficult to estimate. From the limited amount of information available, a guess of the noise background is made.[25] The processed signal level and the estimated background noise level according to Eq. 30 are plotted *vs* frequency in Fig. 34, for the selected media and the specified path lengths. For those zones where PSL is equal to NL, signal detection will be made 50% of the time. For 99% probability of detection, the criteria will be that PSL should be greater than NL by 10 dB i.e.,the signal excess should be $\leq$ 10 dB.

On this basis, it is seen from Fig. 34 that an acoustic flowmeter with a 1-W watt acoustic source must operate at a frequency not higher than 10 kHz in medium C because of a sharp drop-off in PSL. By the same reasoning, an acoustic flowmeter is feasible for frequencies up to 150 kHz for medium B and up to 300 kHz for medium A. The results of this feasibility study, however, will have to be verified with experimental values for attenuation and noise background levels.

2.0 BI-GAS Acoustic Flow/No-Flow Indicator

Of particular concern at the BI-GAS pilot plant is monitoring the char flow. A schematic of the BI-GAS reactor system is shown in Fig. 35. Blockage of the char feed lines between the char cyclone and the char burners has been a recurrent problem. The char first drops approximately 16 m by gravity feed from the cyclone to a steam eductor, where high-pressure steam is added to the char. The char and steam then move horizontally about 3 m to the nozzle of the char burner. Blockage of the char in either the vertical or horizontal section can cause a very serious perturbation of the gasifier operation and can quickly lead to a hazardous temperature excursion in the gasifier.[26]

The safety aspects of this problem made the need for a flow monitor quite urgent, but no suitable unit is commercially available.

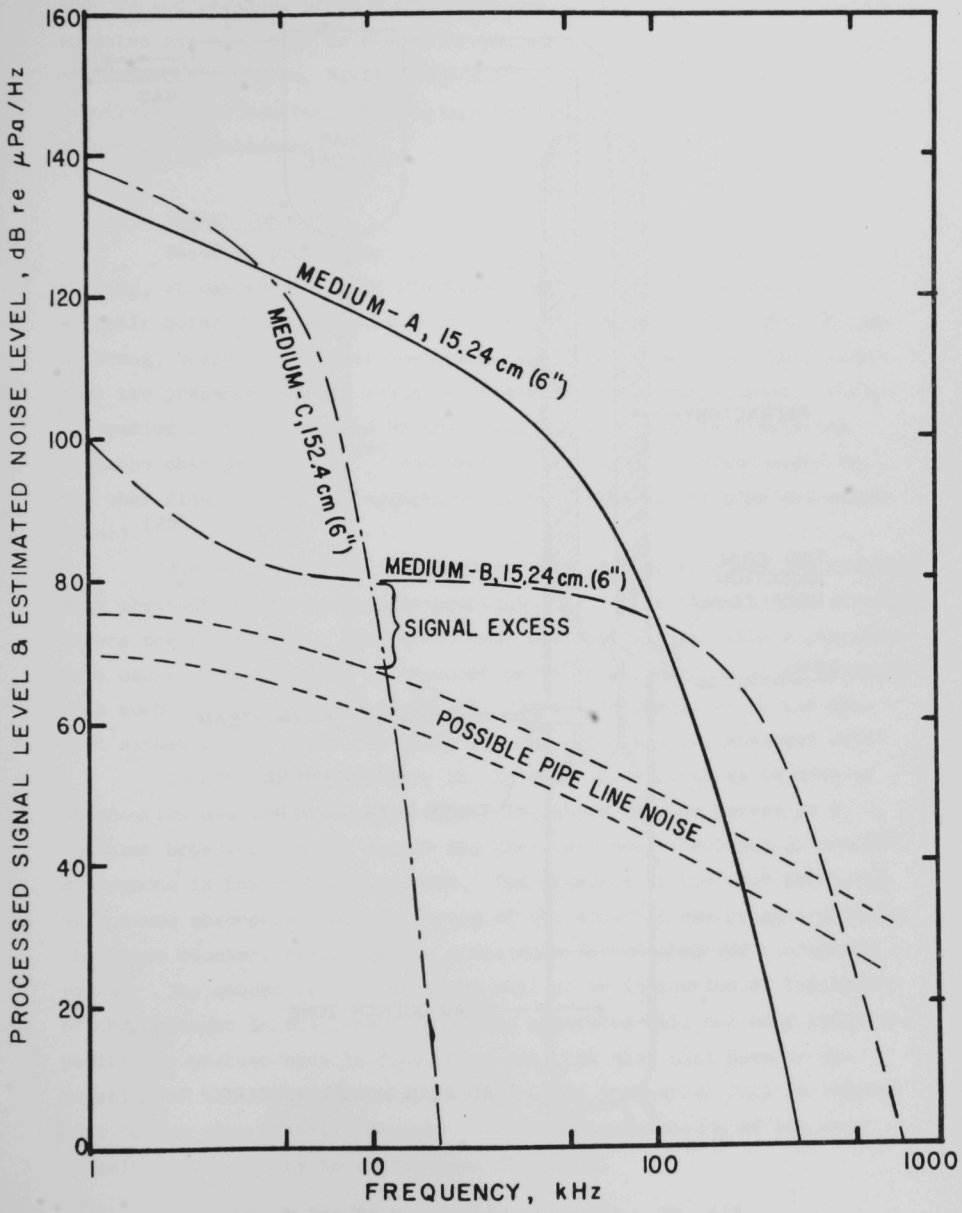

Fig. 34 Determination of Signal Excess.

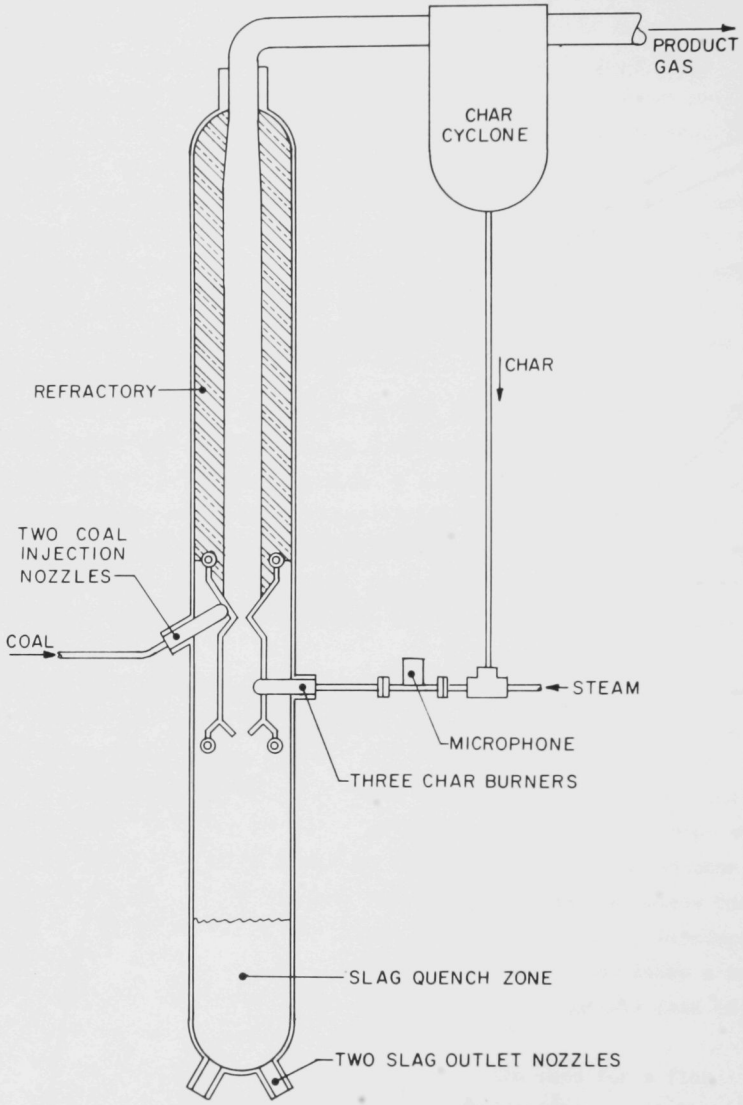

Fig. 35 Schematic Diagram of BI-GAS Reactor.

The design operating conditions in the char line are a temperature of 439°C (800°F) and pressure of 11.4 MPa (1650 psi). The char particles are quite abrasive and also tend to plug orifices and to foul moving parts. Because of these difficulties, BI-GAS requested the assistance of ANL in developing a suitable flow monitor. A flow monitor based on acoustic principles was chosen for development.

(a) Design Concept

Based on preliminary pilot plant measurements with no char flowing, it was evident that the steam eductor was a major source of acoustic noise. A microphone in the location shown in Fig. 35 produced a strong, broad-band signal associated with the steam flow. This meant that the presence of char could be judged in two different ways: first, by looking at the reduction of the steam signal caused by scattering from the char particles,[27] and second, by looking at noise added by the char flow (caused by impingement of particles on the pipe and microphone).[28]

The combination of a relatively streamlined geometry (to minimize flow obstruction and microphone erosion) and a large steam signal strongly favors the first mode. The second mode would be favored with a geometry that caused more particle impingement on the microphone or in a situation with much less background noise. The first mode dominates in the present situation and forms the basis for understanding the observed data.

In effect, the geometry of the char line allows us to make an attenuation measurement on the char. The steam eductor serves as a constant broad-band noise source and the pipe section between it and the microphone is the attenuation path. The presence of the char particles will cause absorption and scattering of the acoustic energy generated by the steam eductor, resulting in a decrease in the observed microphone signal. The amount of this decrease will be an indication of the amount of char present in the line. Thus, the apparatus will not only indicate positively whether char is flowing or not, but also will give an indication of the amount that is flowing. This indication will be related only to the char density, however. An additional measure of the char velocity is necessary to obtain mass flow rate.

(b) Instrumentation

The microphone chosen for this application is a rugged high-temperature unit developed in the Components Technology Division of ANL.[29] As shown in Fig. 36, it uses two identical plates of lithium niobate arranged back-to-back with respect to their piezoelectric polarities. This makes the microphone sensitive to pressure changes on the faces but relatively insensitive to vibration of the device as a whole. This design means the microphone cannot be clamped to the outside of the pipe but must be immersed in the flow. Fortunately, this microphone is well-suited to withstand the severe process conditions, since it is completely encased in type 304 stainless steel and is capable of operating at temperatures up to 650°C (1200°F) and pressures up to 14 MPa (2000 psi). The frequency response of the microphone is fairly constant from 100 Hz to 50 kHz, but is virtually nil above 100 kHz. The absolute sensitivity of the microphone (calibrated in water) is approximately 1.2×10^{-2} PC/Pa.

Microphones have been installed in the horizontal sections of the three identical char feed lines. Figure 37 shows the microphone housing before installation of the microphone. The char line is nominal 1 1/4 in. schedule 160 stainless steel pipe, and connections are made with 2-in. Grayloc fittings. The microphone housing is at the center of this section of pipe and consists of a 2-in. tee with a Grayloc hub welded to the branch. The microphone is supported from a matting hub that forms a demountable seal. A 2.22-cm (0.875-in.) hole in the wall of the char line allows the microphone to sense pressure fluctuations in the process steam but causes minimal disturbance to the flow and negligible erosion of the microphone. Figure 38 shows the microphone as it is supported from the blind Grayloc hub. This support is designed to position the lower edge of the microphone flush with the inner surface of the char line, in the hole that was machined in the pipe wall. The signal lead for the microphone passes through the Conax compression seal as shown. The fitting uses a lava sealant to seal against the high temperature, high pressure gas in the char line.

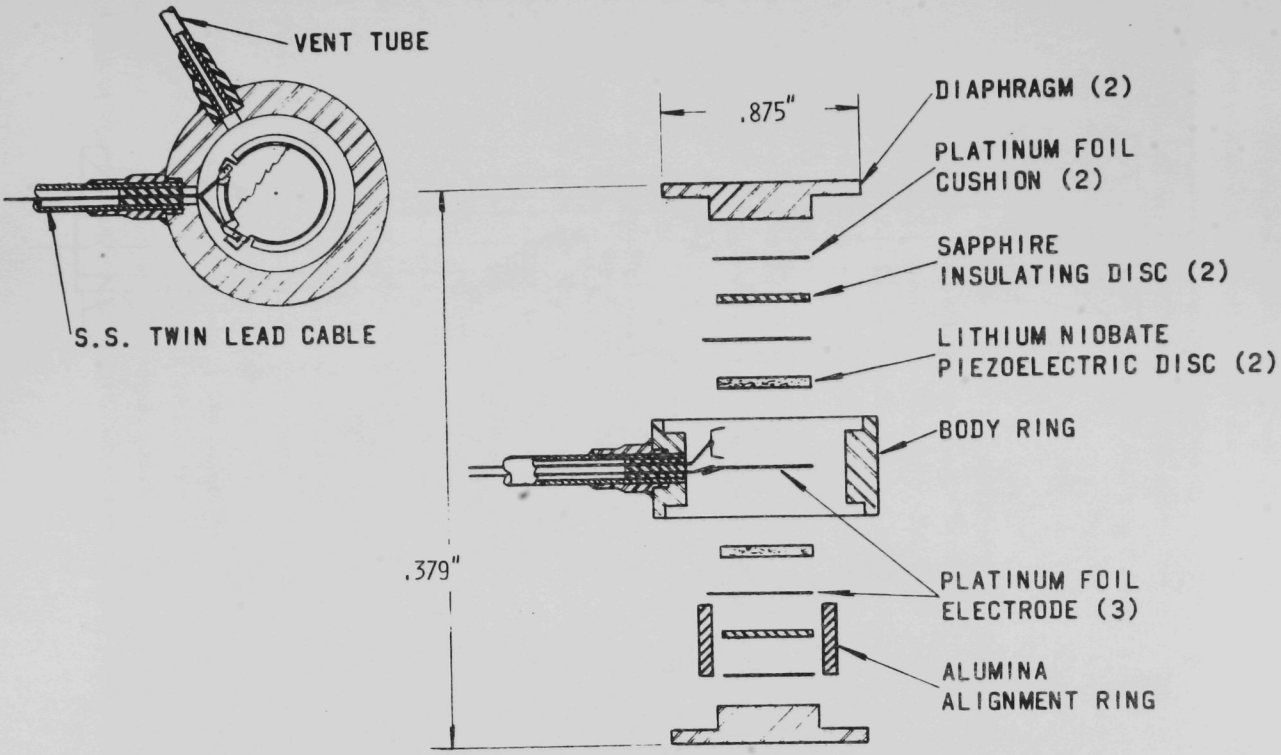

Fig. 36 Construction Details of High-Temperature Microphone.

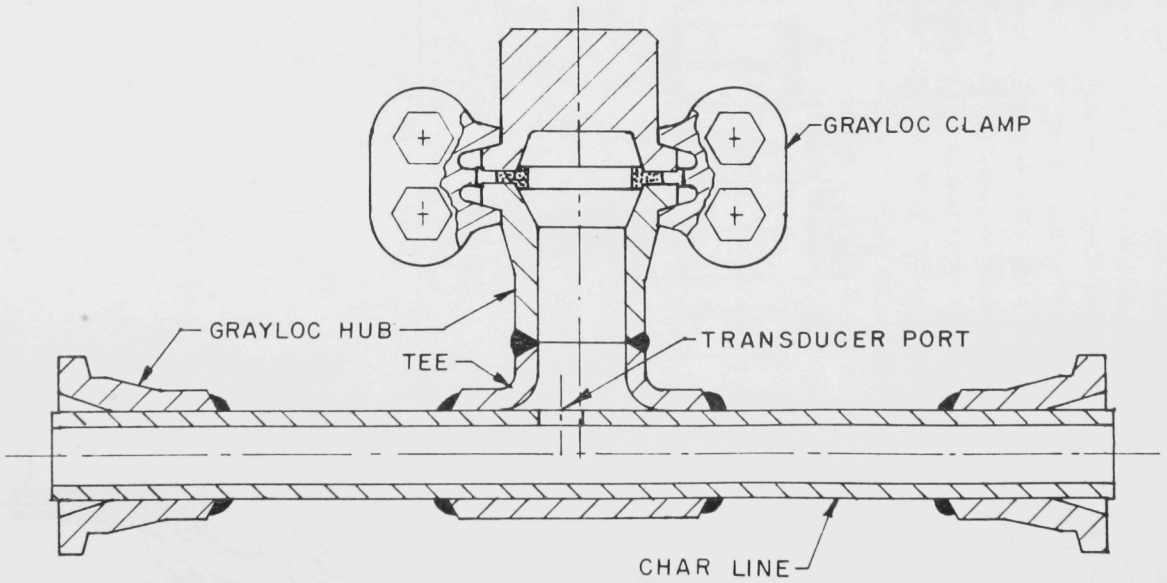

Fig. 37 Microphone Housing for BI-GAS Char Line.

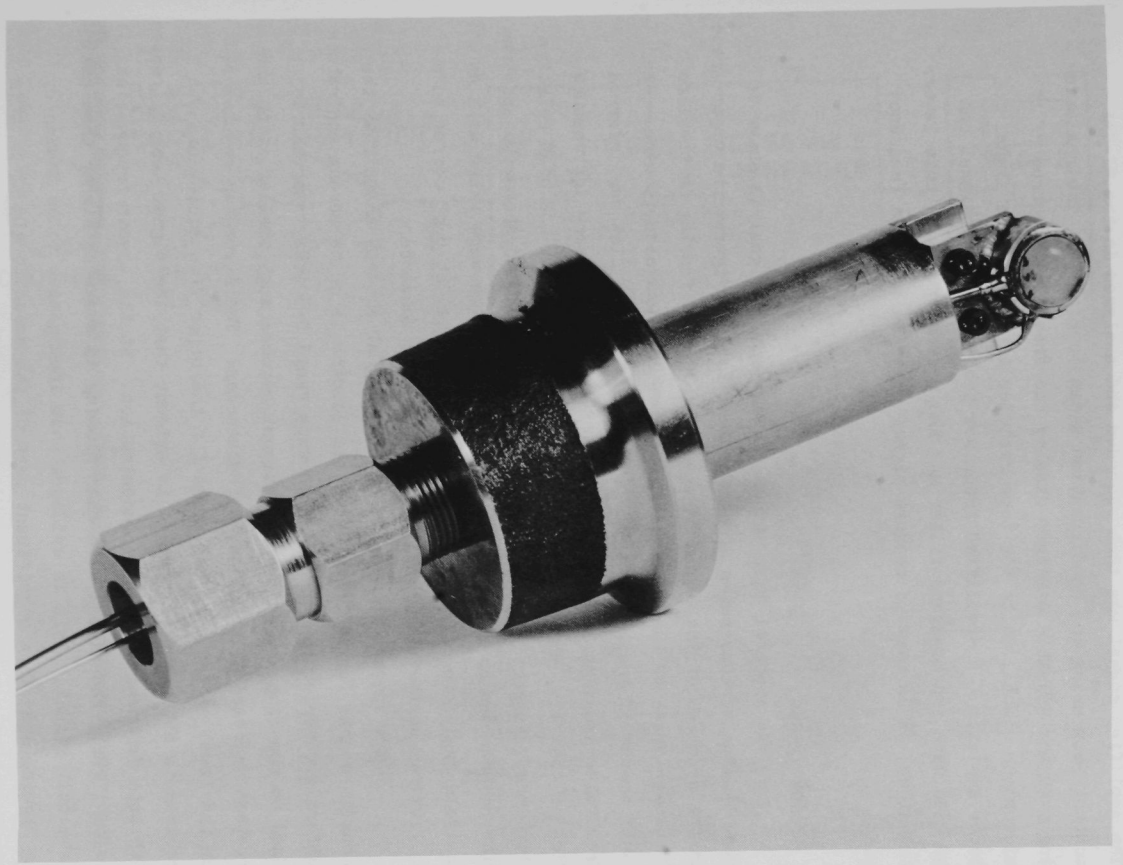

Fig. 38. Photograph of Microphone and Support Assembly.

For the initial studies, the microphone signal was first amplified in a remote charge converter located near the microphone. The amplified signal was then recorded and analyzed in the BI-GAS control room using the configuration shown in Fig. 39. The real-time Analyzer and Ensemble Averager display the frequency spectrum of the microphone signal, while the tape recorder saves the data signal for later analysis. A simplified frequency analysis of the signal can be made with the bandpass filter and RMS voltmeter. With this latter technique, it is easy to measure signal power in selected frequency bands.

(c) Data

The spectral analysis of the microphone signal is shown in Fig. 40, for various rates of char flow. In each figure, the upper trace is the spectrum of the signal when only steam was flowing in the line. The lower trace is the spectrum taken when char was also flowing. The exact amount of char was not known but the relative flow was inferred from valve openings and readings of differential pressure instruments. Figures 40a, 40b, and 40c correspond to low, moderate, and high relative flow rates, respectively. The lower trace in Fig. 40d shows the spectrum with no char and no steam flowing. All the spectra were taken with an analysis bandwidth of 300 Hz. The reference level at 0 dB corresponds to 1.0V rms at the output of the remote charge converter.

The spectrum of the steam-only signal clearly shows that the acoustic signal (noise) from the steam eductor is quite strong and rather uniformly distributed over the frequency range 0-50 kHz. As char is added to the line, the microphone signal becomes much smaller, with the greatest decrease at the highest frequencies. The signal is reduced below the level of the analyzer noise for the upper frequencies and its spectrum is not apparent, but it is evident that the signal loss increases with both frequency and char concentration. At the lowest frequencies (below 1 kHz), the signal with char flowing is somewhat higher than the steam-only signal. This is evidence that impingement noise caused by the flowing char is a significant part of the acoustic signal in this frequency band.

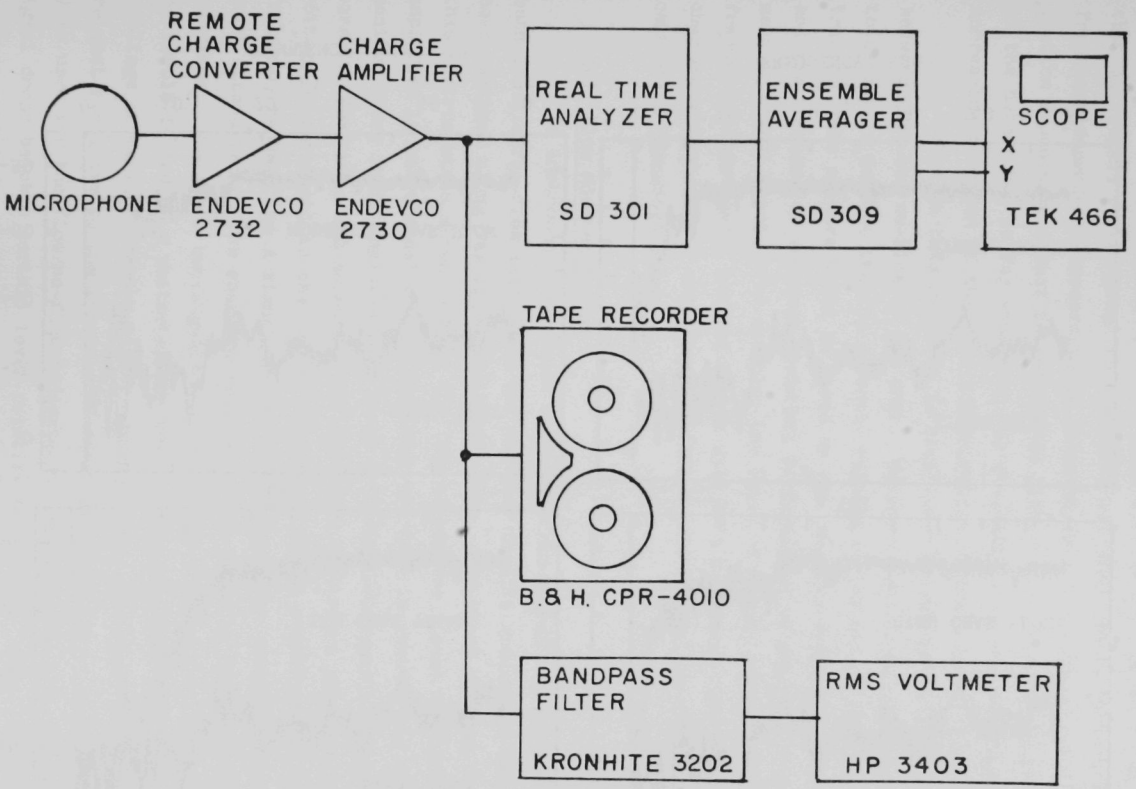

Fig. 39 Electronics for Microphone Signal Processing.

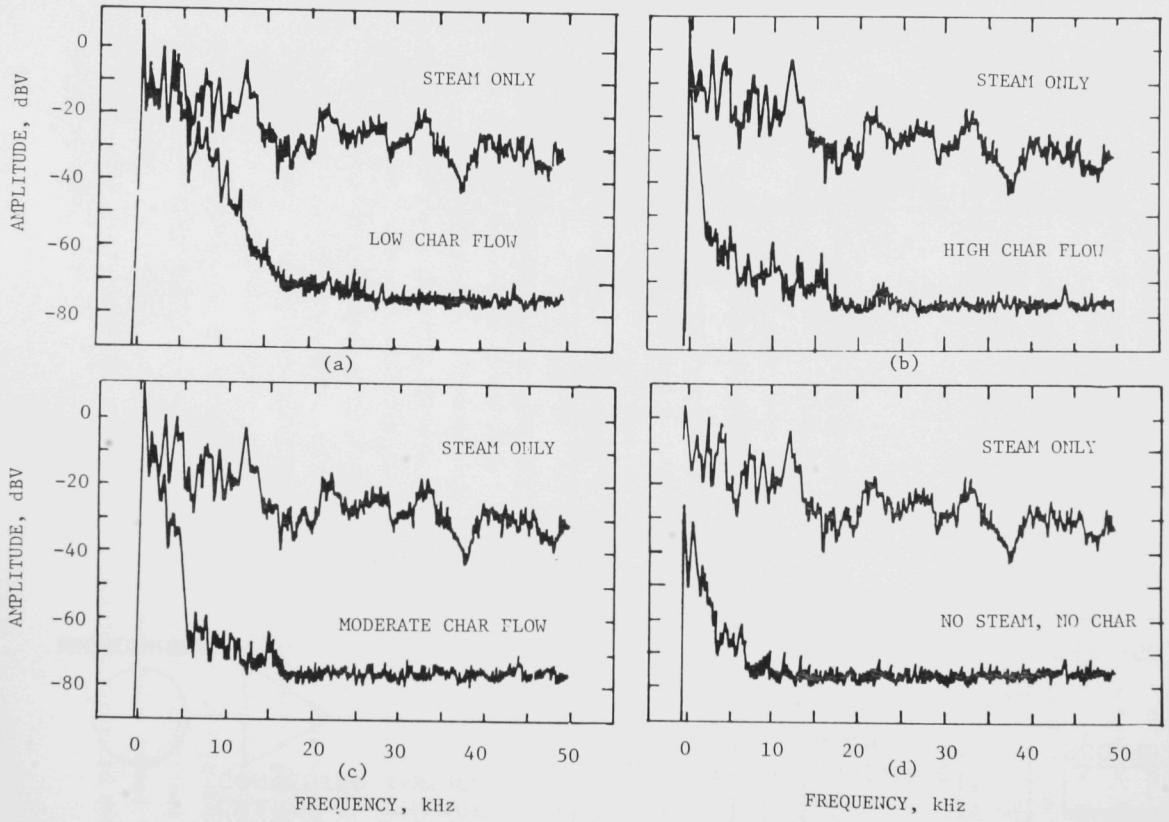

Fig. 40 Spectral Analysis of Microphone Signal.

The change in the microphone signal which we observe as char is added to the line, is consistent with the attenuation model which was discussed earlier. In this case, the char is causing an attenuation that is roughly proportional to frequency and char concentration. The frequency dependence appears to be essentially linear, but the concentration dependence cannot be determined without a calibration. All of the data taken so far show that the attenuation is a monotonically increasing function of the char concentration in the line.

Based on this data, it is clear that we can easily distinguish between flow and no-flow of the char. Moreover, it should be possible to develop a measure that is directly related to the actual char concentration. This measure would be based on the relative attenuation at high and low frequencies and thus would not be dependent on absolute measurement of signal level. For example, the ratio of signal levels in the frequency bands near 1 kHz and 10 kHz will be a monotonic function of char concentration and could be used (after calibration) as a char-concentration (density) meter.

(d) Flow Monitor Design

An instrument to process the microphone signal and provide both the flow/no-flow indication and the char-density indication has been designed along the lines discussed above. The block diagram for this instrument is shown in Fig. 41. The microphone signal is first amplified in an external charge amplifier and then is sent to the flow monitor where it is analyzed into three different frequency bands by band-pass filters. The RMS detectors and LOG RATIO converters generate a dc voltage proportional to the log of the ratios of the amplitudes in the frequency bands. The A signal is the lowest-frequency component and is least attenuated by the char, so this signal is taken as the amplitude reference. The other two signals are then normalized to this reference; the result is fed to a voltmeter for the intermediate band and to a voltage comparator for the high-frequency band. The high frequencies are most sensitive to the presence of char, and this signal (signal C) is used for the flow/no-flow indication. Whenever the high-frequency signal drops below a certain level relative to the low-frequency band, the CHAR FLOW light turns on.

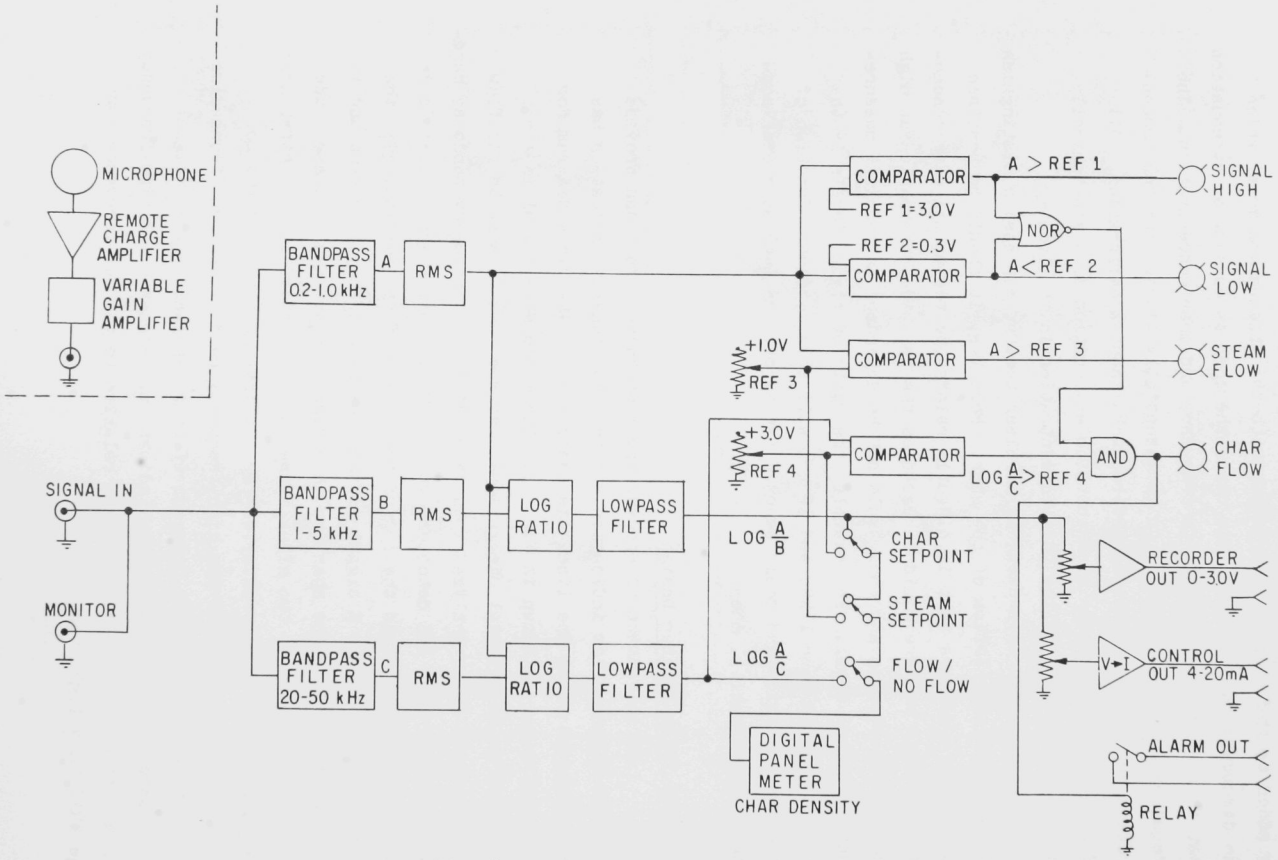

Fig. 41 Block Diagram of Flow Monitor.

The intermediate-frequency band (signal B) is less sensitive to the presence of char but gives a usable signal over a wider range of char density. This band is used to give a continuous indication of char density. It is expected that the signal derived from this intermediate frequency band can be calibrated in terms of actual mass density of char in the pipe. Then if flow velocity can be determined, the mass flow rate of char would be obtained.

Other features which have been incorporated into the flow monitor permit external use of its signals and provide indications of proper operation. Both voltage and current outputs are provided for driving a recorder or a process control system with the char density signal. These outputs have adjustable gain and time constant. The flow/no-flow signal is used to provide a constant closure for an external alarm system. But the contacts will close only if the unit has power and the input signal is within specified bounds. This guards against misleading CHAR FLOW indications that might be based on signals outside the range of accuracy of the circuit.

Front panel indicators show if the input signal is too large or small, the panel meter may be used to check various circuit voltages. For comprehensive testing of circuit function, however, it is necessary to inject known test signals. For this purpose a separate test module has been constructed. This module provides four different signals designed to confirm proper operation of all of the flow monitor circuits. In this way, each flow monitor can be quickly checked out, either as part of a routine maintenance procedure or when the operator suspects a malfunction. The finished flow monitor is shown in Fig. 42. Three identical modules are shown, one for each of the three char feed legs. Also shown is the module used for testing the flow monitor.

Fig. 42. Photograph of Flow Monitor.

(e) Results of the Flow Module Tests

The results from the use of the flow monitor at BI-GAS have been very satisfactory. The instrument has given rapid and clear indications whenever char flow has started or stopped. In addition, the char-density signal has responded well to the variations in char flow as the control valve settings have changed. But the flow monitor indication has not always agreed well with measurements from other instruments, primarily differential pressure indicators. This may be due to the high sensitivity and faster response of the flow monitor, but may also be related to the fact that the differential pressure instruments are quite sensitive to factors such as gas composition, gas temperature, and purge gas flow which do not affect the flow monitor. As more experience is gained with the flow monitor, it is expected that the discrepancies will be resolved.

An example of the output of the flow monitor is shown in Fig. 43. This is a recording of the char-density signal that was made during BI-GAS test G7-A on February 24, 1979. At 2245 hours, the char line plugged and caused a shutdown of the char burner (marked "CLOSE VALVE" on record). At this time, steam flow continued but was diverted by the plug and flowed up the char leg. The operator promptly closed a valve in the char leg, thus forcing steam flow back down along the proper path to the burner and dislodging the plug. At 2256 hours the char burner was relit and char flow resumed (marked "OPEN VALVE" on record). It is observed that char flow is somewhat less stable at this time. This is speculated to be the result of steam flowing up the char leg for a short time during the shutdown. The steam condensed on the char, causing the char to clump and to flow poorly when the valve was opened again.

The sensitivity and speed of response of the flow monitor is clearly seen in Fig. 43. Even though the char-density signal is re-calibrated, it provides valuable information to the plant operator. Stability of the flow is easily judged and the char-density signal allows the operator to know when a previously used flow rate has been attained.

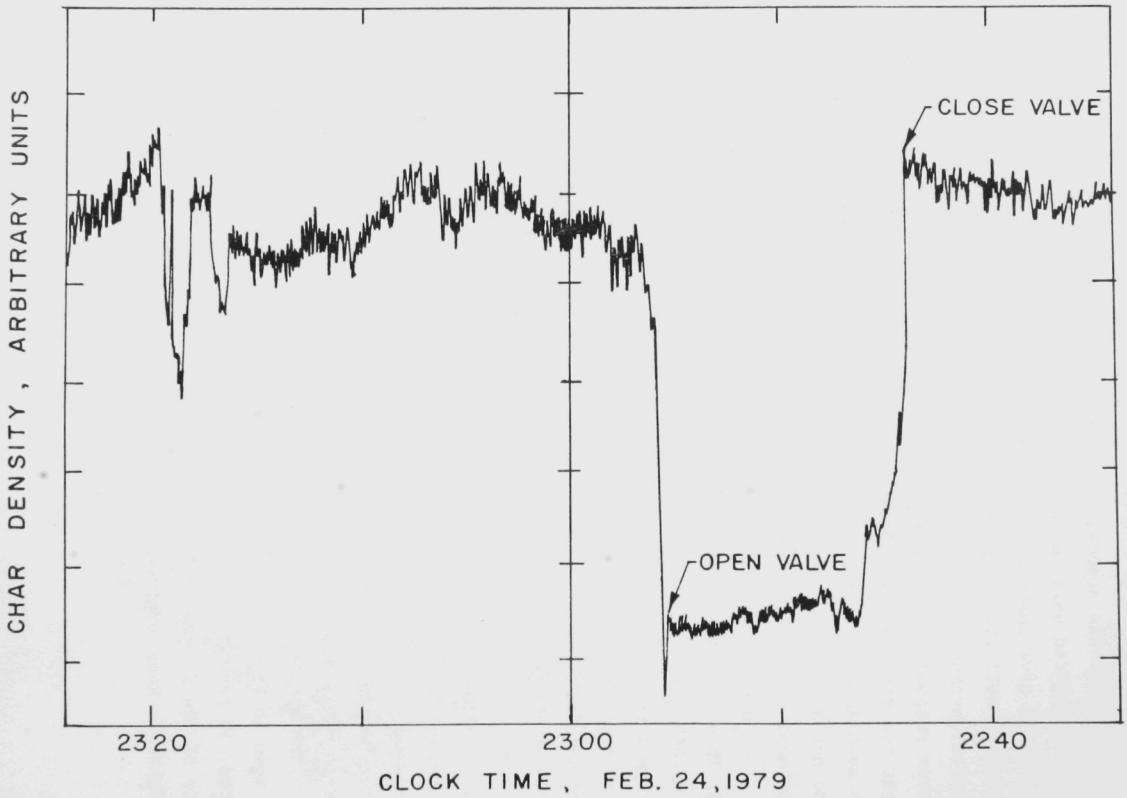

Fig. 43 Recording of Char-Density Signal.

Experience with the acoustic flow/no-flow monitor has been sufficiently encouraging that BI-GAS is considering using the device to control oxygen feed to the lower stage of the gasifier. If this can be done reliably, the supplemental fuel gas feed to this stage can be eliminated, thereby achieving a major milestone for the plant. In the past, the fuel gas has been added to prevent a dangerous oxygen-rich condition from occurring in case of an undetected loss of char feed. But if oxygen flow can be closely matched to char flow, then the fuel gas may not be needed. The acoustic flow monitor is currently the most promising device for providing the necessary char-flow signal.

V. ACOUSTIC TECHNIQUES FOR TEMPERATURE MEASUREMENTS

Many of the pilot plants have reported problems with temperature measurements in their reactors or combustors.[30] The temperatures in the various sections of the reactor vessel and fluidized bed should be precisely controlled for the proper thermodynamic and chemical reactions to occur. The main difficulties in temperature measurement are caused by the corrosive atmospheres that are further accentuated by high temperature and pressure. Detecting fast transients in the process conditions, while protecting the sensing elements from an adverse environment is a challenge in itself. Existing thermowell-protected thermocouples do not adequately meet the challenge. Another type of problem faced by all the conversion and combustion processes is the detection of hot spots on vessel walls and pipes. These hot spots should be detected in advance to prevent damage to the vessel or pipe material. Most plants use a temperature-sensitive paint which indicates hot spots by a change in color, but these paints have a slow response and are strongly dependent on ambient conditions.

In choosing a sensing device to measure temperature, several basic requirements should be considered such as the temperature range of interest, accuracy of measurement, response time, environmental influences, and intended use of the temperature information. The specification of temperature range (1500 - 3000°F) in the coal conversion and combustion processes, narrows the choice of devices to one of several types of commercially available thermocouples. No single instrument-type, however, can meet all the needs of the many varied applications requiring temperature measurement. Alternatives, therefore, to thermocouple sensors have been developed and tested in high-temperature environments. Among the alternatives are acoustic thermometers, whose feasibility and use will be discussed in this report.

1.0 Physical Principle - Acoustic/Ultrasonic Thermometry

Ultrasonic waves are elastic wave motions in materials. A wave is characterized by a phase velocity V and an attenuation α, both of which reflect information about the medium through which the wave is propagating. The success of any process measurement made *via* ultrasound techniques

lies in the accurate determination of one or both of these parameters. Ultrasonic thermometers are based on the dependence of sound velocity on temperature. For ideal gases the velocity is given by

$$V = \sqrt{\gamma RT/M} \tag{35}$$

where γ is the specific heat ratio, R the gas constant, T the absolute temperature, and M the molecular weight. The velocity of sound in liquids is given by

$$V = \sqrt{K/\rho} \quad , \tag{36}$$

where K is the bulk modulus and ρ the density of the liquid. Whereas fluids can support only longitudinal waves, solids can support both longitudinal and transverse waves. The velocity of longitudinal and transverse waves in solids are given by

$$V_\ell = \sqrt{\frac{E(1-\nu)}{\rho(1+\nu)(1-2\nu)}} \quad , \tag{37}$$

$$V_t = \sqrt{\frac{E}{2\rho(1+\nu)}} \tag{38}$$

respectively, where E is Young's modulus, ρ the density, ν Poisson's ratio. In thin wire when the wire size is smaller than the wavelength, the longitudinal waves are called extensional waves. For such waves, ν is negligible, and the velocity is simply given by

$$V_e = \sqrt{E/\rho} \quad . \tag{39}$$

As in the case of gases, there exist no theoretical expressions describing the variation of velocity with temperature for liquids and solids. Figure 44 shows the changes in the velocity of sound in several media with temperature. Whereas the velocity of sound increases in gases at higher temperatures, it generally decreases with increase of temperature in solids and liquids. Solid probes are preferable for process measurements and in this case, rhenium is a good thermometric sensor material showing adequate sensitivity and high melting point (~3180°C).

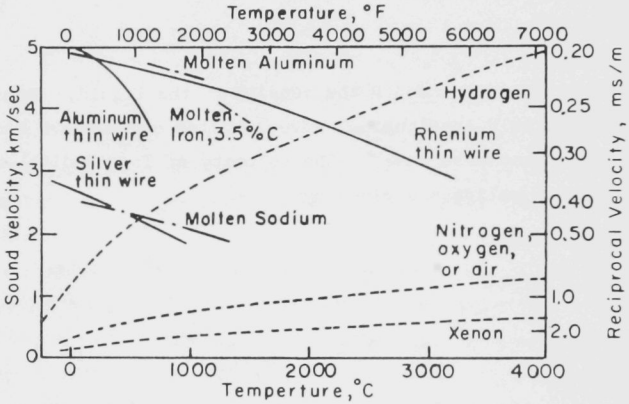

Fig. 44 Velocity *vs.* Temperature.

2.0 Acoustic Temperature-Measurement System

A thin-wire medium is considered for the acoustic transmission, since it provides high echo-signal amplitude and low loss of high-frequency components. Because of the small size of the lead-in and sensor, some mechanical protection is necessary for use in coal conversion plants. The mode of transmission can be either extensional or torsional; but extensional wave transducers are simple in design and generally more reliable than existing torsional wave transducers.[31]

The basic building blocks of the measurement system are a transmitter/receiver, a lead-in (channel), a sensor, and a signal processor. As seen in Fig. 45, the pulser sends out a narrow pulse p(t) which excites the transducer producing an ultrasonic signal x(t) of short duration. This signal is transmitted through the lead-in to the sensor. The sensor, for simplicity, is assumed to have two zones of equal length. The signal x(t) is partly reflected backward at each of the boundaries. The reflected signals, called echoes, trace back the path and, on passing through the transducer, generate an electrical signal r(t). The signal processor estimates the propagation delays in each zone by processing the received signal.

3.0. Mathematical Modeling

Each of the blocks in the measurement system is assumed to be linear, which is justifiable in the case of low-intensity ultrasound. If p(t) is idealized to a delta function, x(t) then represents the impulse response of the transducer. The lead-in is assumed to cause no distortion to the transmitted pulse.

Modeling of the sensor is based on the reflection theory of ultrasonic waves.[32] When a forward-traveling wave meets a plane boundary at normal incidence, some of the energy is reflected backward and the remainder transmitted forward. For such a wave, the sound pressure reflection and transmission coefficients R and T, respectively, are given by

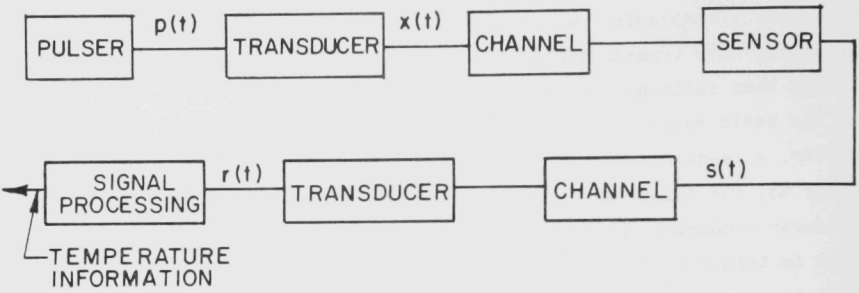

Fig. 45 Block Diagram Representation of a Pulse-Echo Measurement System.

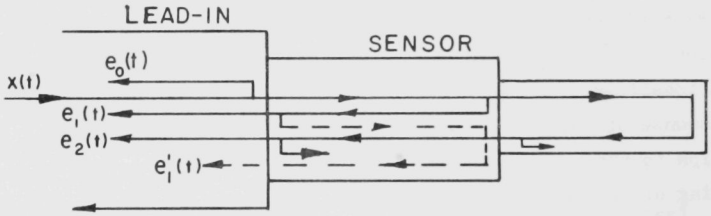

Fig. 46 Echo Paths.

$$R = \frac{(Z_2/Z_1) - 1}{(Z_2/Z_1) + 1} \tag{40}$$

$$T = \frac{2\ Z_2/Z_1}{(Z_2/Z_1) + 1} \tag{41}$$

$$T - R = 1 \tag{42}$$

Where Z_1 and Z_2 are the characteristic impedances of the materials. For extensional waves, the characteristic impedance is given by $Z = \rho vA$ where ρ is the density, v the velocity, and A the cross-sectional area. Thus, one way of incorporating reflectors in the sensor is to change the diameter of the wire.

For a backward-traveling wave, the reflection and transmission coefficients R' and T' are given by

$$R' = -R \tag{43}$$

$$T' = 1 + R' = 1-R \tag{44}$$

Figure 46 shows the echo paths in the sensor. Suppose the reflection coefficients at the boundaries are equal except at the end where R = 1. Let α represent the attenuation in Nepers/unit length and L the length of each sensor zone. Traversing the echo paths as shown in Fig. 46 and using the expressions for the reflection and transmission coefficients, the equations for the echo signals $e_o(t)$, $e_1(t)$ and $e_2(t)$ are given by

$$e_o(t) = R\ x(t) \tag{45}$$

$$e_1(t) = R\ (1-R^2)\ \exp\ (-2\alpha L)\ x(t-T_1) \tag{46}$$

$$e_2(t) = (1-R^2)^2\ \exp\ (-4\alpha L)\ x(t-T_1-T_2) \tag{47}$$

where T_i (i = 1,2) represents the propagation delay corresponding to the ith sensor zone. In the derivation of Eqs. (40) - (42), the echo interactions resulting from reverberations are neglected. Note that the reverberation signal $e'_1(t)$ can interact with $e_2(t)$. However, the relative amplitude given by $e_i(t) = R^3 e_z(t)$ will be negligible when R is small.

The echo-signal equations in the form given above lend themselves to a tapped delay line representation which for the general case is shown in Fig. 47. An additive noise n(t) can be introduced to take into account the model error and the background noise. The combined output resulting from all the echoes is given by

$$s(t) = C_o\, x(t) + C_1\, x(t-T_1) + C_2\, x(t-T_1-T_2) + n(t) \tag{48}$$

where,

$$C_o = R \tag{49}$$

$$C_1 = R\,(1-R^2)\,\exp\,(-2\,\alpha\,L) \tag{50}$$

$$C_2 = (1-R^2)^2\,\exp\,(-4\,\alpha\,L) \tag{51}$$

The transduction of s(t) into n(t) is a convolution operation given by

$$r(t) = \int_o^t h(\tau)\, s\,(t-\tau)\, d\tau \tag{52}$$

where $h(\tau)$ is the impulse response of the transducer and is equal to $x(\tau)$ under the assumption of impulse input.

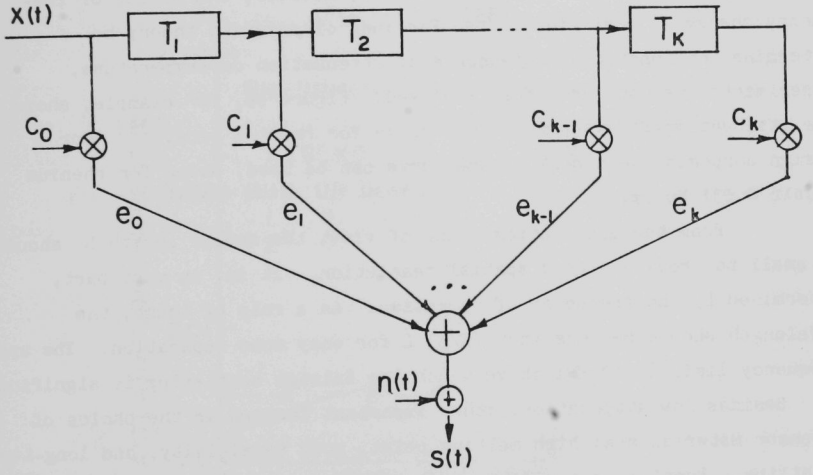

Fig. 47 Tapped Delay Line Representation of the Sensor.

4.0 Design Considerations

Considering Eqs. (48 to 51), the echo-signal amplitudes vary with the reflection coefficient R for the given values of α and L. For easy identification of the individual echoes, the value of R is chosen in such a way that the echo-signal amplitudes are on the same order of magnitude. Also, this enables even distribution of the input signal energy among the echoes.

The attenuation coefficient α of a sensor material varies, in general, with the frequency of operation and the temperature. For the frequency range of interest (below 10 MHz) however, the effect of frequency change is negligible.[33] For lack of adequate theory to determine the functional dependence of attenuation on temperature, experimental methods are often employed. Figure 48, for example, shows the attenuation-*versus*-temperature curve for rhenium wire.[34] For design purposes,the α peak of the curve can be used, which for rhenium equals 0.031 Np/cm.

From the application point of view, the sensor length L should be small to provide a good spatial resolution. It is, in most part, determined by the frequency of operation. As a rule of thumb, the wavelength should be less than (2/3) L for easy echo separation. The upper frequency limit is 10 MHz above which the Raleigh scattering is significant.

Besides low attenuation, other important factors in the choice of a sensor material are: high melting point, good sensitivity, and long-term stability. Rhenium is a widely studied material for thermometric applications. It has good sensitivity, and provides an accuracy of less than 1 percent at 2000°C. Much higher temperatures can be measured using tungsten, but the sensitivity is low compared to that of rhenium. Single crystal aluminum oxide (sapphire) is another good sensor material. It has a melting point of 2050°C, is oxidation resistant, and provides an accuracy of $\pm$2°C at 1900°C.

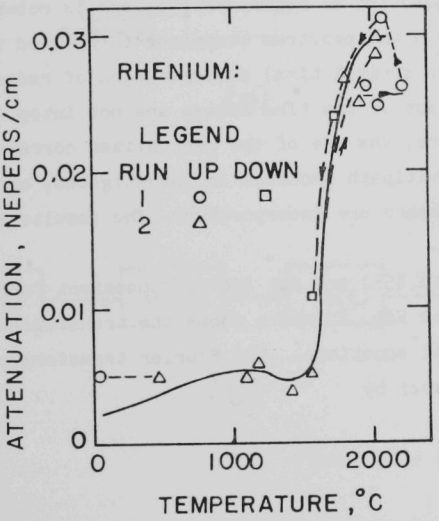

Fig. 48 Attenuation *vs.* Temperature for a Rhenium Wire.

5.0 Signal Processor

The function of the signal processor is to determine/estimate the propagation delays corresponding to the various sensor zones. Time-delay estimation techniques find applications in such diverse fields as sonar and radar detection, voice synthesis, and identification of bio-electric signal origins. Because of its practical significance, several time-delay methods have been proposed in the past. Basically all these methods are based on the idea of correlation, and they pertain to single-path problems. Recently, Knapp and Carter[35-37] have unified many of the existing time-delay estimators in the framework of generalized correlation. However, the solution of multipath problems is relatively little known.[37] Although the cepstrum technique is applied for signal extraction and epoch (echo arrival time) determination of radar/sonar signals, it is not efficient if the time delays are not integral multiples of a basic delay.[38] Here, the use of the generalized correlation techniques to solve the multipath problems is investigated, and certain modifications and improvements are incorporated. The results are compared using a numerical example.

The model Eqs. (48) to (52) are put into a convenient form for time-delay estimation. Consider Fig. 49 which shows the transfer-function representation of the model equations. The Fourier transform of the received signal r(t) is given by

$$R(f) = X(f)\, M(f)\, X(f) + X(f)\, N(f) \tag{53}$$

where X(f) represents the transfer function of the transducer, M(f) corresponds to the transfer function of the sensor, and N(f) is the Fourier transform of the noise. From Eq. (48), M(f) is given by

$$M(f) = C_o + C_1 \exp(-j\,2\pi f T_1) + C_2 \exp[-j\,2\pi f(T_1+T_2)] \tag{54}$$

Equation (53) may be rewritten as

$$R(f) = M(f)\, Y(f) + V(f) \tag{55}$$

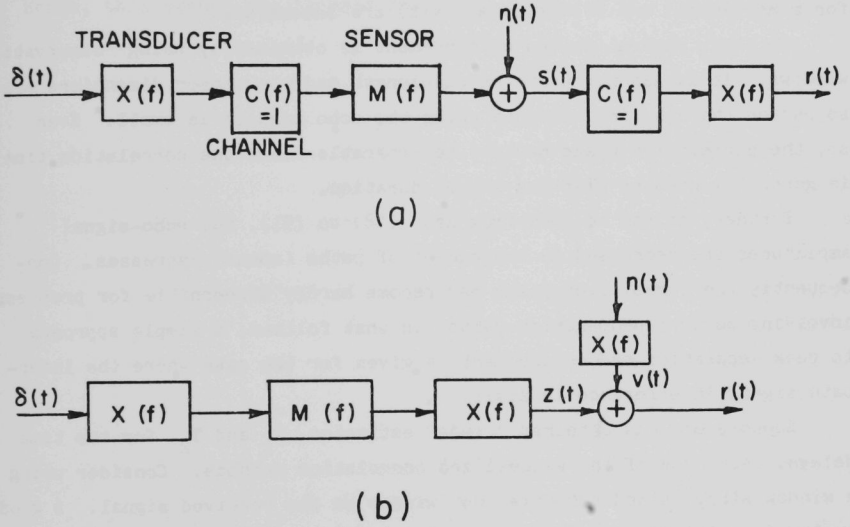

Fig. 49 Transfer Function Representations.

Where $Y(f) = X^2(f)$ and $V(f) = X(f)\,N(f)$. Equation (55), in the time domain, becomes

$$r(t) = C_o\, y(t) + C_1\, y(t-T_1) + C_2\, y(t-T_1-T_2) + v(t) \qquad (56)$$

which is in the standard form for time-delay estimation (see Fig. 49b). It is assumed in the sequel that the input signal y(t) is available for measurement, and that y(t) and v(t) are incoherent.

Peak separation and enchancement is obtained by using "observation" windows. It is assumed that the wavelength and the sensor dimensions are so chosen that the interference among the echo signals is small. Even so, the correlation peaks may not be separable since the correlation time is generally greater than the signal duration.

Further, as can be seen from Eqs. (48) to (51), the echo-signal amplitudes are decreased as the number of paths (zones) increases. Consequently the correlation peaks may become hardly discernible for problems involving several propagation paths. In what follows, a simple approach to peak separation and enhancement is given for the case where the inter-path signal interference is small.

Suppose one has obtained "crude" estimates, $\hat{T}_1$ and $\hat{T}_2$, for the time delays, using one of the generalized correlation methods. Consider using a window w(t), called "observation" window on the received signal. A good choice for w(t) is a cosine (Hanning) window. The window width may be chosen on the order of the correlation time of the input signal. Then, output data corresponding to the individual paths may be obtained as

$$r_1(t) = [C_o\, y(t) + C_1\, y(t-T_1) + C_2\, y(t-T_1-T_2) + n(t)]\; .$$

$$w(t-\hat{T}_1) \qquad (57)$$

$$r_2(t) = [C_o\, y(t) + C_1\, y(t-T_1) + C_2\, y(t-T_1-T_2) + n(t)]\; .$$

$$w(t-\hat{T}_1-\hat{T}_2) \qquad (58)$$

where $r_1(t)$ and $r_2(t)$ represent decoupled versions of the combined multipath signal. Since the neighboring-path signals fall under the tail end of the cosine window, the interference is reduced. Now, using the single-path-maximum-likelihood (ML) estimator for the respective data segments, separate and sharp peaks are possible. It is found from simulation results that the sensitivity of the estimates with respect to the location and width of the window is small near the true delays. Hence, this method can be used for peak separation and enhancement.

6.0. Numerical Results

A typical set of specifications for an ultrasonic thermometer is as follows:

Sensor material	-	rhenium
Sensor length, L	-	50 mm/zone
Sensor size, d	-	4 mm
Frequency, f	-	200 kHz
Type of wave	-	extensional

If the temperature range is between 200°C and 2000°C, the transit time per zone varies between 20.8 μs and 26.3 μs. With the present day electronics, a time interval of 50 ns can be detected, hence a thermometric resolution of ± 16°C is possible.

Taking two sensor zones, the tap coefficients C_o, C_1, and C_2 in Eq. (48) are determined next. The attenuation coefficient α is assigned a value of 0.03 Np/cm, which is the α peak of the curve in Fig. 48. The value of R is then chosen in such a way that the echo peaks are of the same order of magnitude. For R = 0.4, Eq. (49) becomes

$$s(t) = 0.4 \times (t) + 0.25 \times (t-T_1) + 0.39 \times (t-T_1-T_2) + n(t) \quad (59)$$

In order to test the efficiency of the signal-processing techniques described in the previous section, a test signal is selected for x(t). Typically, the impulse responses of the transducer tend to approximate a nyquist pulse[39], whose analytical expression is given by

$$x(t) = \frac{\sin \pi t/\tau}{\pi t/\tau}$$

where τ is the pulse width from the centerline to the first zero crossing. The frequency response of x(t) has the ideal low-pass characteristic given by

$$X(f) = \tau \text{ for } 0 < |f| < 1/2\tau$$

$$= 0, \text{ otherwise}$$

For the problem at hand, $\tau = 4$ μs is suitable. Consider a hypothetical situation in which the time delays T_1 and T_2 are 24 μs and 26 μs, respectively. Figures 50 and 51 show, respectively, the Nyquist pulse and the echo signal from Eq. (59).

A decimation-in-time FFT algorithm was used to compute the Fourier transforms.[40] Corresponding to a sampling time of 2/3 μs, 128 samples were obtained from the output signal. Pseudo-random numbers of normal distribution with zero mean and specified variance were used for the noise term. The output data were zero-padded with 384 zeros to avoid circular effect and time aliasing in the cross-correlation computation. Ten averagings were used to obtain smoothed spectral estimates.

For the noise-free case, the impulse response method yields sharp spikes as shown in Fig. 52. Corresponding to a signal-to-noise ratio of 1.75, the output signal is as shown in Fig. 53. For the noisy signal, the results of a basic cross-correlator, impulse-response estimator, and ML estimator are, respectively, as shown in Fig. 54a, b, and c. In order to check for the aliasing, leakage, and other computational errors, a direct cross-correlation in the time-domain was computed and found to agree with the results of Fig. 54a. In the impulse-response estimator, a rectangular window with a width equal to the bandwidth of the input signal was used, since the generalized filter function goes to zero for frequencies beyond that range. Although each of the estimators correctly identifies the peaks, the ML estimator smooths out the small ripples compared to the other estimators. When the signal-to-noise ratio was increased

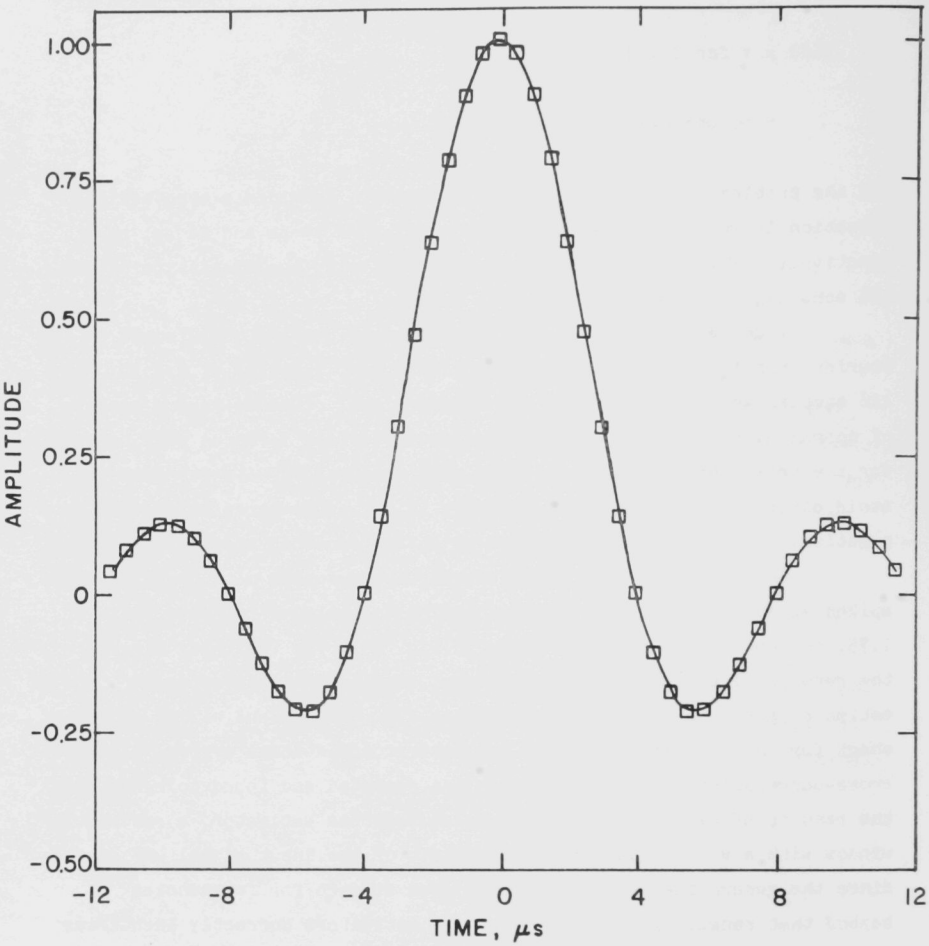

Fig. 50 Nyquist Pulse.

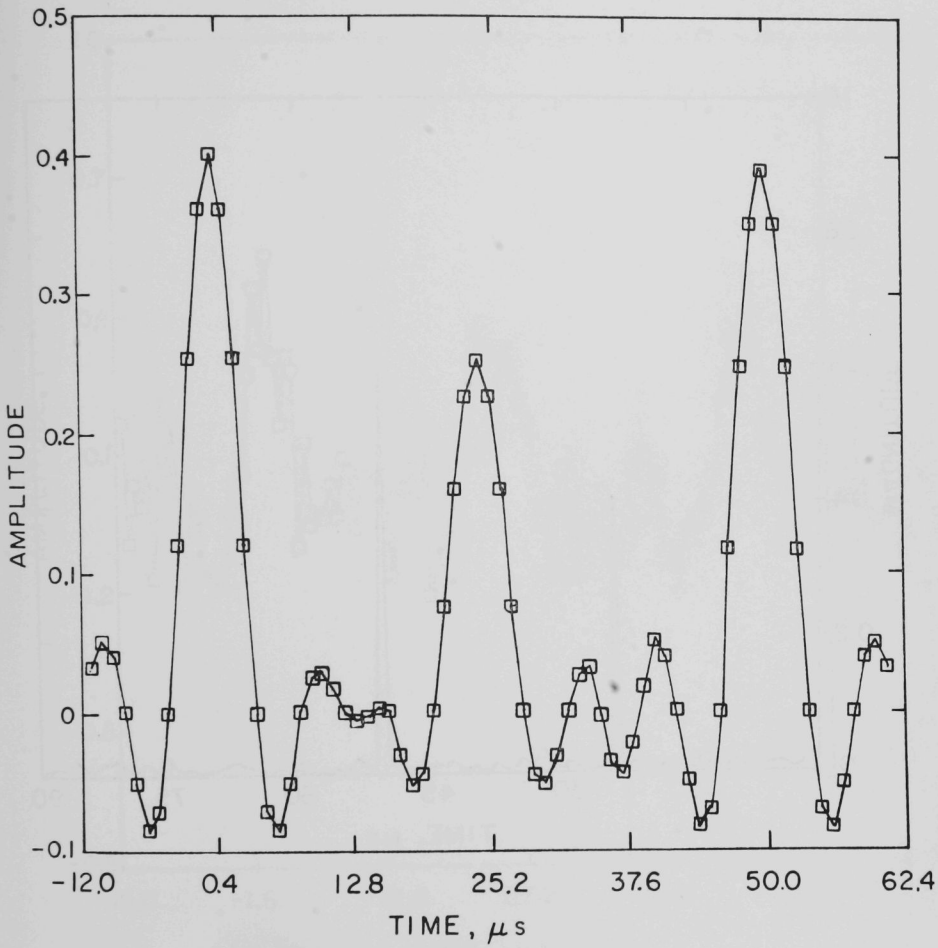

Fig. 51 Echo Signal.

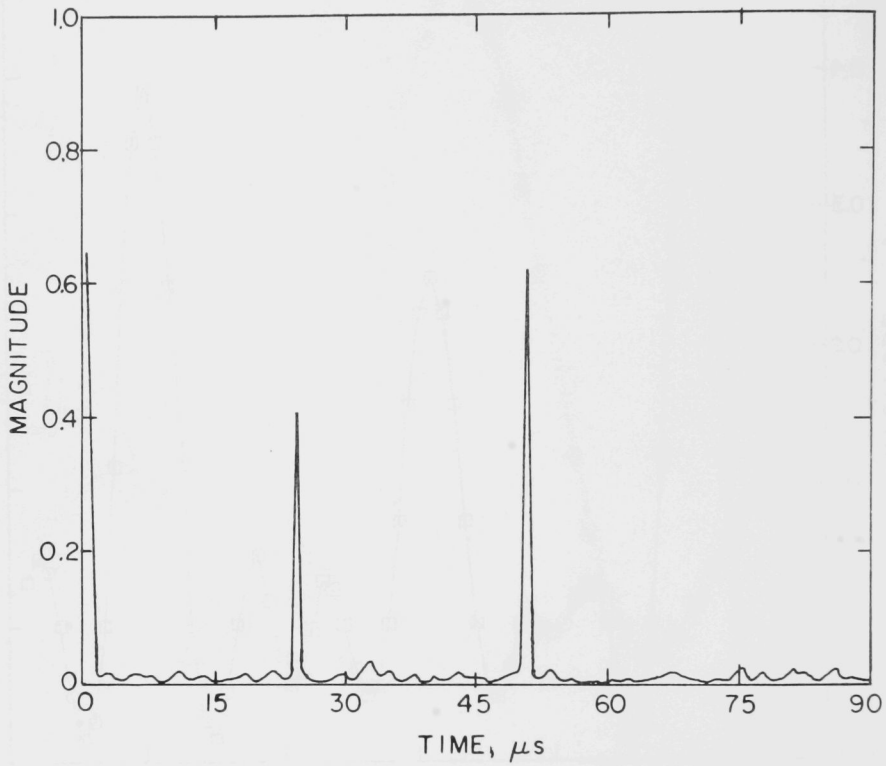

Fig. 52 Impulse Response Method for the Noise-Free Case.

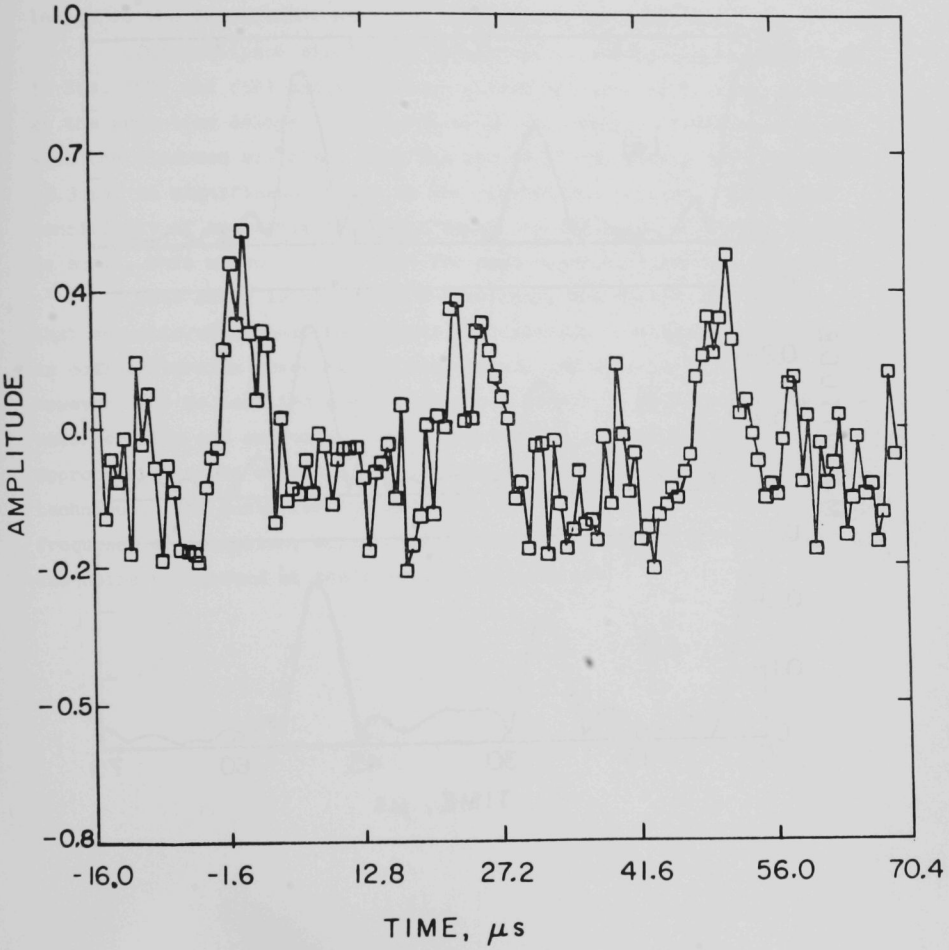

Fig. 53 Output Signal.

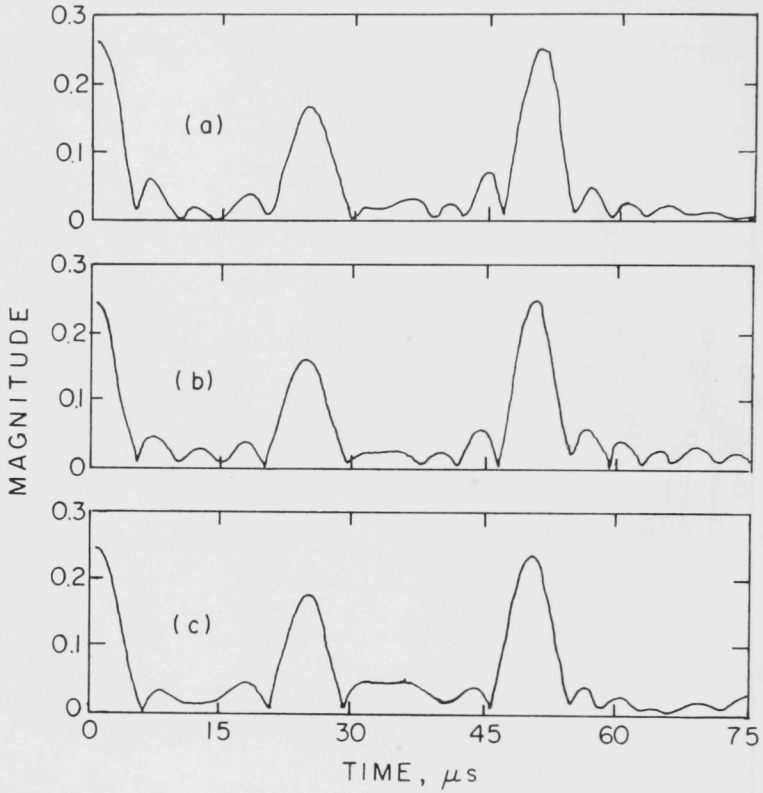

Fig. 54 Time Delay Estimation:

a) basic cross-correlator,
b) impulse response estimator,
c) maximum likelihood estimator.

to 0.0175, false peaks were produced by all three estimators. This is mainly due to the fact that the record length was very small (128 samples with 10 averagings). The limitation of increasing the record length is the requirement of a fast instrument response time.

The multipath signal was decomposed into single-path signals as in Eqs. (57) and (58) using a cosine window of width 40 μs and centered at the true time delays. Figure 55 shows the results of the estimation with the windowed signals. When the center of the window was changed to $\pm$3.3 μs, no significant change in the results was noticed. Since the sensitivity of the estimates with respect to the location of the window is small, this method can be used for peak separation and enhancement.

This study is of course theoretical, but clearly indicates that acoustic/ultrasonic techniques are feasible to measure temperatures in coal-conversion reactors and combustors. It will be necessary, however, (a) to test the available sensor materials at high temperatures under erosive and corrosive conditions and (b) upon the selection of the appropriate sensor material, to validate the proposed signal-processing technique. The basis for the applicability of this technique will be the frequency of operation, which will determine the length of the sensor and the noise background at the frequency of interest.

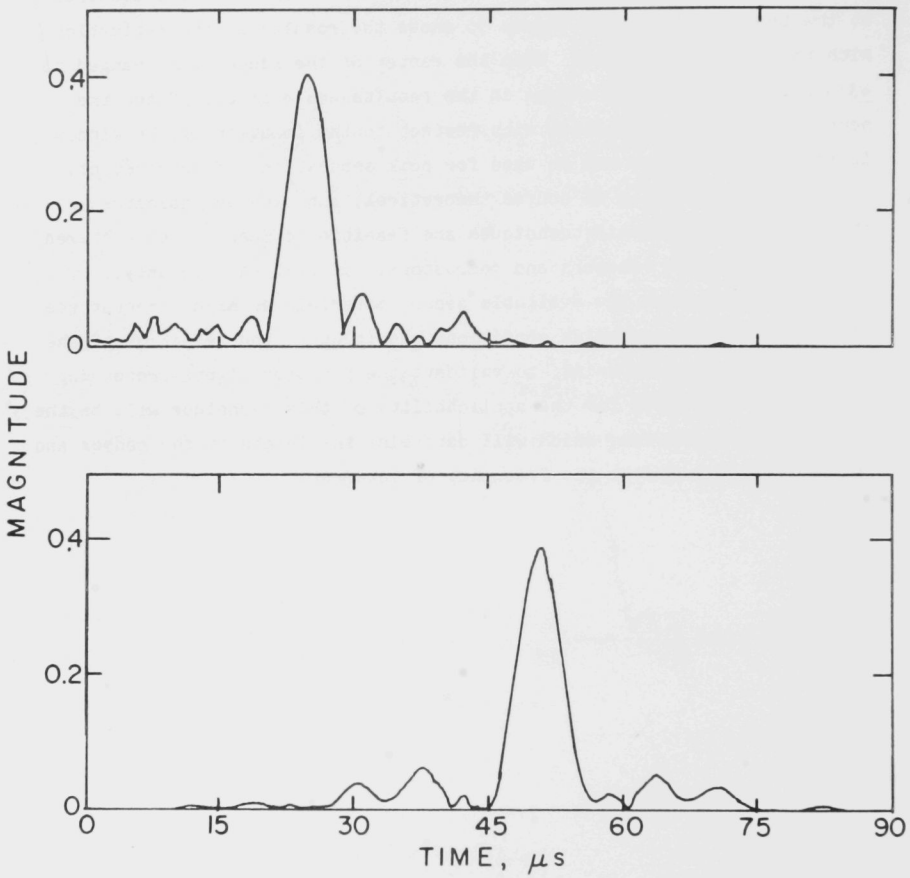

Fig. 55 Peak Separation and Enchancement.

VI. ACOUSTIC LEVEL MEASUREMENTS

Ultrasonic level detectors are commercially available, but as in the case of flow measurement are not directly applicable to measuring level in coal conversion plants because of the adverse environment and, in particular, because of the high-temperature requirements made on the transducers. The measurement usually is based upon the time required for a pulse of ultrasound energy to travel from a transmitter to a free surface, reflect from the surface, and return to a receiver, which may be the same transducer used to generate the pulse.

An acoustic level sensor, like level devices based on other principles, can be used to make the following measurements:

(a) Point measurement: detecting a gas-liquid, gas-solid, foam-liquid, or liquid-liquid interface at a fixed location and,

(b) Continuous measurement: sensing the position of an interface as it moves up or down.

The advantages of the acoustic techniques are that they have no moving parts, are easy to install, and are non-contacting. There do exist, of course, acoustic systems that are in contact, but these require only one opening for the waveguide in order to transmit and receive the acoustic pulses.

The mathematical modeling and data-processing techniques discussed earlier for temperature measurements are directly applicable to level measurements. At the present time a feasibility study on acoustic techniques to measure level is in progress, and preliminary indications are that the techniques are feasible. Final results of the study will be reported in the near future.

VII. CONCLUSIONS AND RECOMMENDATIONS

The work performed at ANL in the last four years has established that acoustic/ultrasonic techniques are usable to measure flow, temperature, and level in coal-conversion plants. Other parameters such as density, concentration and viscosity can possibly be determined through the acoustic properties of materials. Acoustic techniques are attractive because they are nonintrusive, easy to apply, and have inherit fast response.

The results of this study were based on theoretical calculations and experiments in the laboratory and pilot plants. In the case of flow measurements with experiments at the HYGAS, SRC-II, and BI-GAS pilot plants, actual flow-indicating devices were demonstrated and the results were very satisfactory. In the HYGAS tests the active acoustic cross-correlator was demonstrated and can be used as a flow-measuring device at least for small-scale plants. Use of this device in large-scale coal-conversion plants will require additional studies on sound attenuation in coal-slurry media. During the HYGAS tests important parameters in acoustic measurements, such as, noise background and attenuation were determined. It was found that the noise background in the frequency region of interest is small and decreases with concentration and does not restrict the measurements. The sound-attenuation measurements, however, indicated that attenuation increases with frequency and concentration. This results, when used in the sonar equation, indicated that acoustic/ultrasonic techniques are feasible in the frequency range below 500 kHz. The attenuation measurements indicated that the attenuation of sound is proportional to the concentration of particles in the line. This observation indicates that sound attenuation can be used to measure density.

The use of the acoustic doppler flowmeter was demonstrated for low-temperature slurries in the laboratory and high-temperature slurries at the SRC-II pilot plant by using the stand-off scheme. The accomplishment at the SRC-II pilot plant is a first in monitoring high-temperature slurries *via* acoustics in coal-conversion plants. Additional work, however, in developing high-temperature transducers and obtaining operational experience is needed to establish the reliability of the instrument.

The BI-GAS flow/no-flow indicator has enabled BI-GAS to remain operating and is the only dependable device to be used in the char-return line of the plant. Additional work, however, is needed to upgrade the device to a flowmeter by installing another microphone indicator upstream or downstream of the existing one and then using cross-correlation to determine velocity. The observation that signal level is proportional to char concentration in the line might also lead to a density meter and hence, a mass flowmeter, which is very much desired.

The theoretical feasibility studies have established that use of acoustic techniques to measure temperature and level in coal-conversion plants is reasonable, but basic experimental work to characterize the acoustic values is needed to prove the results. Understanding of the fundamental acoustic characteristics in coal streams will enhance further applications of acoustics in such areas as viscosity, and acoustics may become a viable diagnostic and research tool for combustion and reaction studies.

Based on the results to date the following recommendations are made:

1. Study attenuation to establish the effects of particle size and particle-size distribution, scattering, temperature, pressure, entrained fluids and gases, particle fluid velocity differences.
2. Develop high-temperature transducers.
3. Clearly establish the relationship between attenuation and particle concentration for density measurements.
4. Examine the effects of geometries, in particular for the BI-GAS case, on flow measurements.
5. Upgrade the BI-GAS flow/no-flow indicator to a flowmeter which will enable the instrument to be used in other plants.
6. Experimentally prove the feasibility of acoustic techniques for temperature and level sensors.
7. Perform material studies at high temperatures and pressures for the temperature and level sensors.
8. Initiate studies for viscosity measurements.
9. Determine the desired range, sensitivity, and accuracy for the instruments to be used in pilot and demonstration plants.

VIII. ACKNOWLEDGEMENTS

The authors would like to express their appreciation to the Department of Energy, Fossil-Energy for their support of this work. We would also like to thank R. S. Zeno, G. S. Rosenberg, T. P. Mulcahey, and N. M. O'Fallon for their support and encouragement. Thanks are also due to S. H. Sheen, P. D. Roach, H. B. Karplus, G. F. Popper and N. Gopalsami for their contribution and suggestions. And special thanks are due to Nancy Heeg for the excellent typing of this report.

IX. REFERENCES

1. N. M. O'Fallon, et al., "A Study of the State-of-the-Art of Instrumentation for Process Control and Safety in Large-Scale Coal Gasification Liquefaction and Fluidized-Bed Combustion Systems," ANL-76-4 (January 1976).

2. A. C. Raptis, et al, "Instrumentation Needs in Advanced Coal Utilization," Alternative Energy Sources, Vol. 7, pp 3359-3375, Hemisphere Publishing Corporation, Washington, D.C., 1978.

3. "Instrumentation and Process Control for Fossil Demonstration Plants," Annual Technical Progress Report, Oct. 1976 - Sept. 1977, Argonne National Laboratory, ANL-FE-49622-12, Oct. 1977.

4. A. C. Raptis, et al, "Measurements of Noise Background and Attenuation in Coal Toluene Slurries," 1978 Ultrasonics Symposium Proceedings, IEEE Cat. #78CH1344-1SU.

5. P. D. Roach and A. C. Raptis, "An Acoustic Char Flow Monitor for the BI-GAS Pilot Plant, The Proceedings of the 1979 Symposium on Instrumentation and Control for Fossil Energy Processes, pp 195-209, ANL-79-62, CONF-790855, 1979.

6. H. B. Karplus and A. C. Raptis, "Slurry Flow Measurements Using an Acoustic Doppler Flowmeter," The Proceedings of the 1979 Symposium on Instrumentation and Control for Fossil Energy Processes, pp 184-195, ANL-79-62, CONF-790855, 1979.

7. N. Gopalsami, A. C. Raptis and T. P. Mulcahey, "Monitoring Temperatures in Coal Conversion and Combustion Processes via Ultrasound," Argonne National Laboratory, ANL-FE-49622-TM09, Feb. 1980.

8. L. C. Lynnworth, "Ultrasonic Flowmeters," Physical Acoustics, Vol. XIV, pp 407-525, Academic Press, New York, 1979.

IX. REFERENCES (Contd.)

9. A. C. Raptis, et al., "Feasibility Study of Ultrasonic/Sonic Flowmeters for Coal Slurries," Argonne National Laboratory, ANL-CT-77-1, Oct. 1976.

10. R. J. Urick, Principles of Underwater Sound for Engineers, 2nd Ed. McGraw-Hill, 1975.

11. R. J. Urick, "The Absorption of Sound in Suspensions of Irregular Particles," J. Acoust. Soc. Am., Vol. 20, No. 3, pp 283-289, May 1948.

12. A. C. Raptis, G. F. Popper and W. M. Carey, "A Feasibility Study of Ultrasonic/Sonic Flowmeters for Coal Slurries," Alternative Energy Sources, Vol. 7 pp 3377-3395, Hemisphere Publishing Corporation, Washington, D.C. 1978.

13. E. J. Skudrzyk and G. P. Haddle, "Noise Production in a Turbulent Boundary Layer by Smooth and Rough Surfaces," J. Acoust. Soc. Am., Vol. 32, pp 19-34, Jan. 1960.

14. A. C. Raptis, et al., "Acoustic Noise Background and Sound Transmission Tests in a Slurry Line at the HYGAS Pilot Plant," Argonne National Laboratory, ANL-FE-49622-TM04, Jan. 1979.

15. W. G. Bair, "Instrumentation and Data Acquisition Techniques in the HYGAS Pilot Plant," Proceedings of the 1977 Symposium on Instrumentation and Process Control for Fossil Demonstration Plants, pp 64-73, ANL-78-7, 1977.

16. H. B. Karplus and A. C. Raptis, "Investigation Leading to the Development of an Acoustic Doppler Slurry Flowmeter," Argonne National Laboratory, ANL-FE-49622-TM06, 1979.

IX. REFERENCES (Contd.)

17. H. B. Karplus, "Ultrasonic Transducer With Laminated Coupling Wedge," U.S. Patent 3,973,152, Dec. 1976.

18. H. B. Karplus and G. A. Forster, "Interim Ultrasonic Sodium Flow Measurement on the EBR-II Secondary System," Argonne National Laboratory, ANL-CT-78-23, March 1978.

19. L. C. Lynnworth, "Fluid Flowmeter", U.S. Patent 3, 575, 050, April 1971.

20. H. Bazerghi and K. J. Sudula, "Estimation and Reduction of Errors in Flow Measurements with Use of Cross-Correlation Techniques," Presented at Sound Specialists Meeting on Reactor Noise, SMORN-II, Sept. 19-23, 1977, Gatlinburg, TN, USA.

21. P. S. Epstein and R. R. Garhart, "The Absorption of Sound in Suspensions and Emulsions; I. Water Fog in Air," JASA, Vol. 25, No. 3, pp 553-565, 1968.

22. K. F. Herzferld and T. A. Litovitz, Absorption and Dispersion of Ultrasonic Waves, Academic Press, New York, N. Y. p 44, 1959.

23. H. Lamp, Hydrodynamics, 6th Edition, Dover Publications Inc., New York, N. Y., pp 514-518, 1945.

24. S. N. Foner and B. H. Wall, "Attenuation of Sound by Rigid Spheres: Measurements of the Viscous and Viscous and Thermal Components of Attenuation and Comparison with Theory," JASA, Vol. 57, No. 1, 1975.

25. D. H. Tack, M. W. Smith and R. F. Lambert, "Wall Pressure Correlations in Turbulent Air Flow," JASA. Vol. 48, No. 4, pp 410-418, 1961.

IX. REFERENCES (Contd.)

26. A. L. Wilson, "Safety Assurance Study of High BTU Coal Gasification Pilot Plants," Interim Report, ERDA Report No. FE-2240-8, Aug. 1976.

27. J. W. Zink and L. P. Delsasso, "Attenuation and Dispersion of Sound by Solid Particles Suspended in a Gas," JASA, Vol. 30, No. 8, pp 765-771, Aug. 1958.

28. D. L. Mallins, W. F. Baldwin, and P M. Berry, "How Detectors Measure Flow Line Sand," Oil and Gas Journal, p 101, Feb. 3, 1975.

29. A. P. Gavin, T. T. Anderson and J. J. Janicek, "Sodium Immersible High-Temperature Microphone-Design Description," Argonne National Laboratory, ANL-CT-75-30, Feb. 1975.

30. J. F. Schooley, "State-of-the-Art of Instrumentation for High Temperature Thermometry," Proc. 1977 Symp. on Instrumentation and Process Control for Fossil Demonstration Plants, Chicago, IL, 1977.

31. L. C. Lynnworth and E. P. Papadakis, "Ultrasonic Thermometry," Proc. 1970 Ultrasonics Symp., San Francisco, CA, Oct. 1970.

32. L. C. Lynnworth and D. R. Patch, "New Sensors for Ultrasound: Measuring Temperature Profiles," Materials Research and Standards, Vol. 10, pp 6-11, Augu. 1970.

33. J. Blitz, Ultrasonics: Methods and Applications, Van Nostrand, New York, N.Y. 1971.

34. E. Papadakis, K. A. Fowler and L. C. Lynnworth, "Ultrasonic Measurements of Young's Modulus and Extensional Wave Attenuation in Refractory Wires at Elevated Temperatures with Application to Ultrasonic Thermometry," Journal of Applied Physics, Vol. 45, pp 2409-2420, 1974.

IX. REFERENCES (Contd.)

35. C. H. Knapp and G. C. Carter, "The Generalized Correlation Method for Estimation of Time Delay", IEEE Trans. Acoust., Speech, Signal Processing, Vol. ASSP-24, pp 320-327, 1976.

36. J. C. Hassab and R. E. Boucher, "Optimum Estimation of Time Delay by a Generalized Correlator," ibid, Vol. ASSP-27, pp 373-380, 1979.

37. J. S. Bendat and A. G. Piersol, Engineering Applications of Correlation and Spectral Analysis, John Wiley, New York, N.Y., 1980.

38. R. C. Kemerait and D. G. Childers, "Signal Detection and Extraction by Cepstrum Techniques," IEEE Trans. Information Theory, Vol. IT-18, pp 745-759, 1972.

39. E. P. Papadakis, "Theoretical and Experimental Methods to Evaluate Ultrasonic Transducers for Inspection and Diagnostic Applications," IEEE Trans. Sonics and Ultrasonics, Vol. SU-26, pp 14-27, 1980.

40. L. R. Rabiner and B. Gold, Theory and Application of Digital Signal Processing, Prentice-Hall, Engelwood Cliffs, N.J., 1975.

Distribution for ANL/FE-49628-TM04

Internal:

P. B. Abramson
E. F. Bennett
E. L. Carls
C. E. Cohn
S. A. Cox
L. R. Dates
R. W. Doering
J. J. Eichholz
W. A. Ellingson
N. Gopalsami
E. F. Groh
C. L. Herzenberg
A. A. Jonke
H. B. Karplus
P. Kehler
L. G. LeSage
W. H. Lin
A. A. Longnecker
N. M. O'Fallon (4)
T. P. Mulcahey
E. G. Pewitt
K. G. Porges
A. C. Raptis (10)
J. J. Roberts
G. S. Rosenberg
S. H. Sheen
D. L. Smith
W. J. Sturm
C. E. Till
R. S. Zeno
A. B. Krisciunas
ANL Patent Dept.
ANL Contract File
ANL Libraries
TIS Files (6)

External:

DOE-TIC, for distribution per UC-90h (226)
Manager, Chicago Operations Office, DOE
President, Argonne Universities Association
Components Technology Division Review Committee:
- A. Bishop, U. Pittsburgh
- F. W. Buckman, Consumers Power Co.
- R. A. Greenkorn, Purdue U.
- W. M. Jacobi, Westinghouse Electric Corp., Pittsburgh
- M. A. Schultz, Mashpee, Mass.
- E. E. Ungar, Bolt, Beranek and Newman, Inc., Cambridge, Mass.
- J. Weisman, U. Cincinnati

Applied Physics Division Review Committee:
- P. W. Dickson, Jr., Clinch River Breeder Reactor Project, Oak Ridge
- K. D. Lathrop, Los Alamos Scientific Lab.
- W. B. Loewenstein, Electric Power Research Inst.
- J. E. Meyer, Massachusetts Inst. Technology
- R. Sher, Stanford U.
- D. B. Wehmeyer, Detroit Edison Co.

G. A. Atwood, U. Akron
K. C. Baczewski, Dravo Corp., Pittsburgh
D. L. Basdekas, Office of Nuclear Regulatory Research, USNRC
C. W. Busch, Spectron Development Labs., Costa Mesa
L. L. Chyi, U. Akron
A. C. Dolbec, Electric Power Research Inst.
A. K. Dubberly, Pace Co., Denver
D. Duffey, U. Maryland
R. Forde, Gulf Research and Development Co., Pittsburgh
W. Fuchs, Pittsburgh Energy Technology Center, USDOE
H. W. Goldstein, General Electric Co., Space Sciences Lab., Philadelphia
E. C. Guyer, Dynatech R/D Co., Cambridge, Mass.
D. S. Hacker, U. Illinois, Chicago
R. King, Oak Ridge National Lab.
T. K. Lau, Fossil Energy, USDOE (10)
C. Leffert, Wayne State U.
B. G. Liptak, Liptak Associates, Stamford, Conn.

W. W. Managan, Technology for Energy Corp., Knoxville
H. March, Procon, Inc., Des Plaines, Ill.
L. B. Mattson, Jet Propulsion Lab.
Y. Nakamura, Jet Propulsion Lab.
D. Rapley, Stearns Roger, Inc., Denver
L. N. Rubow, Gilbert Associates, Inc., Reading, Pa.
S. Sami, Southern Illinois U., Carbondale
C. K. Sanathanan, U. Illinois, Chicago
J. F. Schooley, National Bureau of Standards, Washington
M. A. Scott, U. Tennessee Space Inst., Tullahoma
A. J. Simpkin, Bell Aerospace Textron, Buffalo
R. F. Stewart, Morgantown Energy Technology Center, USDOE
E. S. Van Valkenburg, Leeds & Northrup Co., North Wales, Pa.
F. A. Zenz, Garrison, N. Y.